IOWA STATE UNIVERSITY
Digital Repository

Retrospective Theses and Dissertations

Iowa State University Capstones, Theses and Dissertations

1987

Protein precipitation with acids and polyelectrolytes: the effects of reactor conditions and models of the particle size distributions

Rod R. Fisher
Iowa State University

Follow this and additional works at: https://lib.dr.iastate.edu/rtd

 Part of the Chemical Engineering Commons

Recommended Citation
Fisher, Rod R., "Protein precipitation with acids and polyelectrolytes: the effects of reactor conditions and models of the particle size distributions " (1987). *Retrospective Theses and Dissertations*. 8536.
https://lib.dr.iastate.edu/rtd/8536

This Dissertation is brought to you for free and open access by the Iowa State University Capstones, Theses and Dissertations at Iowa State University Digital Repository. It has been accepted for inclusion in Retrospective Theses and Dissertations by an authorized administrator of Iowa State University Digital Repository. For more information, please contact digirep@iastate.edu.

INFORMATION TO USERS

While the most advanced technology has been used to photograph and reproduce this manuscript, the quality of the reproduction is heavily dependent upon the quality of the material submitted. For example:

- Manuscript pages may have indistinct print. In such cases, the best available copy has been filmed.
- Manuscripts may not always be complete. In such cases, a note will indicate that it is not possible to obtain missing pages.
- Copyrighted material may have been removed from the manuscript. In such cases, a note will indicate the deletion.

Oversize materials (e.g., maps, drawings, and charts) are photographed by sectioning the original, beginning at the upper left-hand corner and continuing from left to right in equal sections with small overlaps. Each oversize page is also filmed as one exposure and is available, for an additional charge, as a standard 35mm slide or as a 17"x 23" black and white photographic print.

Most photographs reproduce acceptably on positive microfilm or microfiche but lack the clarity on xerographic copies made from the microfilm. For an additional charge, 35mm slides of 6"x 9" black and white photographic prints are available for any photographs or illustrations that cannot be reproduced satisfactorily by xerography.

8716766

Fisher, Rod R.

PROTEIN PRECIPITATION WITH ACIDS AND POLYELECTROLYTES: THE EFFECTS OF REACTOR CONDITIONS AND MODELS OF THE PARTICLE SIZE DISTRIBUTIONS

Iowa State University PH.D. 1987

University Microfilms International 300 N. Zeeb Road, Ann Arbor, MI 48106

PLEASE NOTE:

In all cases this material has been filmed in the best possible way from the available copy. Problems encountered with this document have been identified here with a check mark __✓__.

1. Glossy photographs or pages __✓__
2. Colored illustrations, paper or print _____
3. Photographs with dark background __✓__
4. Illustrations are poor copy _____
5. Pages with black marks, not original copy _____
6. Print shows through as there is text on both sides of page _____
7. Indistinct, broken or small print on several pages __✓__
8. Print exceeds margin requirements _____
9. Tightly bound copy with print lost in spine _____
10. Computer printout pages with indistinct print _____
11. Page(s) _____ lacking when material received, and not available from school or author.
12. Page(s) _____ seem to be missing in numbering only as text follows.
13. Two pages numbered _____. Text follows.
14. Curling and wrinkled pages _____
15. Dissertation contains pages with print at a slant, filmed as received _____
16. Other _____

_____

_____

University
Microfilms
International

Protein precipitation with acids and polyelectrolytes: The effects of reactor conditions and models of the particle size distributions

by

Rod R. Fisher

A Dissertation Submitted to the
Graduate Faculty in Partial Fulfillment of the
Requirements for the Degree of
DOCTOR OF PHILOSOPHY
Major: Chemical Engineering

Approved:

Signature was redacted for privacy.
In Charge of Major Work

Signature was redacted for privacy.
For the Major Department

Signature was redacted for privacy.
For the Graduate College

Iowa State University
Ames, Iowa

1987

TABLE OF CONTENTS

DEDICATION

To my father and my father-in-law, for their examples of integrity.

GENERAL INTRODUCTION

In an increasing number of industrial systems, the process requires the separation of proteins from dilute aqueous solutions. Examples of such protein-containing streams include wastewater from food production, where the goal is to reduce protein disposal; solutions of plant or animal tissue extract, where the protein is sought as a primary or by-product for use in food, feed, or other products; and, of high interest currently, solutions from fermentation broths or cell homogenates carrying the protein products of biotechnology.

In all of these applications, chemical engineers can employ their traditional expertise to solve important and unique design and operation problems. In illustration, let us consider the use of precipitation to separate the proteins derived from biotechnological processes.

Products of Process Biotechnology

The industrially important products from the biochemical process/fermentation technologies are used in (1) human health care (vaccines, hormones, specialty drugs), animal health care (vaccines and hormones), agriculture (fine chemicals), and specialty chemical applications (vitamins, amino acids, and enzymes). Enzymes, produced in the largest scale (from 400 to 500 tons annually (2)), include proteases used in cleaning agents and as clarifying agents in beverages, amylases and isomerases used in conversion of starch to sugars, and rennin used in cheese manufacture.

Given that many of the benefits of process biotechnology will be realized in the manufacture of proteinaceous compounds, development of

this industry will require research and design advances in 1) modification of the protein-producing organism, 2) cell growth and protein synthesis processes, 3) protein recovery and purification, and 4) utilization and application of the protein product. The third step, often called downstream processing, commands up to ninety percent of the overall process. Yet a base of fundamental engineering information on protein recovery and purification operations is lacking.

Production of the biopolymer

Advances in the past decade have made it possible to alter the gene code of a given cell and induce that cell to synthesize a desired protein. The manufacture of such bioproducts from plant, animal, or microbial cells requires integration of the production operations--usually fermentation--and the recovery stage.

The sequential steps for recovery and purification of the bioproduct are (3, 4)

1) physical or chemical extraction from the cell (if the product is intracellular), where physical methods include homogenization, milling, sonication, freezing, and osmotic shock; and where chemical methods include detergent treatment and chemical or enzymatic hydrolysis,
2) particulate removal by filtration or centrifugation,
3) primary isolation or concentration of product, by extraction, sorption, evaporation, phase partition, membrane techniques (ultrafiltration or reverse osmosis), or precipitation,

4) purification, by chromatography, adsorption, membrane techniques, electrophoresis, or fractional precipitation,

5) final product preparation for end use, by crystallization, drying, suspension, or solubilization.

To be of value, most of the proteinaceous products of biotechnology must maintain their bioactivity. The maintenance of activity can present an extremely difficult problem. Safe limits (usually near physiological conditions) on pH, ionic strength, temperature, and mechanical forces must be maintained. Some proteins are prone to surface denaturation, as when contacting an air-liquid interface; thus, foaming must be minimized. Also, the cell or tissue in use may produce a number of significant proteolytic enzymes, which, when released during the cell-breakage step, act to degrade the desired protein. A number of protease inhibitors have been used to minimize this effect (5).

Applications of Precipitation

Protein precipitation involves the destabilization of a protein solution in order to form particles that are separable by gravity settling, centrifugation, filtration, or other physical means. The size, shape, density, and strength of the precipitates govern the efficiency of the solid-liquid separations (6); thus, the control of these properties is desirable.

Clearly, from the five-step recovery sequence listed above, precipitation can play an advantageous role in protein separations. Applying fractional precipitation may permit one to skip the particulate removal step and perform the primary isolation and purification steps in a single

unit operation. An important advantage of precipitation is that it is a bulk process, and less scale-dependent than methods such as chromatography. Currently, for low-unit-value products--where the emphasis of the separation method should be on energy cost, recovery efficiency, and environmental impact--precipitation often proves economically favorable.

The selectivity of precipitation for a specific protein from a mixture is usually lower than that of other purification methods. Selectivity can be increased, however, by exploiting highly specific protein-precipitant interactions, such as in affinity precipitation (7).

Precipitation can be achieved by a wide variety of methods, providing engineers flexibility in choosing the optimal process for a given system. Generally, precipitation is caused by

1) changing the solvent to reduce the stability of the colloidal sol; one can adjust ionic strength (salting out), pH (isoelectric precipitation), dielectric character (solvent precipitation); temperature (causing denaturation and solubility changes), or free volume (through addition of inert solutes or polymers).
2) adding the precipitant, which binds to the protein, so that the precipitate is necessarily a mixture of the two. The precipitant may be a small MW compound, a multivalent metal ion (Ca^{++}), an uncharged polymer, or a polyelectrolyte (flocculation); the binding may be due to nonspecific forces (electrostatic or hydrophobic) or specific interactions (affinity).

Specific examples for the application of precipitation include the recovery of milk-whey protein with polyelectrolytes (8), other food industry applications (9), and the fractionation of blood plasma proteins

by ethanol precipitation (10). Precipitation is also used widely in mineral and inorganic systems. Examples include treatments to clarify raw water (11) and processes in papermaking to precipitate (i.e., affix) the fines into the paper web (12).

Fundamentals of Colloid Aggregation

This work focuses on two specific precipitation systems: isoelectric precipitation of soy proteins and polyelectrolyte precipitation of egg white proteins. Any discussion of either requires a basic understanding of the physico-chemical aspects of colloidal behavior in aqueous solution.

Proteins as colloids

As generally defined, a colloid is a system of solid-like particles with diameters ca. 1 nm to ca. 1 μm. The proteins of the soy and egg white system in aqueous solution are in the range of a colloidal dispersion (13), allowing the theory of colloidal aggregation to be applied to precipitation. In this work, the following definitions will be used (6, 14):

Aggregation--the generic term to refer to any type of reversible or irreversible association of particles.

Coagulation--aggregation in which charge neutralization of the colloid and/or double layer compression (to be described below) are the predominant mechanisms by which the individual colloidal particles come together.

Flocculation--aggregation characterized by a bonding agent, usually a high molecular-weight polymer, which acts upon the colloid.

This agent may act either by physically bridging the colloidal particles or by attaching to and neutralizing surface charges.

A protein is a polyampholyte coiled such that the hydrophobic (apolar) amino acid residues are predominantly oriented away from the surface, with positive and negative charges of weakly acidic and basic groups, as well as other polar groups, exposed to the solvent. Most proteins possess a net negative charge in neutral pH solutions. The final charge depends on the ionizable residues, their exposure to the surface, their pK values, and the solution pH. The pH which gives a net charge of zero is known as the isoelectric point, usually ranging from pH 4 to 6 for proteins. In addition to charged and hydrophilic groups, the surface of the protein also carries a substantial number of hydrophobic patches which are quite important in determining the protein solubility (15).

A charged colloid in an electrolyte solution is described by the double-layer theory of colloid stability (16, 17). According to this theory, the charged surface attracts oppositely charged ions into a closely associated Stern layer, across which much of the net potential drops. The more diffuse Gouy-Chapman layer of counterions, from which ions of similar charge to the surface are repelled, extends out from the Stern layer. Hydrodynamically, the inner layer is strongly adsorbed and moves with the colloid, while most of the Gouy-Chapman layer is in closer association with the solvent. The ζ-potential is an electrophoretically measured characterization of the double layer, with typical values for a stable, non-aggregating colloid in the range of ± 10 to ± 40 mV (6).

The DLVO theory of colloid stability (18) sums the double-layer repulsive force--proportional to the square of the ζ-potential and significant over a distance on the order of a nanometer--with the attractive London-van der Waals induced-dipole interaction--proportional to the colloid diameter and significant over a longer distance, on the order of tens of nanometers--to yield an overall potential energy barrier to collision. Each of these forces is influenced by the properties of the solvent, ionic strength and dielectric constant. If the repulsive energy maximum is less than approximately 5 kT, then particles can overcome this barrier and coagulate (17).

The solubility of the protein is also affected by the solution ionic strength (and the type of ions present), dielectric constant, temperature and by the presence of organic solvents.

Isoelectric precipitation--coagulation

A solution of protein molecules is made less stable by reducing the repulsive component of the interaction potential; in the case of isoelectric precipitation, by adjustment of the pH to where the protein surface has a lower net potential. In a destabilized protein sol; the molecules will aggregate due to diffusive motion to form a primary particle (19), the final size of which is dependent on the mechanism of formation, or nucleation (20). The primary particles continue to grow to a size where convective flows become important and fluid-driven particle-particle collisions lead to the formation and growth of aggregates--where aggregate now implies an assemblage of primary particles.

Collision rates of aggregating colloids have been theoretically described for zero-shear cases (perikinetic) and for uniform shear (orthokinetic) (21). However, most precipitations of practical importance are done in turbulent conditions, so other mechanisms and rate relations should be considered. When the aggregate attains a sufficiently large size, aggregate breakage due to environmental effects becomes important, and has been shown to be a predominant factor in the dynamic equilibrium of growth and breakup which determines the final aggregate size (22).

Breakage has been attributed to the following mechanisms: 1) deformation and rupture caused by dynamic pressure fluctuations (23), related to velocity fluctuations (24); 2) loss of primary particles by erosion due to hydrodynamic shear, aggregate-aggregate or aggregate-solid surface interactions (23); 3) fragmentation of the aggregate by hydrodynamic shear; and 4) fragmentation due to aggregate-aggregate collisions, expected to be most important between similarly sized aggregates (25).

Collisional breakage has been supported experimentally for isoelectric precipitation of soy proteins, in laminar (26) and turbulent shear (27). Other investigations of breakup have considered surface erosion by turbulent drag (28), turbulent rupture (29), and shear of the polymer chain (30). Others (27) have reported that breakage of isoelectrically precipitated soy protein appears to be second order with particle concentration, indicating a collision-breakup mechanism.

Previous work on isoelectric precipitation: kinetics and mixing

Since physical separation of the precipitate from the fluid phase is ultimately desired, the particle size distribution is an important

characteristic of a precipitating system. Much previous work has considered protein precipitation where measurements of particle size distributions by electronic particle counter techniques were made. Also, number population models have been constructed using empirical and mechanistic terms to account for aggregate growth, breakup, and flow into and out of the system.

Grabenbauer and Glatz (19) investigated the isoelectric (HCl) precipitation of soy in a CSTR (continuous stirred-tank reactor) in order to extract kinetic aggregate-growth information. They used the Coulter counter to monitor steady-state particle size distributions of the protein aggregate, and presented population-balance models analogous to those used in crystallization (31), in which they employed empirical terms accounting for a constant growth rate and breakage (into two fragments) as a power-law function of aggregate size. The protein concentration, agitation, and ionic strength were varied and found to significantly affect the particle size distributions.

Petenate and Glatz (32) theoretically derived mechanistic terms for growth and breakup, and derived values for the kinetic parameters associated with these terms from their data. For growth, they concluded that a growth rate linear with aggregate diameter was sufficient in fitting the data; physically, this finding implies that the collision efficiencies for large aggregate-primary particle contacts and small aggregate-primary particle contacts are not different. Their data supported a thorough breakage mechanism, in which hydrodynamic shear disrupts the aggregate into separate particles, too small to measure.

They studied effects of concentration, stirrer speed, and pH on kinetic constants, finding that mixing affected breakage rate more than it did growth.

Glatz, Hoare, and Landa-Vertiz (22) further investigated the kinetic mechanisms using data from CSTR, batch, and tubular reactors. Their model assumes breakage into a small number of daughter fragments. The important influence that mixing has on the phenomena of growth and breakup is again made clear.

In studying reaction and crystallization in an CSTR, Tavare and Garside (33) compared the effects of two extremes in mixing--maximum mixedness and complete segregation--on theoretical models. Their solutions predicted that the products would differ significantly in physical properties (particle size distributions) but differ little in chemical composition (reaction conversion).

In all of these efforts the effects of the mixing on the physical properties (size, density) of the precipitate are made clear. In the application of precipitation for fractional recovery of selected proteins, we must also be concerned how mixing affects the final resolution of the fractionation. The physical properties govern the efficiency of the solid/liquid separation, and the compositional or chemical properties govern the quality of the product and thus the efficiency of the overall process.

Applications of Polyelectrolyte Precipitation

Polyelectrolytes have been used as precipitating and flocculating agents for many years, especially for water clarification. Within the last decades, they have been used increasingly for protein removal or

recovery. Advantages of using polyelectrolytes include their effectiveness at low concentration (in salting out for water treatment, up to 95 percent of the precipitate is made up of the inorganic salt precipitant, whereas for polymer flocculation, on the order of five percent (17)), the low cost of most polyelectrolytes, the high protein yields they provide, and the improved solid-liquid separation properties of the precipitate (34). The wide array of different polyelectrolytes allows choices of different properties (pH, molecular weight, chain stiffness, etc.) in order to customize the polymer to fit the application.

Polyacrylic acid and lysozyme

As a flocculant, PAA has been used in water clarification, in the treatment of sugar solutions, in paper manufacture, and in sewage disposal (35). Others (36, 37) have done extensive work applying PAA to the precipitation and fractionation of proteins.

Lysozyme is responsible for lysis of invading bacterial cells in the egg. Other properties of lysozyme and the other proteins constituting the egg white are given in Table 1 and detailed in other reviews (38).

Fundamentals of Polyelectrolyte Precipitation

With the application of polyelectrolytes as precipitants in the recovery of proteins, the questions regarding mixing become more interesting; much less is known of the mechanisms of aggregation, for example, and polyelectrolytes present special problems in dispersion and diffusion due to their high molecular weights. Properties and phenomena relevant to polyelectrolyte precipitation are now briefly considered.

Table 1. Protein composition of egg white (39)

Protein	% of total protein	V_{20} ml/g	MW x 10^{-3}	pI	Biological property
ovalbumin	65	0.75	45	4.58	
conalbumin	13.8	0.73	76.6	6.8	metal binding
lysozyme	3.3	0.72	14.8	11.3	bacterial lysis
ovomucoid	12	0.69	27.9	3.9	trypsin inhibitor
avidin	<0.1		66	10	biotin binding
ovomucin	1.9				hemagglutinin
globulins	4.4				

Polyelectrolytes

The properties of the polyelectrolyte which are important to the precipitation are affected to a large extent by the solution environment. An excellent overview of the properties of dissolved polymers is given by Robb (40). The polyelectrolyte in solution will usually configure to a random coil of roughly spherical shape if it is nonionic and, if ionic, a more extended rodlike configuration due to repulsion of the charges along the backbone. The counterions and fixed charges therefore affect three properties of extreme importance to flocculation: 1) the polyelectrolyte solubility, 2) its conformation in solution and when adsorbed, and 3) its ability to associate with a charged colloid.

Formation of the solid phase

The destabilization of a protein solution with a polyelectrolyte precipitant occurs in analogous steps to isoelectric precipitation.

First, the formation of the primary particle is understood to occur very rapidly. No mechanisms for the formation of the primary particle have been reported in the literature. One hypothetical mechanism is that the protein diffuses into a nearby polymer domain and attaches due to charge-charge attractions, reducing the total potential of the polymer. (For the egg white proteins-PAA system, the polymer radius of gyration will be on the order of 200 Angstroms, while the protein radius of gyration will be on the order of 50 Angstroms.) This attachment induces the polymer to coil, allowing the polymer-protein ensemble to diffuse to another such ensemble and adsorb by van der Waals or polymer entanglement. Such diffusive growth occurs until the polymer or protein in the nearby fluid is depleted. In a sense, in this mechanism the polyelectrolyte acts as the colloid and the protein acts as the precipitant. In those instances where the polymer and the protein have the same charge, adsorption can still occur by hydrophobic and hydrogen bonding and by the action of divalent salts acting as binders (41).

Next, once the primary particles have formed, aggregation begins, where polymer adsorption may cause charge neutralization, bridging, or patch formation (17). In bridging, for example, an adsorbed polymer may extend 10-100 nm into the solution (when ionic strength <0.1 M for a 10^5 molecular weight polymer); this is sufficiently long to penetrate a repulsive double layer between the particles (with thickness much less than 10 nm) (40).

Kinetic considerations

The overall rate of flocculation will depend on the rates of one or more of the following steps (6) (see Figure 1):

For primary particle formation:

1) introduction of the polyelectrolyte and the protein to the solution,
2) diffusion of these two species into close proximity,
3) adsorption of one species onto the other and possible rearrangement,
4) growth of a solid phase by continued diffusion until the local supply of protein is depleted.

For aggregation (flocculation):

1) diffusive or convective movement of the polymer to the primary particle,
2) adsorption of the polymer onto the particle and possible rearrangement,
3) collision of the primary particles driven by convection of the fluid,
4) growth of the aggregate by one or more of the mechanisms given for flocculation: charge neutralization, bridging, or patch formation,
5) breakage of the aggregates due to one or more of the mechanisms given:
   -- deformation and rupture as a result of fluctuation dynamic pressures

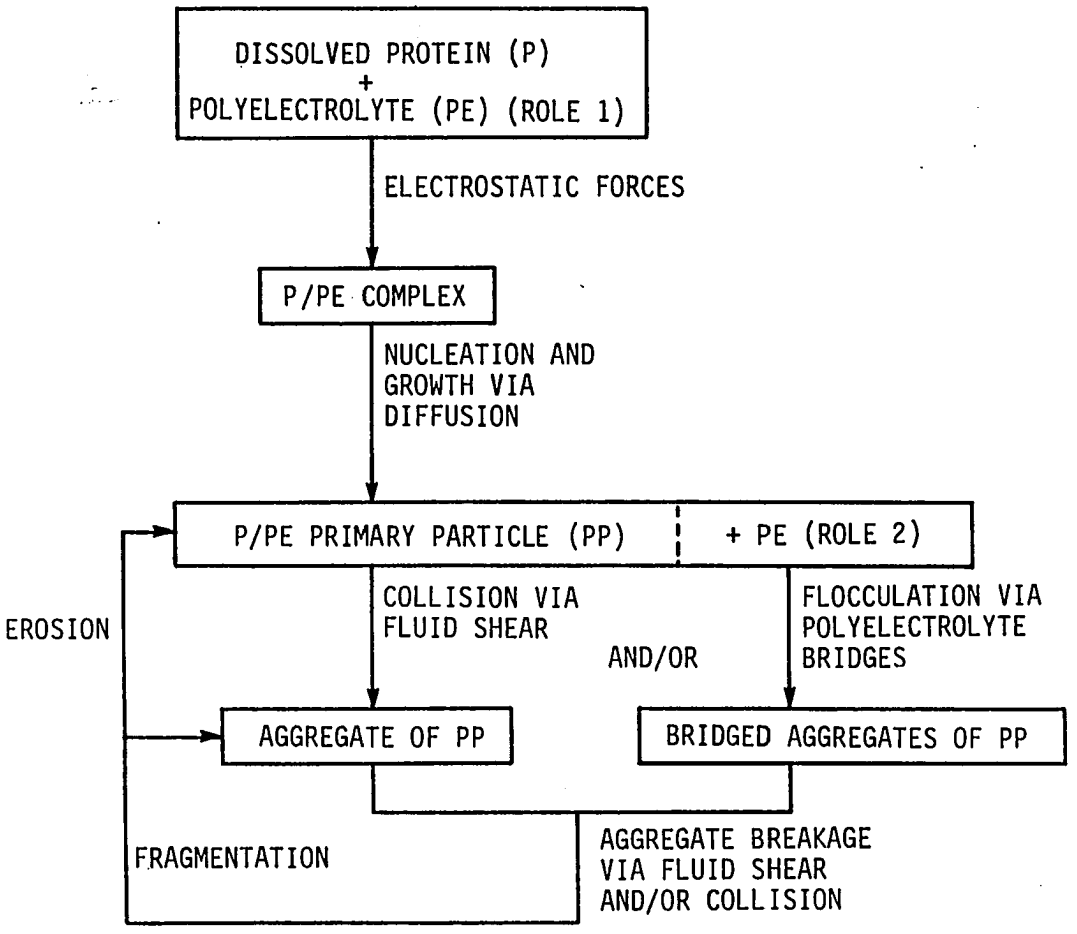

Figure 1. Fundamental phenomena expected to occur during precipitation of biological macromolecules by polyelectrolytes. Shown are two direct influences of the polyelectrolyte

-- erosion of primary particles from the aggregate by hydrodynamic shear

-- fragmentation by hydrodynamic shear

-- fragmentation by aggregate-aggregate collisions

Successful reactor design requires an understanding of the precipitation kinetics and other controlling phenomena. The events describing the formation and growth of the solid phase will be briefly discussed here. Mixing, which exerts influence on all steps, and breakage, in dynamic equilibrium with growth at sufficiently long times, will then be considered.

Polyelectrolyte diffusivities differ dramatically from those of low molecular-weight electrolytes, and may be low enough to make this step rate-limiting in the formation of the primary particle. Adsorption of oppositely charged polymers on proteins is a relatively fast process (17) (on the order of 0.01 second (42)), and rearrangements occur in seconds (43).

Collision rates have been described using a modified Smoluchowski theory for orthokinetic aggregation (21), and give an indication of how different process variables will affect the precipitation. Experimental and theoretical considerations of the kinetics of flocculation are documented (17, 20, 44).

Mixing considerations

As is clear from the previous sections, the level of agitation is a very influential factor in precipitation processes. Of concern is the early distribution of the precipitant, where irreversible attachment and

rapid polymer adsorption necessitate thorough admixing at introduction (40, 42).

Mixing is quantified by V_g, the root-mean-square fluid velocity gradient (45)

$$V_g = (P/\mu V)^{\frac{1}{2}}$$

for tank volume V and viscosity μ, and where expressions for P (the power input) as a function of impeller speed and type and fluid viscosity exist. The literature gives power characteristics of various tank configurations and impellers (46).

Reactor considerations

The precipitation reactor is any device or devices making possible these events:

1) Initial contacting of the protein and precipitant

2) Growth of the floc

3) Aging and breakage of the floc

The objectives in precipitation reactor design (6, 47) are to promote contacting for efficient growth, to minimize denaturation or over-precipitation, to minimize breakage of the precipitate, and to maximize aggregate strength through aging.

In the precipitation of enzymes, continuous processing can give number of advantages, including reduced residence time and exposure of the enzyme to fewer extremes (6); with thorough mixing, the inlet protein is exposed quickly to the final, bulk conditions. Also, because continuous operation--either in tubular flow reactors or continuous stirred tank

reactors (CSTR)--gives uniform and temporally unchanging conditions during the precipitation, it is amenable to modeling.

Research Objectives and Overview

Overall, this work is intended to provide information based on mechanistic considerations of experimental data that will allow improved design and operation of reactors for the precipitation of proteins from aqueous solution. The specific objectives are to understand the mixing environment of the precipitation--mean shear rate, V_g, and mean residence time, τ--through experimentation and modeling. We are interested in the role these parameters have on the physical and compositional properties of the precipitate product.

In Section I, the fractionation of soy proteins by isoelectric precipitation under two extremes of agitation during acid addition is studied. The objective here is to quantify the differences in the product and to relate these differences to the precipitation environments. This work acts as a preliminary study in that it verifies the mixing environment to be an important parameter during precipitation. It also demonstrates the difficulties in interpreting results using the complicated soy protein, and motivates the transition to the egg white system.

Section II presents experimental results characterizing the continuous fractionation of lysozyme from egg white by polyelectrolyte precipitation. Here, the objectives are to identify the effects of shear and residence time, to test these trends statistically, and to interpret these trends in light of the possible phenomena at play during the precipitation. Because this work represents the first such study of protein precipitation using

high molecular-weight polyelectrolytes, any unique or unexpected results with regard to the mixing environment are of special interest. A tangential objective is to survey the efficacy of polyacrylic acid precipitation of proteins by assessing the yield and enrichment of active lysozyme and by studying the recovery of the enzyme from the solid-phase complex.

In Section III, the data from Section II are used to test the applicability of a population-balance model. This model has been previously applied to precipitations using small-molecule precipitants. One objective is to identify, through the model, any phenomena unique to the polyelectrolyte. Another objective is to derive and incorporate the types of terms needed in the model to reflect these unique phenomena, and to test the altered model against the data.

Explanation of Dissertation Format

The three parts contained in this dissertation are written in a form suitable for publication in a technical journal. This general introduction is intended to orient the reader and provide additional background and literature review. References cited in this section are given at the end of the dissertation. I have provided a more thorough literature review elsewhere (48). Except for work attributed to others in the acknowledgements, the research presented in the three parts represents original work that I have conducted.

SECTION I. EFFECTS OF MIXING DURING ACID ADDITION ON FRACTIONALLY PRECIPITATED PROTEIN

ABSTRACT

Isoelectric fractionation of the two major proteins of soy is characterized. Fractions are acid precipitated and centrifugally collected at pH 6.0 (glycinin) and pH 4.8 (β-conglycinin). Two extremes in the speed of acid addition (rapid, with no mixing, and slow, via acid dialysis, with complete mixing) are compared to determine their effects on the properties of the precipitate. Total protein yield, fraction composition, and aggregate microstructure do not depend significantly on the method of acid addition. Particle size distribution and hindered settling behavior do differ and are explained using a model of aggregate strength. The rapid acid addition produces larger primary particles, because of higher supersaturation, and yields larger aggregates, because of higher inter-particle potential and stronger aggregates. Further aggregation in low-shear hindered settling is faster for the slowly precipitated aggregate because few of these bonding sites could survive the high-shear precipitator, whereas more can contribute to aggregation during hindered settling.

NOMENCLATURE

d_1 primary particle size (L)

d50 diameter at which 50% of the total aggregate volume is in larger particles (L)

d90 diameter at which 90% of the total aggregate volume is in larger particles (L)

F attractive force per contact (mL/t^2)

g gravitational force (mL/t^2)

n_c number of interparticle bonds per area (L^{-2})

Q interaction potential function (m/t^2)

Greek

μ ionic strength (M)

ϕ particle solid fraction

τ tensile stress ($mL^{-1}t^{-2}$)

INTRODUCTION

The recovery of proteins by large-scale processes is becoming more important as fermentation and genetic engineering technologies increase in application and volume. Precipitation followed by filtration, centrifugation, or gravity settling is one such process that has been used for many years and through which crude fractionation of the different proteins is possible. Precipitation also permits more discriminating large-scale fractionation to be done. Bell and co-workers (1) list a number of techniques for fractional precipitation: salting out, isoelectric and solvent precipitation, phase separation with such polymers as PEG, flocculation with polyelectrolytes, and precipitation with multivalent cations. The prediction and control of events during any protein precipitation process require an understanding of the parameters that affect the process.

Some investigators have been concerned with whether it is important in isoelectric precipitation to control mixing during the addition of acid to the protein solution. Local extremes in pH can cause irreversible denaturation of the proteins (1), which will alter the precipitation behavior. Hoare (2) has reported that the precipitate properties differ with extremes in operating conditions. One extreme exploited in inorganic precipitations is homogeneous precipitation, as reported by Berg (3), which involves the homogeneous production of the precipitant, usually by a controlled chemical reaction, within the solution. Advantages of this technique include the production of denser precipitate and reduced co-precipitation, evident when thorium is homogeneously precipitated as the

iodate. Homogeneous precipitation has been used by Gorden and co-workers (4) for fractional precipitation of rare earths, wherein they report greater reproducibility of conditions. Another method of controlled release of precipitant was performed by McMeekin (5) in the separation of serum albumin by salting out with ammonium sulfate. He suspended a rotating cellophane bag filled with the precipitant in the solution, effecting a gradual release--usually 48 h duration--and producing a granular, relatively pure, easily separated protein isolate. Michaels (6) has discussed using ultrafiltration membranes in the same way. Blood plasma fractionation is another process where the importance of mixing is clearly noted (7).

This dependency on the method of precipitation suggests that the rate of acid addition--or equivalently, the level of mixing during acid addition--in the fractional precipitation of soy proteins will affect composition, structure, or both. Salt et al. (8) have shown that the level of mixing has differing effects on the protein structure, depending on the type of precipitating acid used. Nelson and Glatz (9) initiated an investigation of the soy protein system to determine if fractionation occurs at the primary particle level; their results suggest that the soy system is suited to a fractional precipitation study of acid addition.

The major storage protein fractions in the soybean seed are glycinin and β-conglycinin. Glycinin, represented in the 11S fraction by ultracentrifugal analysis, constitutes ca. 50% of the total protein in the whole seed, and β-conglycinin, in the 7S fraction, constitutes ca. 18% (10). Glycinin exists in its native form as a dodecamer of associated subunits

for a total molecular weight of approximately 3.2×10^5 D, and β-conglycinin exists as a trimer of ca. 1.5×10^5 D. The remaining components are 2S and other proteins (11), fat, carbohydrates, fiber, ash, and water, with trace amounts of phytates within the protein storage units (12). Many of these compounds are believed to have an effect on protein behavior in solution (13).

Previous work on the fractionation of these soy proteins has been done by Okubo and Shibasaki (14) (by column chromatography), Hasagawa and co-workers (15) (by gel filtration), Wolf and Sly (16) (by cryoprecipitation of the 11S fraction), Roberts and Briggs (17) (by salting out of the 7S fraction), and Eldridge and Wolf (18). Thanh and Shibasaki (19) have outlined a procedure for the isoelectric fractional precipitation of 11S and 7S protein fractions in a Tris-buffered system to control ionic strength. Starting with an artificial system--a mixture of isolated 11S and 7S--they have investigated the effects of pH, Tris concentration, protein concentration, and ionic strength on the fractionation. Their characterization included ultracentrifugal analysis but no measurement of the properties important to subsequent isolation of the precipitate from the whey.

In this work, we contrast the effects of slow and rapid acid addition and characterize the system properties important to separation: composition, microstructure, particle size distribution, and hindered settling behavior.

EXPERIMENTAL

Extraction

Soy protein was extracted from defatted soy flakes (Nutrisoy 7B high protein-solubility flakes, Archer Daniels Midland Co., Inc., Decatur, Illinois) in a 1:10 dilution with water held at pH 7.6 for 30 m by the dropwise addition of 2.5 M NaOH. The resultant slurry was strained and centrifuged at 14.7 x 10^3 g (10^4 rpm, Du Pont Sorvall RC-5 Superspeed Centrifuge) at 18-25°C for 25 min; the supernatant, with a total protein concentration of ca. 35 mg/mL, was stored overnight with no observable change in protein concentration.

Selection of Optimum pH for Fractionation

To determine the pH at which to best fractionate the glycinin (11S) and β-conglycinin (7S), a serial precipitation of diluted soy extract (12 mg/mL) was performed. Aliquots of fractions at the pH values 6.6, 6.4, 6.2, 6.1, 6.0, and 5.8 were characterized by SDS-PAGE on a 10-15% gel, and total protein was measured by the biuret method standardized against bovine serum albumin (20). The PAGE gel of this fractionation is shown in Figure 1. We obtained reasonably pure glycinin at pH 6.0; considering that a dramatic cutoff point does not exist between glycinin and β-conglycinin, this pH was used in the remaining experiments for the first fraction. This result differs from that of Thanh and Shibasaki (19), who recommend pH 6.4, but whose system was more dilute, at different ionic strength, and devoid of phytate (suspected of affecting protein solubility (21)), and which consisted of a mixture of 7S and 11S isolates.

Figure 1. SDS-PAGE gel (10-15% acrylamide gradient, stained with coomassie blue) of supernatant after serial precipitation to determine the optimum pH for fractionation of glycincin and β-conglycincin. Shown are aliquots at specified pH values; the major bands are identified

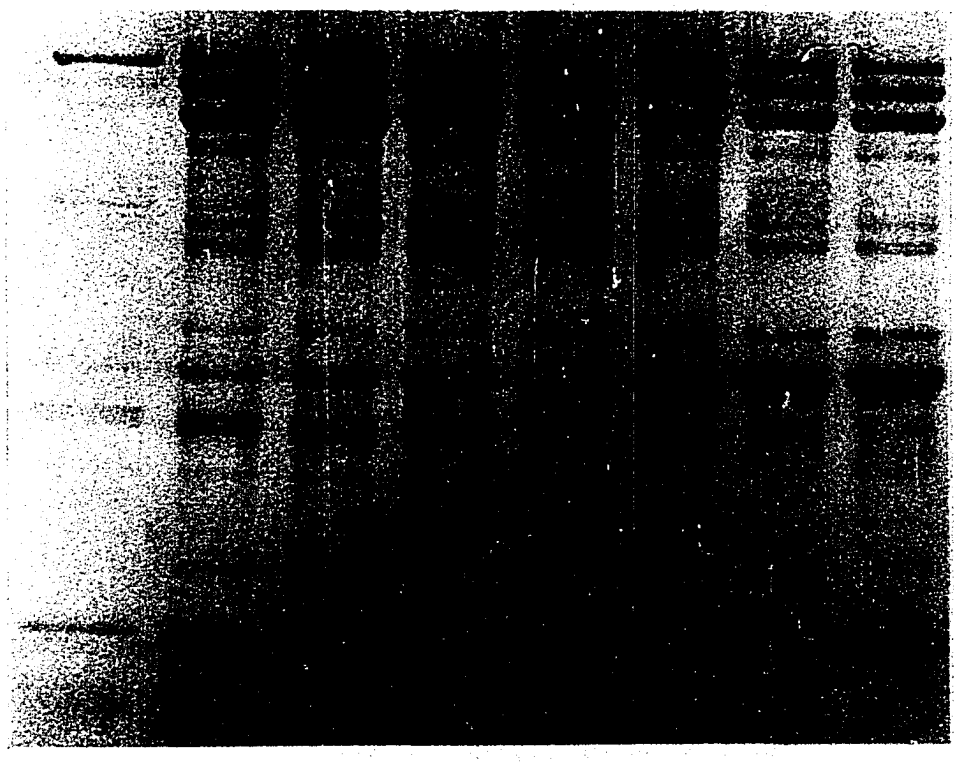
β-CONGLYCININ
GLYCININ
(ACIDIC SUBUNITS)
GLYCININ
(BASIC SUBUNITS)
pH 4.8 5.8 6.0 6.1 6.2 6.4 6.6 7.6
(EXTRACT)

Fractional Precipitation with Acid

The precipitations, for both slow and rapid acid addition, began with 525 mL of the soy extract at 9.0 mg/mL in a 600-mL beaker. A dialysis bag (dialyzer tubing, 12 kD cutoff, tied at each end) filled with 50 mL of 0.1 M HCl and mounted on a rotating shaft allowed the gradual release of acid in the slow case. In the rapid case, a similar bag was used filled with water so that the mixing environments would be identical. For both rapid and slow addition, the bag was positioned just above a 4-cm magnetic stirring bar. Stirring bar speeds, dialysis rotation rates, and mixing times were equal for each case, the first two chosen to give thorough mixing with rotation in opposite directions.

Slow acid addition

Once mixing was established with the stirring bar, the dialysis bag, filled with 50 mL of 0.1 M HCl, was lowered into the extract. At pH 6.0 ± 0.03 (after ca. 11 min) the bag was lifted, and stirring with the bar continued. At 15.0 min, aliquots were taken for the analyses described below. The remainder of the slurry was centrifuged at 14.7×10^3 g for 25 min. The supernatant was returned to the precipitation beaker and the precipitation was continued to pH 4.8 ± 0.03, with mixing being allowed to continue for 33.0 min. Aliquot sampling was repeated.

Rapid acid addition

A titration of a sample of the 9.0 mg/mL extract was performed to determine the volume of 0.1 M HCl required to lower the pH to 6.0 ± 0.03. This volume was dumped quickly into the beaker of stagnant extract, with

no mixing for 1.0 min; then the dialysis bag, filled with 50 mL water, was lowered, and mixing was implemented as before for 15.0 min. Similar steps were taken to titrate the pH 6.0 supernatant to pH 4.8 ± 0.03. Added ionic strength values were ca. 4.7 mM at pH 6.0 and 8.3 mM at pH 4.8; ionic strength was estimated by the added ions of NaCl and NaOH only, while the contributions of protein charges or other flake compounds to ionic strength were not included. Aliquots for analysis were taken at each cutoff.

Analyses

Coulter counter measurements

Two replicate 1:101 dilutions of the slurry (drawn with a widened pipette tip to avoid shear breakup) were made immediately at the completion of each pH cutoff. The pH 6.0 samples were diluted with Tris-Maleate buffer (pH 6.0, μ = 0.20 M), and the pH 4.8 fractions were diluted with NaAc buffer (pH 4.8, μ = 0.095 M). All buffers used for particle size determination were filtered twice through a sandwich filter of 0.45 and 0.2 µm (Sartorius Sartobran capsule). A model T_{AII} Coulter counter with a 70-µm aperture and calibrated with a latex standard was used to obtain duplicate particle size distributions and total particle volumes.

Scanning electron microscopy

A 1:31 dilution of the slurry was made with 1% gluteraldehyde, mixed gently, and was allowed to fix for at least 15 min (22). Approximately 0.1 mL of this dilution was coated onto a freshly sanded aluminum stub, air dried, and stored in a desiccator. Samples were sputter-coated with

Au for 2.0 min and viewed at 15 keV on a JEOL model JSM-U3 scanning electron microscope.

Hindered settling

An adaptation of Michaels and Bolger's (23) hindered settling method was used to gain insight into the characteristics of the precipitated aggregate. A 50-mL aliquot of the pH 6.0 or 100-mL aliquot of the pH 4.8 slurry was immediately and gently poured into a 50- or 100-mL graduated cylinder. The positions of the slurry-supernatant interface were measured with time and reported as percent of original height. When the precipitate-supernatant interface fell to ca. 15% of the original height, the absorbance of the supernatant at 588 nm (the wavelength where the dissolved protein has least absorbance) was determined. Tests were run at room temperature (22°C).

Protein yield and composition

Aliquots (10.0 mL) of each fraction were centrifuged at 14.7×10^3 g, 18-25°C, for 25 min. The supernatant of each, as well as 10.0-mL aliquots of the slurry, were diluted 1:2 with double-strength phosphate buffer. The precipitate of the centrifuged sample was redissolved in 10.0 mL of single-strength phosphate buffer (pH 7.6, μ = 0.5 M (24), without 2-mercaptoethanol). These buffered samples were stored at 4°C and characterized by biuret analysis, SDS-PAGE (24, 25), and rocket gel immunoelectrophoresis (10).

Time would not allow all of the analytical procedures to be performed during any one experiment; therefore, the experiment was replicated four

times, with three of the total six analyses being performed on each. Overlapping analyses gave results showing variation between replicates to be within the experimental error of the analyses.

RESULTS AND DISCUSSION

Protein Yield and Composition

Table 1 contrasts the products of the two extremes of acid addition--rapid vs. slow--at pH cutoffs of 6.0 and 4.8. The rapid-slow differences have been assigned confidence values based on standard t-tests. Rapid acid addition resulted in more protein being precipitated at pH 6.0 but less at pH 4.8 so that, overall, the final yields are not significantly different.

The compositions of the fractions (Table 1) indicate that separation of the glycinin and β-conglycinin does occur, with substantial enrichment of the glycinin phase in the pH 6.0 fraction. The immunologically identified glycinin and β-conglycinin make up a relatively small fraction of the total protein (27 and 17%, respectively); in the native soybean seed, these two proteins make up ca. 50 and 30% of the total protein, respectively, although genetic and environmental variations exist (10). After storage for one to three days in single strength phosphate buffer at 4°C, ca. 75-90% of the precipitate redissolved (assay by biuret) with no significant variation due to method of mixing. This solubility would account for some but not all of the low content of glycinin and β-conglycinin in the final protein.

An explanation for these low fraction yields is that glycinin or β-conglycinin which has been altered during preparation of the soy flake will not be identified by rocket immunoelectrophoresis; however, this material will still appear in the biuret and SDS-PAGE assays, resulting in lower apparent contributions of the fractions to the total protein.

Table 1. Protein yield and composition (mg/mL) of the fractions

Fraction	Total protein[a]		Difference[b]
	Rapid	Slow	
Extract	9.00	9.00	--
pH 6.0 precipitate	3.77	3.55	<50
pH 6.0 supernatant	4.65	5.34	>99
pH 4.8 precipitate	2.79	3.4	97
pH 4.8 supernatant	1.69	1.77	89
Final yield[e] (%)	72.9	77.2	<20

[a]This was determined by biuret, as the mean of three replicate experiments.

[b]This is the percent significance of difference between rapid and slow precipitation, by t-test.

[c]Measurements were made by rocket immunoelectrophoresis based on one experiment with three replications on measurement, concentrations normalized to 9.00 mg/mL extract.

[d]The standard deviation was equal to zero.

[e]This is the percent total protein recovered as precipitate.

Glycinin[c]		Difference[b]	β-Conglycinin		Difference[b]
Rapid	Slow		Rapid	Slow	
2.48	2.48	--	1.50	1.50	--
1.86	1.87	50	0.149	0.147	<20
0.216	0.204	35	1.44	1.28	--[d]
0.278	0.275	30	0.766	0.742	35
0.	0.	--	0.	0.	--
		--			

When we assume that any fractionation of components in the immunologically unidentified fraction is no better than that for the identified components, Table 1 shows that no differences in the fractionation of glycinin or β-conglycinin can be attributed to the mixing during acid addition. These results are supported qualitatively by the SDS-PAGE gels (Figure 2).

Physical Properties

Microstructure

The aggregates precipitated at pH 6.0 and 4.8 differ dramatically, as can be seen from their photomicrographs (Figure 3). The pH 6.0 protein forms a very loose, weak aggregate that flattens under its own weight when not suspended in liquid. The mean diameters of the primary particles making up the aggregates, as estimated from the photomicrographs and corrected for the sputter coating thickness, are ca. 0.2 μm for both rapid and slow acid addition (Table 2). There is no significant size difference between the rapid and slow pH 6.0 aggregates. The pH 4.8 aggregates, however, do show dependence on the mixing during acid addition, with the rapid addition producing a significantly larger primary particle. The pH 4.8 aggregates appear similar to total soy protein precipitate (i.e., those where the extract is adjusted directly to pH 4.8) and were quite durable to shear forces. Nelson and Glatz (9) found no effect of precipitation pH--varying from 4.3 to 4.9--on primary particle size, but recognized that in their case the pH was lowered slowly enough (acid addition required ca. 1 min) to allow the protein to precipitate over the pH range from that of the extract to the final pH.

Figure 2. SDS-PAGE gel (10-15% acrylamide gradient, stained with coomassie blue) of collected fractions: wells 1 and 2, hindered settling supernatant of pH 4.8 slurry for slow and rapid precipitation, respectively; well 3, initital protein extract; wells 4 and 5, supernatant at pH 6.0, rapid and slow; wells 6 and 7, supernatant at pH 4.8, rapid and slow; wells 8 and 9, precipitate at pH 6.0, rapid and slow; wells 10 and 11, precipitate at pH 4.8, rapid and slow; wells 12 and 13, aggregate slurry at pH 6.0, rapid and slow; wells 14 and 15, aggregate slurry at pH 4.8, rapid and slow. The major bands are identified

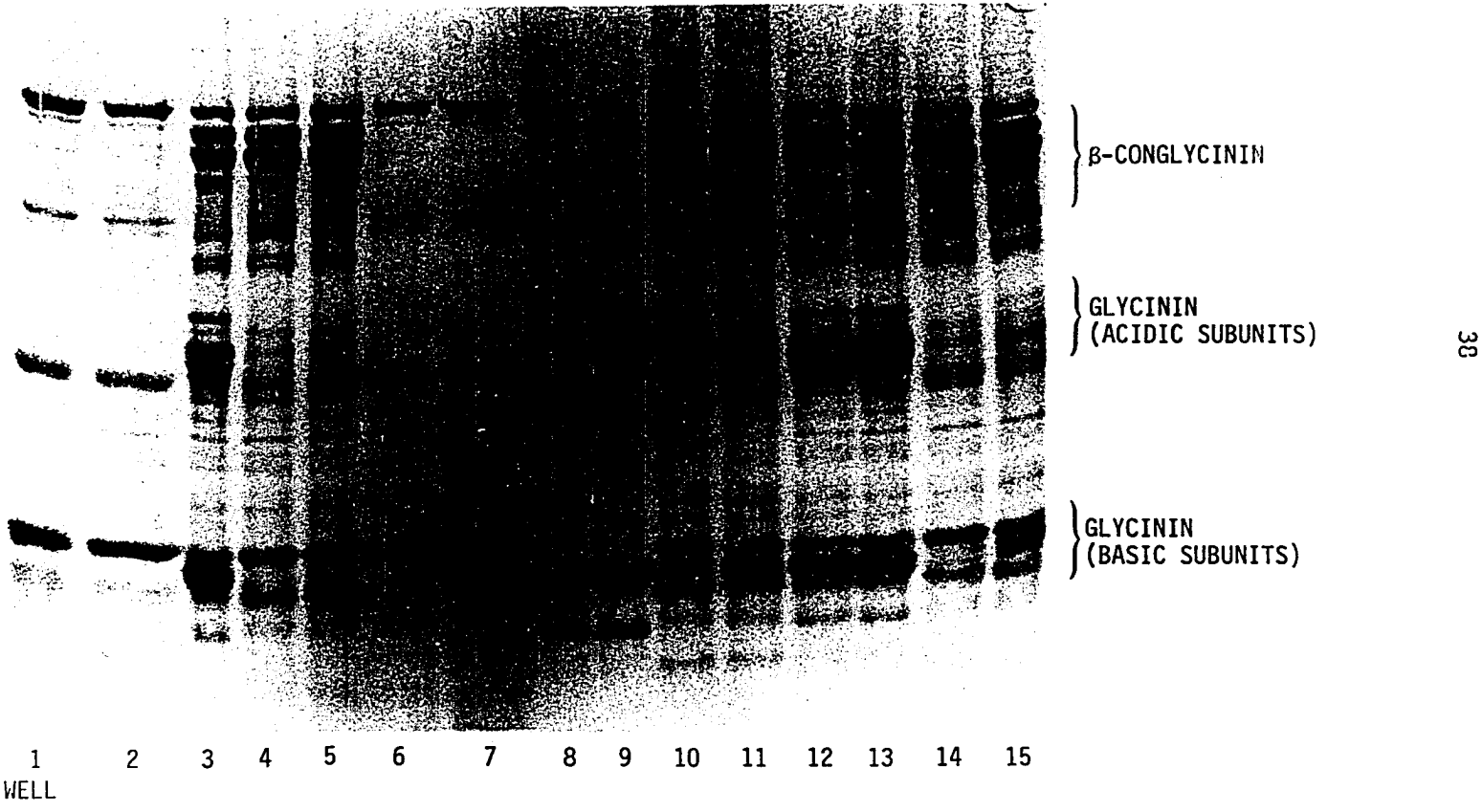
β-CONGLYCININ
GLYCININ
(ACIDIC SUBUNITS)
GLYCININ
(BASIC SUBUNITS)
1 2 3 4 5 6 7 8 9 10 11 12 13 14 15
WELL

Figure 3. Scanning electron photomicrographs of aggregates: (A) rapid precipitation at pH 6.0, (B) rapid precipitation at pH 4.8, (C) slow precipitation at pH 6.0, (D) slow precipitation at pH 4.8

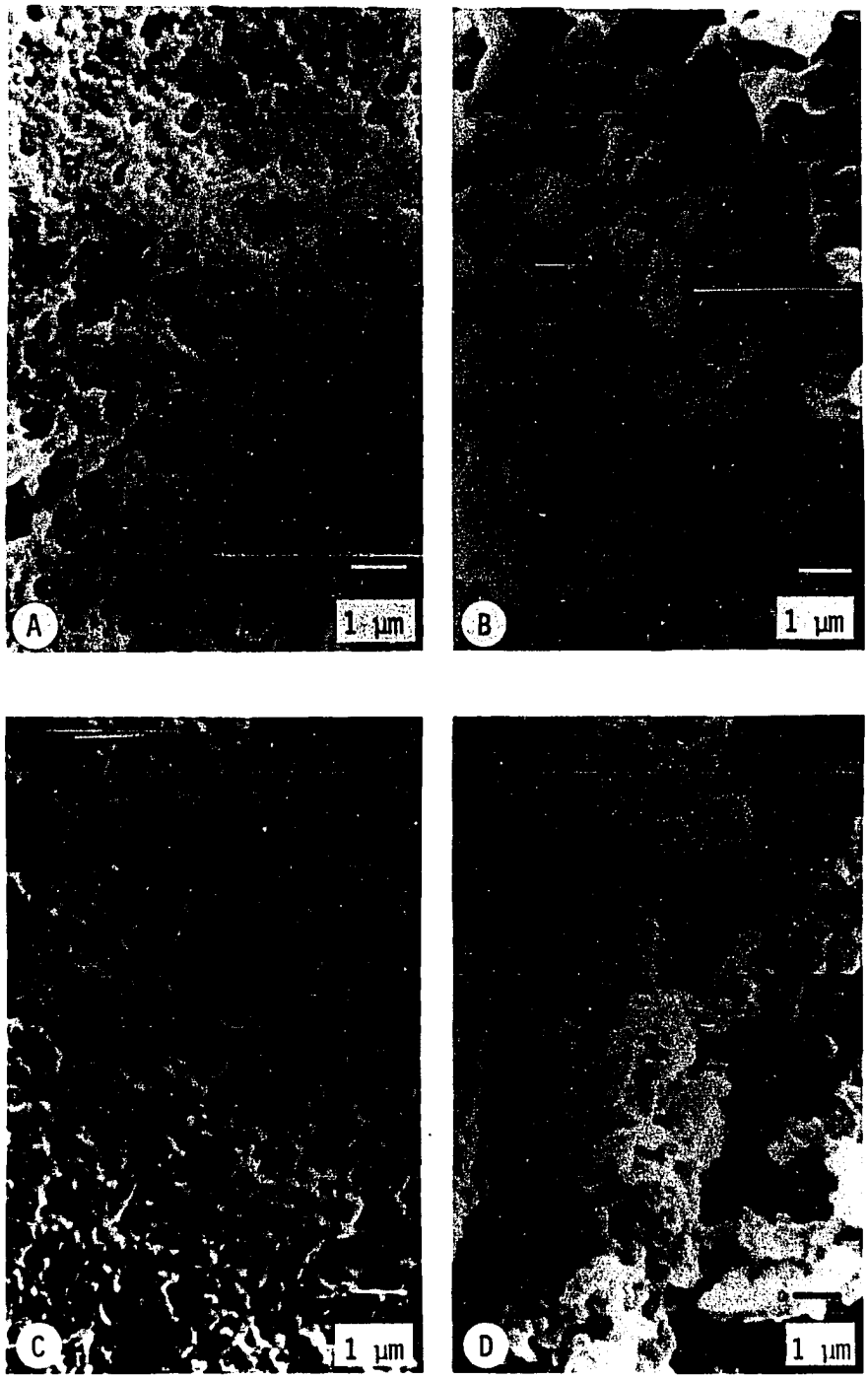
A
1 µm
B
1 µm
C
1 µm
D
1 µm

Table 2. Properties of the pH 4.8 precipitate. The pH 6.0 rapid and slow precipitates had d_1 values of 0.13 and 0.19 μm, respectively, which are not significantly different

Property	Rapid precipitation	Slow precipitation	Difference significance[a] (%)
d_1 (μm)	0.51	0.36	98
d90 (μm)	6.79	6.02	>99
d50 (μm)	11.31	7.88	>99
Aggregate density[b] (kg/m^3)	1143	1122	--
ϕ	0.48	0.41	--

[a]Percent significance of difference between rapid and slow precipitation was found by the t-test.

[b]The densities are calculated assuming that the protein density is 1296 kg/m^3, the whey density is 1007 kg/m^3 as measured, and the Coulter counter measures 80% of the total aggregate volume (ref. 25).

In our experiment, the mixing differences during acid addition are thought to affect the primary particle in the following way: during slow precipitation, the fraction of protein in solution that is inherently insoluble is small at any given time, but during rapid precipitation, the abrupt change in pH brings a much larger fraction of protein to insolubility. This higher supersaturation, as Nelson and Glatz (9) found, produces the conditions that lead to larger primary particles.

Particle size distribution

The particle size distributions for the pH 4.8 fractions are shown in Figure 4. (The pH 6.0 aggregates were too small and/or may have been too weak to withstand the shear forces of normal handling or Coulter counter sampling to be characterized usefully with the 70-μm aperture.) Table 2 lists the d90 and d50 aggregate densities--as calculated from corrected Coulter size distribution volumes and precipitate concentrations (26)--for the pH 4.8 fractions. The calculated densities compare well with those of Bell et al. (26), who report the density of soy aggregate from Coulter counter data to equal 1156 kg/m^3. The density of the pH 6.0 aggregates was estimated to be near that of the whey since they did not settle. Repetition of the precipitation experiments and particle size measurements revealed that the distributions are reproducible; thus, the differences in d90 and d50 between rapid and slow acid addition are significant. Similarly, for ethanol precipitation of soy protein in a tubular reactor, Chan and co-workers (27) found that mixing conditions affect the aggregate size; however, in their case, poorer mixing gave smaller aggregates.

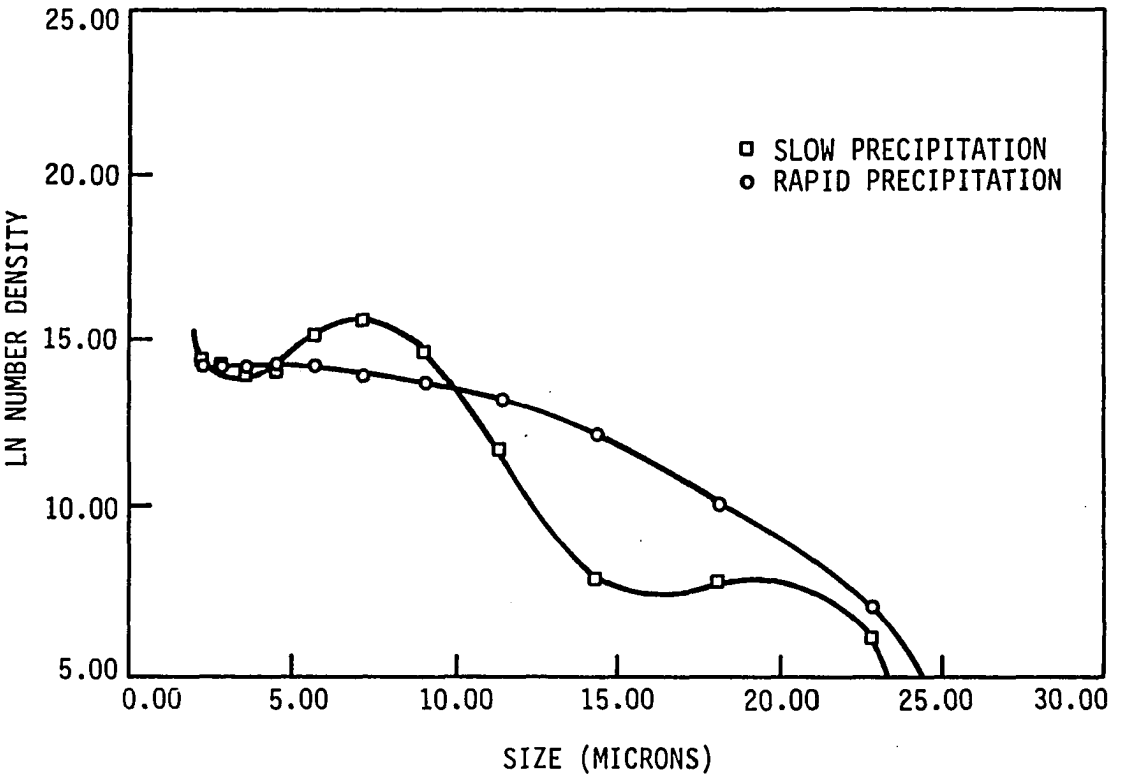

Figure 4. Particle size distributions for the protein precipitates aggregated at pH 4.8. The lines show the polynomial fits used in calculation of total volumes

The particle size distributions clearly show that the slowly prepared aggregate has undergone breakup of the larger particles into the 8-μm range. The upturn of the curve at the small end is indicative of the greater concentration of fines and the higher turbidity of the whey after settling, shown later in the hindered settling data. Thus, it appears that the aggregation of smaller primary particles gives a weaker aggregate. In contrast, Smith and Kitchener (28) found that, for a constant interparticle potential function, mean aggregate size increases as primary particle size decreases.

The floc model developed by Firth and Hunter (29) holds that aggregate strength, τ, is the product of the number of bonds per area, n_c, and the force per bond, F:

$$\tau = n_c F \tag{1}$$

In this equation, $n_c = \phi/d_1^2$ and $F = d_1 Q$, where ϕ is the solid fraction in the particle; Q is the interaction potential available for interactions between primary particles; and d_1 is the primary particle size. It is then evident that

$$\tau = \phi Q/d_1 \tag{2}$$

Considering that the particle size distributions for the pH 4.8 fractions show the rapidly formed precipitate to be stronger and to have a higher τ, and using the experimentally derived values for ϕ and d_1, we conclude that $Q_{rapid} > 1.2Q_{slow}$ (i.e., that the attractive potential is greater for the rapid precipitate).

Such surface potential differences between rapid and slow precipitation could occur as a result of different orientations of the proteins within the primary particles. During slow acid addition, the aggregating proteins are able to arrange so as to minimize the potential within the particle, thereby reducing the potential available for surface-surface interactions between primary particles. In contrast, the rapid addition of acid reduces the opportunity for intraparticle orientation, leaving more of the bonding potential of the proteins to exist at the primary particle surface. In this way, the potential between surfaces of primary particles is a function of how the material is incorporated into the surface.

Hindered settling

The result of the hindered settling tests on the pH 6.0 and 4.8 aggregates are shown in Figure 5. The pH 6.0 suspension is quite stable, with no change in the slurry after 3 h; the slurry remains milky with no apparent aggregation occurring in the stagnant tube. The pH 4.8 aggregate prepared by slow acid addition clearly settles faster than that by rapid acid addition, in agreement with McMeekin's (5) result, yet it has a more turbid whey. Since aggregate density, as measured prior to settling, cannot account for the different settling rates, another reason must be sought.

Hoare (30) found experimentally that flocculation occurs in the hindered settling tube, leading to conditions suitable for settling. Thus, the controlling characteristic of the settling becomes the aggregate's ability to aggregate further and become large enough to settle.

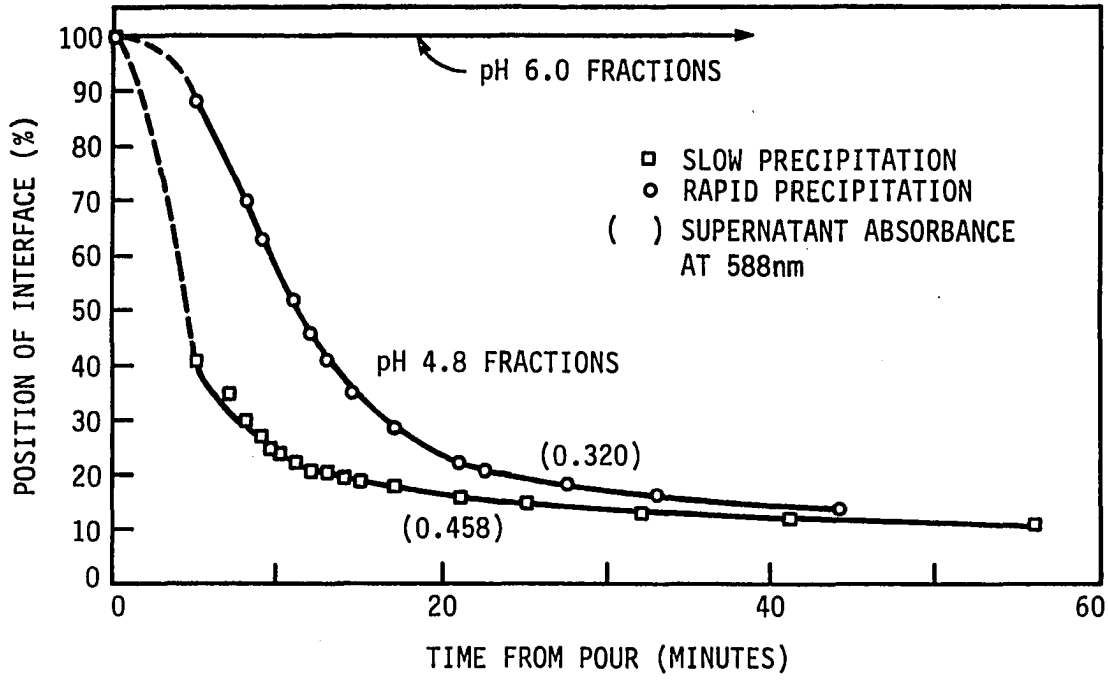

Figure 5. Hindered settling profiles of the fractions

The aggregating properties of the precipitate are expected to be dependent on the history of preparation (30); in this work, the size and primary-particle makeup of the precipitates do differ between rapid and slow precipitation. Furthermore, increases in properties such as aggregate elasticity (31) or porosity (32) would increase the aggregate's ability to grow in hindered settling; the aggregate prepared by slow addition of acid does have a lower volume fraction of solids (higher porosity), is a weaker aggregate under shear, and may therefore be expected to be more deformable. Also, a larger number of fines in the slow precipitation case may be responsible for the higher growth rates during settling (2). Another possible explanation is that since the aggregates in rapid acid addition have a longer mean residence time in the shear environment, they may be described by that part of the curve defined by Hoare (2) where hindered settling growth rate increases as aging time increases.

In explaining the hindered settling behavior, a consideration of the potential function is again helpful. As described earlier, the interparticle potential for aggregation is greater for the product of rapid precipitation. Because of this, a larger fraction of interparticle bonds can survive the high-shear environment of the precipitator. Furthermore, these particles have a longer mean residence time in the shear, allowing for more rearrangement of particles to maximize use of available aggregation potential. These two effects--more surviving bonds and aging to saturate available bonding sites--produce a larger aggregate and cause a lower number of available sites to exist on the aggregate when the slurry is transferred to the low shear hindered settling tube. Conversely, for

slow precipitation, a larger fraction of sites are not able to bond in the high shear precipitator and are thus available in hindered settling, where they are effective in inducing faster aggregation and settling. In effect, because the aggregate produced by slow precipitation is weaker, it will predominantly aggregate in the low-shear, hindered settling conditions.

CONCLUSIONS

Isoelectric precipitation of soy proteins can give substantially enriched protein fractions. Two extremes in the speed of acid addition--or alternatively, of mixing during acid addition--do not show differences in fraction composition, microstructure, or overall protein yield. However, other properties are affected. Rapid acid addition gives primary particles that are larger and a particle size distribution showing a larger, stronger aggregate. Hindered settling of the aggregate produced by rapid acid addition occurs more slowly than that of the slowly precipitated protein.

These findings are consistent with previous floc models where the potential term of the attractive force is used to account for the differences in aggregate behavior. The supersaturation during precipitation influences the sizes of the primary particles; high supersaturation produced by rapid acid addition gives a larger primary particle. Rapid precipitation also reduces the opportunity for arrangement of the proteins to a favorably low potential, resulting in a higher surface potential on the primary particle. These potentials affect the aggregate strength so that the rapid precipitation produces a stronger, larger aggregate having a greater fraction of its bonding sites attached in the precipitator. Finally, in hindered settling, the attractive potential of the precipitates produces further aggregation and settling; the aggregates from slow precipitation have a greater fraction of available bonding sites still unmatched that do bond in the low-shear environment, leading to faster hindered settling.

These results indicate that the particle size distribution is not sufficient in itself as an indicator of the aggregate's ability to settle from solution.

To capitalize on the advantages of controlled acid addition on a larger scale, a different reactor design than used here would be required. For example, incremental addition of the precipitant via static mixers in a recycle loop (33) would accomplish such an objective.

ACKNOWLEDGEMENTS

This work was supported by a grant from the National Science Foundation (CPE-8120568), whose support is gratefully acknowledged. The authors would also like to thank Adoracion Resurreccion, who performed work with immunoelectrophoresis and gave valuable assistance with PAGE.

REFERENCES

1. D. J. Bell, M. Hoare, and P. Dunnill, Adv. Biochem. Eng. Biotechnol., 26, 1 (1983).

2. M. Hoare, Trans. Inst. Chem. Eng., 60, 79 (1982).

3. E. W. Berg, Physical and chemical methods of separation (McGraw-Hill, New York, 1963).

4. L. Gorden, M. L. Salutsky, and H. H. Willard, Precipitation from homogeneous solutions (Wiley, New York, 1959).

5. T. L. McMeekin, J. Am. Chem. Soc., 61, 2284 (1939).

6. A. S. Michaels, "Innovations in separations: Key to success in adapting modern biology to industrial practice," Second Engineering Foundation Conference on Recovery of Fermentation Products, Sea Island, GA, January 29 - February 3, 1984.

7. F. Rothstein, "Technological problems in large-scale plasma fractionation," in Proceedings of the International Workshop on Technology for Protein Separation and Improvement of Blood Plasma Fractionation, H. E. Sandberg, ed., U.S. Department of Health, Education, and Welfare, Publication No. (NIH) 78-1422, 1978.

8. D. J. Salt, R. B. Leslie, P. J. Lillford, and P. Dunnill, Eur. J. Appl. Microbiol. Biotechnol., 14, 144 (1982).

9. C. D. Nelson and C. E. Glatz, Biotechnol. Bioeng., 27, 1434 (1985).

10. P. A. Murphy and A. P. Resurreccion, J. Agric. Food Chem., 32, 911 (1984).

11. B. Hu and A. Esen, J. Agric. Food Chem., 29, 497 (1981).

12. J. R. Brooks and C. V. Morr, J. Agric. Food Chem., 32, 672 (1984).

13. E. Dickinson and G. Stainsby, Colloids in food (Applied Science Publishers, London, 1982).

14. K. Okubo and K. Shibasaki, Agric. Biol. Chem., 30, 939 (1966).

15. K. Hasagawa, T. Kusano, and H. Mitsuda, Agric. Biol. Chem., 27, 878 (1963).

16. W. J. Wolf and D. A. Sly, Cereal Chem., 44, 653 (1967).

17. R. C. Roberts and D. R. Briggs, Cereal Chem., 42, 71 (1965).

18. A. C. Eldridge and W. J. Wolf, Cereal Chem., 44, 645 (1967).

19. V. H. Thanh and K. Shibasaki, J. Agric. Food Chem., 24, 1117 (1976).

20. B. T. Doumas, Clin. Chem., 21, 1159 (1975).

21. A. K. Smith and J. J. Rackis, J. Am. Chem. Soc., 79, 633 (1957).

22. R. J. Carroll, M. P. Thompson, and G. C. Nutting, J. Dairy Sci., 51, 1903 (1968).

23. A. S. Michaels and J. C. Bolger, I & EC Fundam., 1, 24 (1962).

24. S. A. Hughes and P. A. Murphy, J. Agric. Food Chem., 31, 376 (1983).

25. U. K. Laemmli, Nature, 227, 680 (1970).

26. D. J. Bell, D. Heywood-Waddington, M. Hoare, and P. Dunnill, Biotechnol. Bioeng., 24, 127 (1982).

27. M. Y. Y. Chan, M. Hoare, and P. Dunnill, Biotechnol. Bioeng., 28, 387 (1986).

28. D. K. W. Smith and J. A. Kitchener, Chem. Eng. Sci., 33, 1631 (1978).

29. B. A. Firth and R. J. Hunter, J. Colloid Interface Sci., 57, 266 (1976).

30. M. Hoare, Trans. Inst. Chem. Eng., 60, 157 (1982).

31. B. Dahneke, J. Colloid Interface Sci., 40, 1 (1972).

32. P. G. Wolynes and J. A. McCammon, Macromolecules, 10, 86 (1977).

33. F. Rothstein, Bio-Separations Consultants, Long Beach, CA, personal communication, 1984.

SECTION II. POLYELECTROLYTE PRECIPITATION OF PROTEINS
I. THE EFFECTS OF REACTOR CONDITIONS

ABSTRACT

Lysozyme was recovered from egg white by continuous precipitation with polyacrylic acid (MW 4 x 10^6). Precipitator residence time and shear rate had significant effects on the size distribution of the precipitate, but no clear effects on the compositions. Precipitate mean size increased with higher shear, indicating growth phenomena predominating over breakage. Also, an enhancement of growth rate at small sizes was noted. The Camp number successfully characterized the interaction of shear rate and residence time on the particle size. Resolubilization of the precipitate and recovery of the lysozyme produced high yield.

NOMENCLATURE

C_{PAA} concentration of injected PAA (m/L^3)

D_{50} diameter at 50% by volume oversize of particle size distribution (L)

D_{90} diameter at 90% by volume oversize of particle size distribution (L)

F total flow rate into precipitator (L^3/t)

V_g mean shear rate (t^{-1})

LCF lysozyme concentration factor

n number density ($\#/L^4$)

V volume of precipitator (L^3)

Greek Letters

τ mean residence time of precipitator = V/F (t)

ζ zeta potential (mL^2/t^2)

μ ionic strength (M)

INTRODUCTION

In the biochemical process industry, product separation and purification can command a large percentage of the overall production cost. The process may demand converting a stream very dilute in final product (less than 0.5%) and contaminated with organic and inorganic materials to a stream of pure product. Precipitation is one method used for bulk recovery of solutes, and its application to the fractionation of proteins makes it a promising process for purification in biotechnology, as well as food and other industries. The potential applicability of precipitation is being expanded with the incorporation of novel precipitants and processes. However, in order to apply these modifications, the fundamental engineering information describing the basic system needs to first be assembled. The overall objective of this work is to provide information, based on mechanistic interpretation of experimental data, that will aid in the improved design and operation of reactors for the precipitation of proteins from solution.

In this study, the recovery of proteins from dilute solution by polyelectrolyte precipitation will be considered; of specific interest are the reactor conditions--shear rate and residence time--during the precipitation process and the effects that these conditions have on the physical and chemical properties of the recovered precipitate. The physical properties of interest include size distribution, strength, microstructure, and surface charge, properties which will affect solid-liquid separation as well as functional behavior of the solid phase. The chemical properties include yield and enrichment of the target protein.

Much work has been reported concerning general solubility behavior in the polyelectrolyte precipitation of proteins (1-10). When a protein solution is destabilized by the addition of polyelectrolyte, the system is expected to display phenomena found using other, smaller precipitants, such as acids or bases, divalent metal ions, or organic species. First, the protein and polymer will combine by diffusion to form primary particles. In isoelectric precipitation the final size of the primary particle, on the order of 0.1 μm, has been shown to be dependent on the mechanism of formation or nucleation (11). Next, fluid-driven particle-particle collisions lead to the formation and growth of aggregates (1, 12). In polymer precipitations, this second stage of aggregation may incorporate the long-chain polymers in three possible ways (13):

1. charge neutralization of the primary particle by an oppositely charged polyelectrolyte, where the polymer is distributed roughly evenly over the colloid surface (1);
2. the "patch" model of flocculation (14, 15), characteristic of systems where the charge density of the polymer is higher than that of the particle, resulting in oppositely charged patches on the particle surface;
3. bridging, which involves polymer attachment between two particles which would not otherwise meet readily by diffusion (16-18).

When the aggregate attains a sufficiently large size, aggregate breakage due to environmental effects (all driven by power input to the liquid (19-22)) becomes important, and has been shown for isoelectric

precipitation to be a predominant factor in determining the final aggregate size (19).

Mixing in Precipitation

The level of agitation is an influential factor in precipitation processes. Adsorption of oppositely charged polymers and proteins is a relatively fast process (14) (on the order of 0.01 second (23)); therefore, the rapid dispersion of the polymer is important for polymer-protein complex formation. Agitation also determines the shearing rate for a given system, which affects polymer rearrangement (14), desorption (24), degradation (25) and, ultimately, the particle size distribution (26) through aggregate growth and breakage.

Some workers have shown that mixing conditions are more important than the properties of the precipitant in optimizing precipitation (27), yet many neglect to consider mixing conditions. Much of the work that does consider mixing and reactor conditions reports the effect on physical properties of the precipitate. It is necessary to determine if, in fractional precipitation, the shear environment affects also the product's compositional properties.

Recent work which has emphasized mixing has been reported by Goossens and Luner (28) for the polyelectrolyte flocculation of cellulose, where agitation intensity and time were evaluated. Sylvester and Toure (25) have considered the effect of shear on the optimum polymer dosage for flocculation and on the polymer properties. Keys and Hogg (29) give careful consideration to the mixing process in a standard batch stirred tank. They attempted to quantify and understand parameters important to

the mixing of polymers and particles in suspension. Walles (18) and Keys and Hogg (29) advised incremental addition of polymer in batch operation or continuous operation to prevent high local concentrations of precipitant.

The role of agitation in stabilizing (aging) isoelectric precipitates has been studied by Hoare (30, 31), who monitored and modeled aggregate growth. Bell and Dunnill (21) also considered aging, and found an optimum in the aging parameter $V_g\tau$, originally suggested as a design parameter by Camp (32). Salt et al. (33) varied mixing conditions and acid type during isoelectric precipitation of soy proteins, and found little effect of agitation during precipitation on the solubility of H_2SO_4-precipitated protein, but they found substantial mixing differences for HCl. Petenate and Glatz (34) showed, for their system of dilute isoelectrically precipitated soy proteins, that mixing speed had a significant effect on each of the kinetic parameters used in a model of growth and breakage. Recent work in this lab (35) has shown the effects of two extremes of mixing on the properties of an isoelectrically precipitated soy protein.

Polyelectrolytes and Protein Precipitation

Polyacrylic acid (PAA), widely used as a model of normal polyelectrolyte behavior (36), was used in this work as the precipitant. PAA is a linear polymer of weakly acidic carboxylic monomers. Others (5, 37, 38), through work applying PAA to the precipitation and fractionation of proteins, have found polyelectrolytes well-suited to the large-scale recovery of industrial enzymes.

We chose to use PAA for the recovery of lysozyme from egg white. Reasons for this choice were:

-- Egg white is a naturally occurring aqueous solution of proteins, containing no lipid or other organic constituents and small levels of free carbohydrate or enzymes other than lysozyme.

-- Previous work (5) has shown that lysozyme precipitation with PAA produces sufficient yields for study.

-- Lysozyme has a high pI (10.7), allowing the effective use of anionic polyelectrolytes such as PAA in the neutral pH range.

-- Enzyme activity assays are available to indicate denaturing effects of the separation processes on the lysozyme.

In this work, precipitator residence time (τ) and mean shear rate (V_g) were varied in a 3 x 4 incomplete factorial design, in which various physical and compositional properties were monitored. This design allows the Camp number ($V_g\tau$) to be tested as a unique determinant of aging in a precipitator. The concentration of the injected polymer was varied in a limited number of runs to assess the effects of higher polymer feed viscosity and concentration on the precipitate properties.

EXPERIMENTAL

Materials

All protein solutions were buffered to prevent isoelectric precipitation through pH shifts and to hold ionic strength constant. Ionic strength was required to be of sufficiently high conductivity to operate the particle counter with reasonably low background noise. The buffer chosen was a pH 5.4 sodium acetate buffer, 0.05 M in acetate and 0.02 M in NaCl (μ = 0.07 M, with conductivity of 6.0 mmho/cm). In order to avoid any changes in ionic strength during analysis of the precipitate, it was necessary to perform the protein solubilization, precipitation, and slurry dilution using this single buffer.

Egg white was reconstituted from powder (Henningsen Type P-110, spray-dried pasteurized egg white) by gentle mixing into the buffer to give a 10 wt % solution. After 60 minutes of stirring the solution was centrifuged for 60 minutes at 15 x 10^3 g, 15°C to remove insoluble material. This supernatant was diluted to 4.0 mg/mL using the buffer. Because changes in ionic strength upon dilution cause some proteins to precipitate (the reconstituted egg white has an ionic strength of approximately 0.12 M whereas the buffer's ionic strength is 0.07 M, giving a final ionic strength after dilution of 0.073 M), two filtration steps were required to lower the particle count in the feed. The final feed concentration was verified by biuret assay after filtering. Because air contact can denature ovalbumin (39), all mixing and handling of the protein solution required gentle action.

Polyacrylic acid (powder, MW 4 x 10^6; Polysciences, Warrington, PA) was dissolved in deionized water by gentle mixing for two hours. Care was taken to prevent contact of any PAA-containing solution with untreated glass (contact surfaces were pretreated with dimethyldichlorosilane) or metal, which will adsorb PAA (14, 36).

Continuous Precipitations

A standard configuration baffled tank with a six-blade flat-pitch impeller (29) was used (Figure 1). Adjusting the height of the apex of the outlet tube allowed steady control of the tank liquid level. The tank top was open to atmosphere. The PAA was injected via small-bore tubing 3 mm below the center of the impeller.

The egg white protein and PAA solutions were prepared fresh for each run to minimize lysozyme denaturation and hydrolysis of the PAA. The protein feed was prefiltered (3 μm canister filter) into a 20 L carboy, from where it was peristaltically pumped through final filters (Pall 0.45 μm nylon) and flow meters to the precipitator. The PAA solution required no filtration; a peristaltic pump was used for the 0.1 % wt/v PAA and a syringe pump for the 1.0 % wt/v PAA. Both input flow rates were set for each experiment by volume-time measurements and continuously monitored by rotameters; flows varied (due to pump variations) no more than 3%.

To start the precipitation, the precipitator was filled with protein solution (825 mL), then the protein flow rate was stopped. The impeller speed was then set. The PAA flow was switched to the inlet tube of the reactor and allowed to flow for one residence time, at which time the

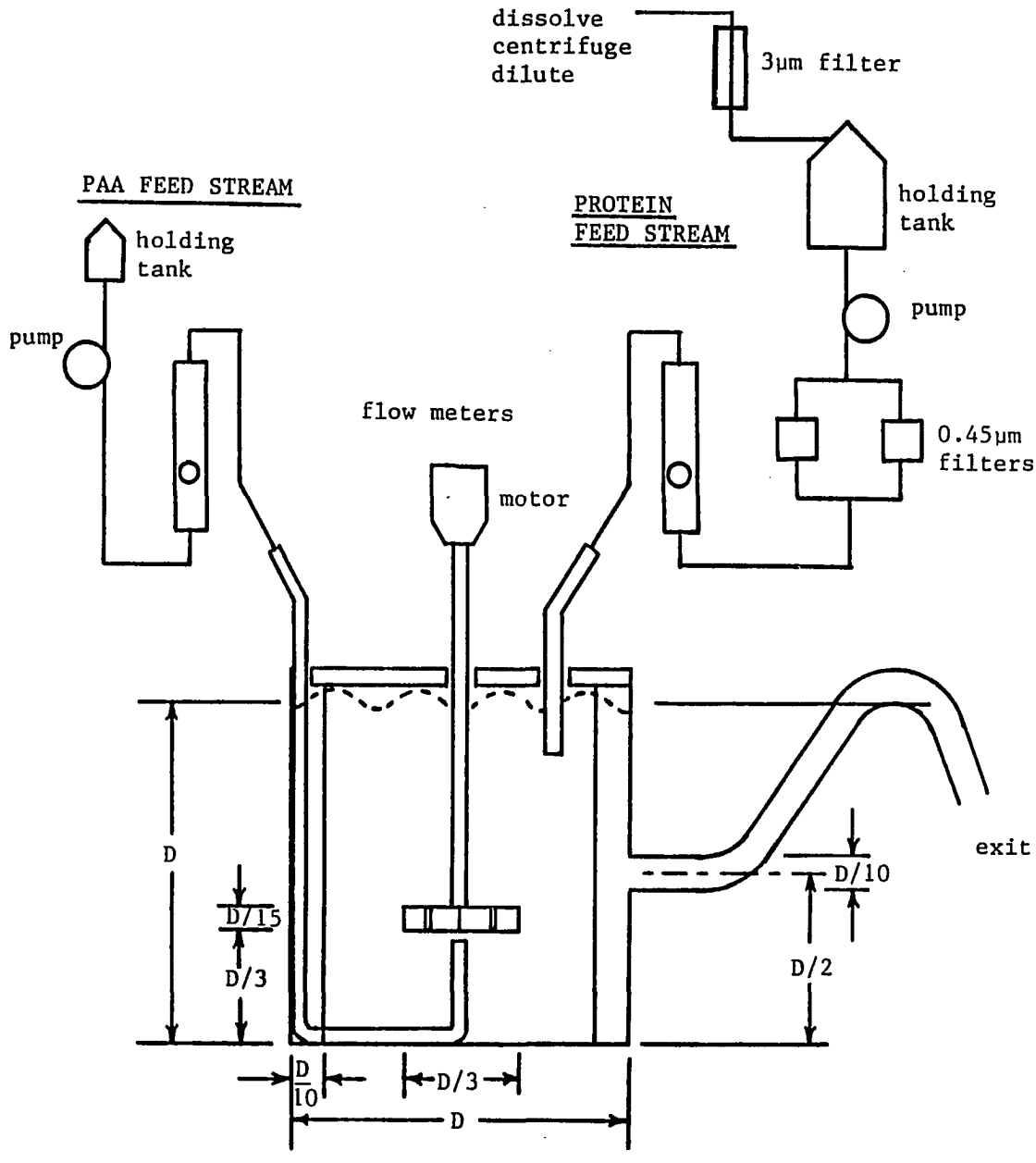

Figure 1. Schematic of process and detail of precipitator: standard baffled tank, 6-blade flat-pitch impeller, D ≡ diameter = 10.3 cm, V ≡ volume = 825 mL

protein flow was started. This method provided rapid approach to steady state while preventing locally high concentrations of PAA during startup. Steady state, as indicated by insignificant changes in PSD, was usually achieved after four residence times had elapsed; aliquots for analysis were collected after five residence times. (Often, two or more samples were withdrawn a few minutes apart to guarantee that steady state had been reached for a particular run.)

Sampling

All samples were drawn directly from the precipitator tank with a widened pipette tip to minimize aggregate breakage and nonisokinetic sampling. Sample PSDs and zeta potentials were measured within 5 minutes of being withdrawn, and biuret and lysozyme assays were completed within four hours.

Analysis

Particle size distribution

Slurry samples were suspended (dilutions from 1:400 to 1:660) in filtered pH 5.4 acetate buffer and analyzed in triplicate on a Coulter Counter model T_{AII} with population accessory (Coulter Electronics, Hialeah, FL) using a 70 μm aperture tube as calibrated with latex size standards (Polysciences polystyrene microspheres, 4.06 μm). Operation allowed counting of particles larger than 1.26 μm; results showed that less than 1% of the actual total particle volume would be smaller than 1.26 μm. Reported size distributions are means of three measurements on each sample. It was found that the size distributions in the diluted

suspensions were stable for over an hour; therefore, it is expected that this method provided accurate measurement of the actual aggregate size in the precipitator.

Zeta potential

The particles' zeta potentials, ζ, were measured via electrophoretic mobility on a Zeta-Meter 3.0 (Zeta-Meter, Inc., New York, NY). Slurry samples were diluted 1:10 in pH 5.4 acetate buffer and viewed in a Type II-UVA cell at 40 to 100 V.

SEM

To obtain photomicrographs, a small drop of the slurry was spread directly onto a freshly sanded Al stub, air dried, and desiccated. Samples were sputter coated with Au for 2.0 minutes and viewed at 25 KeV on a JOEL model JSM-U3 scanning electron microscope.

Protein

Twenty mL aliquots of slurry were centrifuged 15 x 10^3 g for 60 minutes. The supernatant of each was assayed for total protein (biuret assay (40) calibrated with BSA) and for lysozyme (Parry et al. (41), monitoring the optical clearing as lysozyme lyses the cell walls of killed Micrococcus lysodeikticus cells).

The centrifuged precipitate, after 1 to 3 days storage at 4°C, was washed by suspension in pH 5.4 acetate buffer and centrifuged again. The precipitate was stored at -20°C (for up to 4 months), then freeze dried, weighed, dissolved and diluted to 10.0 mL in phosphate buffer (pH 7.0, 0.067 M in KH_2PO_4, 0.5 M in NaCl; μ = 0.62 M) for analysis. (Phosphate

molecules have been shown to cause desorption of PAA from cationic materials (42).)

The polymer dosages varied slightly among runs, and in this range of variance the dosage is proportional to the lysozyme recovery. To adjust for dosage differences, the values of lysozyme recovery and enrichment for each run have been multiplied by the ratio of mean dosage (7.5 mg PAA/g protein) to run dosage.

Recovery of Protein from Polyelectrolyte

The eventual separation of the PAA-lysozyme complex and recovery of enriched lysozyme are obvious goals of fractional precipitation. To investigate the efficacy of polyelectrolyte precipitation, experiments were performed to assess the conditions necessary to dissolve the total precipitate, to fractionally resolubilize the lysozyme, and to remove lysozyme from the resolubilized mixture.

Precipitate resolubilization

Precipitate was prepared in the same manner as above (4 mg/mL protein, 0.1% PAA injected, 7.5 mg PAA/g protein) except in batches of 2.0 L rather than continuously, the shear rate being approximately 200 s^{-1} for 3.8 minutes. Half of the precipitate collected after centrifugation (45 min at 9.4 x 10^3 g) was resuspended in 200 mL pH 5.4 acetate buffer, recentrifuged, and then suspended in 100 mL deionized water with stirring for 60 minutes. The pH of this slurry was raised using 1.0 M NaOH; aliquots at selected pH values were centrifuged and their supernatants assayed for total protein and lysozyme activity.

Fractional resolubilization

In a second recovery method, the washed slurry was adjusted to pH 10.50 and centrifuged. The collected precipitate was suspended in 100 mL of water and adjusted to pH 11.48, centrifuged, and assayed. The aim was to extract non-lysozyme components and concentrate lysozyme in the precipitate.

Ultrafiltration

In a final experiment, half of the washed precipitate from 2.0 L of slurry was resolubilized at pH 11.48 in 200 mL water and centrifuged as above. Approximately 120 mL of the supernatant was passed through an Amicon XM100A or XM300 ultrafiltration membrane (with 10^5 and 3×10^5 Dalton cutoffs, respectively; Amicon, Danvers, MA) using 15-20 psig N_2 in a stirred UF cell (150 mm dia.). The initial solution and permeate were assayed for total protein and lysozyme.

RESULTS AND DISCUSSION

Preliminary Considerations

Dosages

Preliminary batch experiments showed that PAA dosage (from 0.63 to 4.4 mg PAA/g added protein) did not strongly affect particle size (D_{50} of 6.9 to 7.3 μm); these tests did show a relatively high enrichment (4x) and 80% recovery of lysozyme at a dosage of 2.5. However, preliminary continuous experiments demonstrated that using higher PAA dosages (up to 10 mg PAA/g added protein) gave an increased particle size (D_{50} of 9.5 μm) and lysozyme enrichment (4.5x) with 96% recovery. Using these data, a dosage of 7.5 mg PAA/g added protein was selected for all continuous precipitations. (Experimentally, dosages varied from 7.31 to 7.66.) The pH (5.40) and temperature (22°C) were held constant and not optimized.

Physical properties and operating conditions

The specific viscosity (to water) of the filtered feed protein (4 mg/mL, s.g. = 1.00) was determined by a Cannon-Fenske viscometer (ASTM (43)) to be 1.04, while that of the slurry (by a Haake RV-12 viscometer at 1200 s^{-1} shear) was 1.15. The latter value represents that found during the precipitation runs; therefore, a viscosity of 1.1 cP was used for calculations of mean shear.

The range of impeller speeds was limited by the apparatus; below 250 rpm (V_g = 123 s^{-1}) the mixing in the tank, as monitored by injected dyes, was incomplete (>5 s to macroscopic homogeneity) and above 1000 rpm (V_g = 984 s^{-1}) excessive air entrainment occurred (although one run at 1500 rpm (V_g = 1810 s^{-1}) is reported). The root-mean-square fluid velocity

gradient (44) (mean shear rate, V_g) within the precipitator was calculated from correlations for a standard tank with a 6-blade flat-pitch impeller using N_p, the power number, equal to 4.0 (45), and density and viscosity shown above.

Residence time (τ) conditions were selected so that the diagonal of the factorial design (Figure 2) would be occupied by the Camp number ($V_g\tau$) optimum, which, according to Huck and Murphy (46)--using a nonionic polyacrylamide to precipitate metal hydroxides--is 8×10^4. This design varied $V_g\tau$ from 1×10^4 to 64×10^4.

Utilizing the factorial design, an analysis of variance (ANOVA, SAS (47) General Linear Models using unbalanced data) was implemented to test the effects of V_g, τ, and the interaction of these two parameters ($V_g x\tau$) on the product properties. Table 1 summarizes these tests.

One set of runs for C_{PAA} = 1.0% at τ = 230 s was characterized and is included in the discussion and figures to follow; however, these data were not included in the ANOVA because they represent a third dimension on the factorial design which was not sufficiently complete to statistically analyze.

Properties of the Continuous Precipitations

Particle size distributions

Representative particle size distributions (PSDs), shown in Figures 3 and 4, compile the effects of V_g and τ, respectively, for representative runs. (The number density, n, is the number of particles per volume of slurry divided by the width of the size range in which the count is made.) The distributions are markedly different from those obtained using low

N (rpm)	250	500	1,000	1,500
V_g(l/s)	123	348	984	1,810
Re	4460	8920	17,800	26,800
τ (s)				
650	8.0×10^4 4b	2.3×10^5 4c	6.4×10^5 4a	
230	2.8×10^4 5b,7c	8.0×10^4 5c,7a,7d, 8a,8a	2.3×10^5 7b,8c	4.2×10^5 8d
81.6	1.0×10^4 5a	2.8×10^4 3b	8.0×10^4 3a	

C_{PAA} = 0.1%w/v

230	2.8×10^4 6b	8.0×10^4 6a,6d	2.3×10^5 6c

C_{PAA} = 1.0%w/v

Figure 2. 3x4 factorial design of experimental conditions; top cell entry is $V_g\tau$, bottom cell entries are experiments run at that condition

Table 1. Analysis of variance of selected responses[a,b] giving probabilities that variable (V_g, τ or $V_g x \tau$) does not affect the response (SAS, Type III sum of squares)

Response	V_g			τ			$V_g x \tau$		
	df	F	Pr>F	df	F	Pr>F	df	F	Pr>F
D_{50}	3	345.7	0.0001	2	159.7	0.0001	4	9.92	0.0009
D_{90}	3	315.6	0.0001	2	287.7	0.0001	4	7.49	0.0029
lysozyme recovery	3	3.07	0.1125	2	7.31	0.0246	4	0.43	0.7809
protein recovery	3	2.97	0.1191	2	7.71	0.0220	4	11.96	0.0051
lysozyme conc. factor	3	7.84	0.0169	2	10.17	0.0118	4	35.07	0.0003

[a]Compositional properties have been adjusted to account for differences in PAA dosages.

[b]Order of experiments not randomized, but residuals show no temporal trends.

molecular weight precipitants with protein (19) and suggest that rather different phenomena are prevalent in polymer precipitation.

All of the PSDs, represented in Figures 3 and 4, display two features in common. First, the distributions show more linearity in the intermediate range (4-20 μm) compared to isoelectric precipitates of protein, indicating that breakage of the aggregates is less predominant. Second, the slopes of the distributions become more level at the smaller sizes, increasingly so for lower shear rates. At small sizes where breakage can be neglected, the slope of the PSD is inversely proportional to the linear growth rate of the particles (48); thus, the PSDs show enhanced growth at the small sizes, with greater enhancement at the lower shear rates. This indicates that a mechanism in addition to the shear-driven collisions is acting to cause aggregation for the smaller particles. Further consideration of such a mechanism will be included in a subsequent paper on modeling of the PSDs (49).

Among the distributions, effects very different from those expected or shown previously are evident. Most significantly, for higher shear (Figure 3) the distributions show increased growth and larger particles. The PSDs show a depletion of particles between 3 and 12 μm and an increase in the number of particles above 12 μm. Typically, greater shear causes breakage to become predominant, giving a depletion of large particles and more smaller aggregates. In the current system, it appears that the aggregate growth, driven by particle-particle collisions, predominates over breakage with increasing shear. In addition, it may be postulated that enhanced dispersion of the polymer at higher shear rates allows for

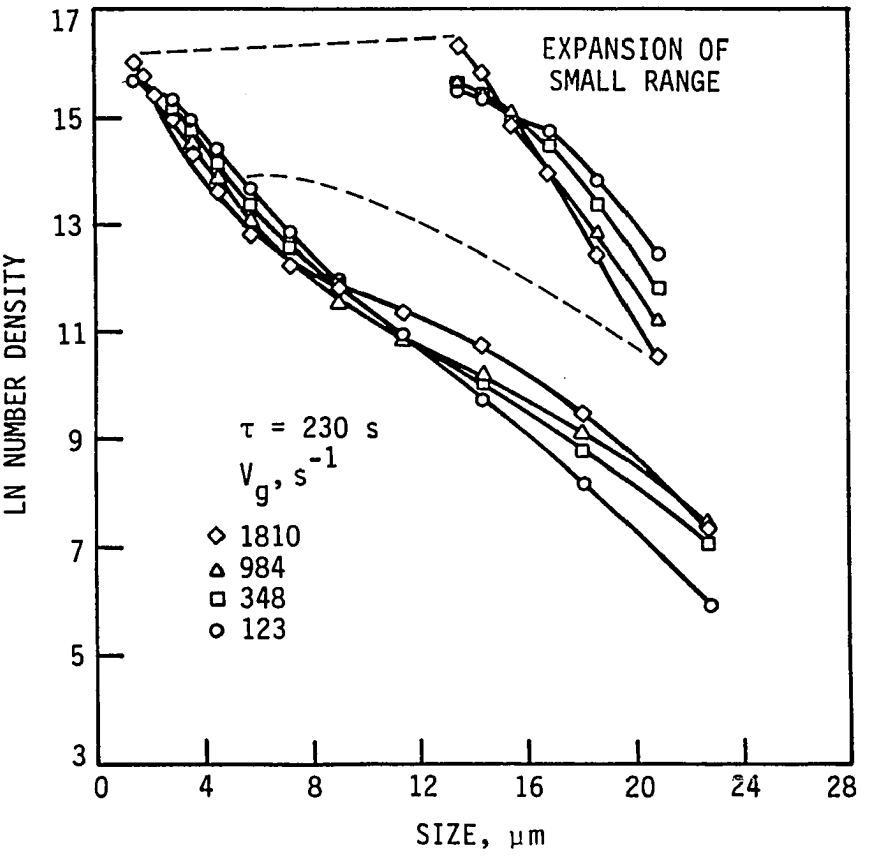

Figure 3. Size distributions for four values of V_g

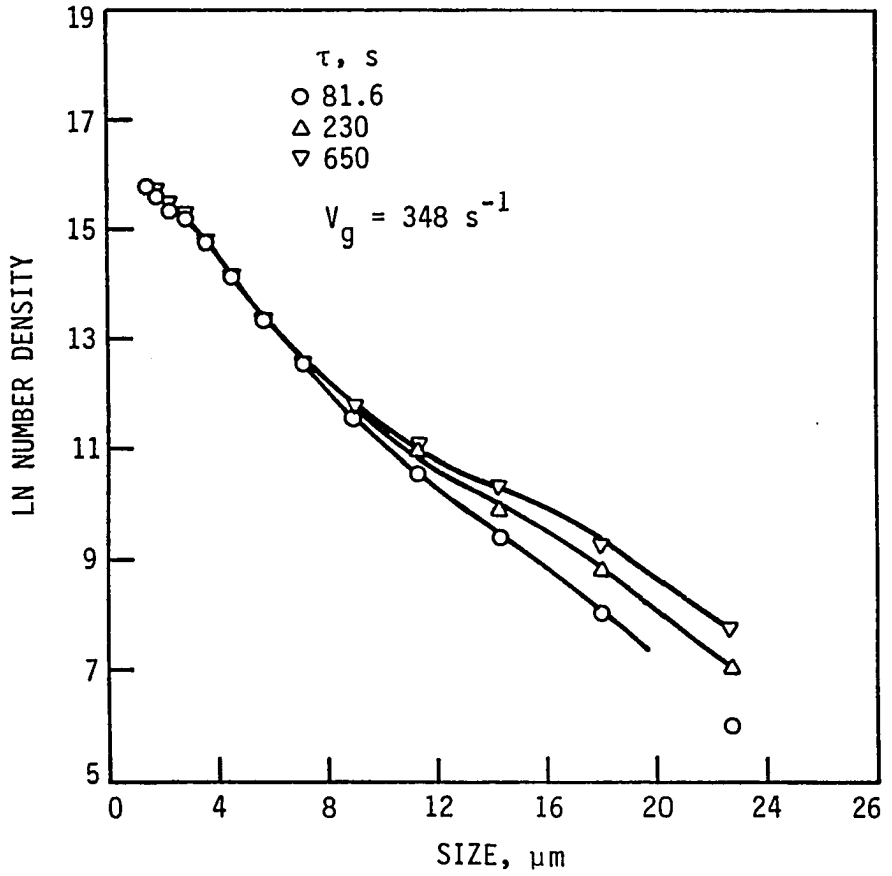

Figure 4. Size distributions for three values of τ

its more efficient use, leading to stronger aggregates or improved collision efficiency. However, if polymer dispersion were important, the effect of V_g on size distribution should be more pronounced for a more viscous injected polymer, such as in the precipitations using 1.0% polymer. Such enhancement is not evident; the PSDs for the 1.0% polymer feed (not shown) indicate effects identical to those for 0.1% polymer (Figure 3).

The PSD variations with residence time (Figure 4) show that the distributions are almost identical up to 8 μm, after which increases in residence time produce increases in numbers of larger particles. Apparently, longer times in the precipitator allow more protein to be removed from solution (confirmed by protein recovery data, not shown).

Mean diameter

D_{50}, the diameter above which 50% of the total measured particle volume can be found, was determined by integration of the size distributions. Figure 5 summarizes the effects of mean shear and residence time on D_{50}. As noted above, particle sizes increase with shear rate and with residence time.

The increase of D_{50} with mean residence time may result from the increased protein precipitated from solution, as identified above, and/or from the longer time required for the polymer-aggregate complexes to come to an "equilibrium" orientation and stoichiometry. When compared to precipitation times using small-molecule precipitants (up to 16 s (50)), the precipitation using high-molecular weight polyelectrolytes would be

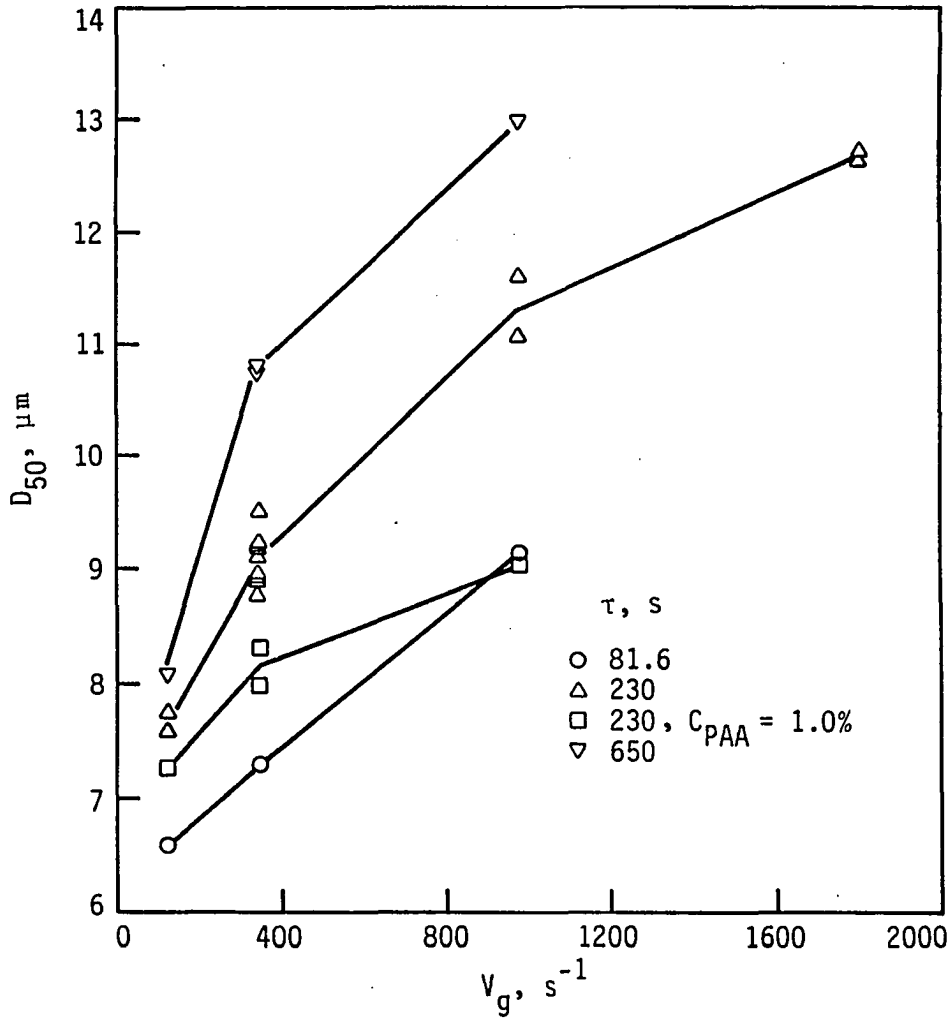

Figure 5. Dependence of mean size, D_{50}, on V_g and τ

expected to require more time for rearrangement of the particles and polymers in the aggregate (from several hours (51) to minutes (52)).

The ANOVA shows a significant nonadditive interaction between V_g and τ; this is supported by Figure 6, which shows the product $V_g\tau$ determinant for particle size, consistent with Camp and Stein (44). This system, however, does not display a maximum in the particle size up to a $V_g\tau$ value of 64×10^4, further evidence of strong aggregates. Bell and Dunnill (21) found maximum strength, for an isoelectrically precipitated soy aggregate in capillary shear, at $V_g\tau = 10 \times 10^4$.

The precipitations using 1.0% PAA produced PSDs identical to those for comparable conditions using 0.1% PAA. The sizes are slightly smaller (Figure 5), but trends in D_{50} are similar. Overall, the effect of increasing the injected PAA concentration ten-fold cannot be considered significant on physical properties.

Microstructure

Scanning electron photomicrographs of aggregates (Figure 7) reveal no qualitative differences in microstructure due to precipitation conditions. They do show the primary particles (approximately 0.5 to 1 μm diameter) that make up the aggregates (which have collected into super-aggregates during drying for the microscopy). The aggregates show much elongation and display numerous appendages; these properties have not been seen when using lower molecular weight precipitants with proteins (12, 35) and may be causally linked to the larger, stronger aggregates produced by this system.

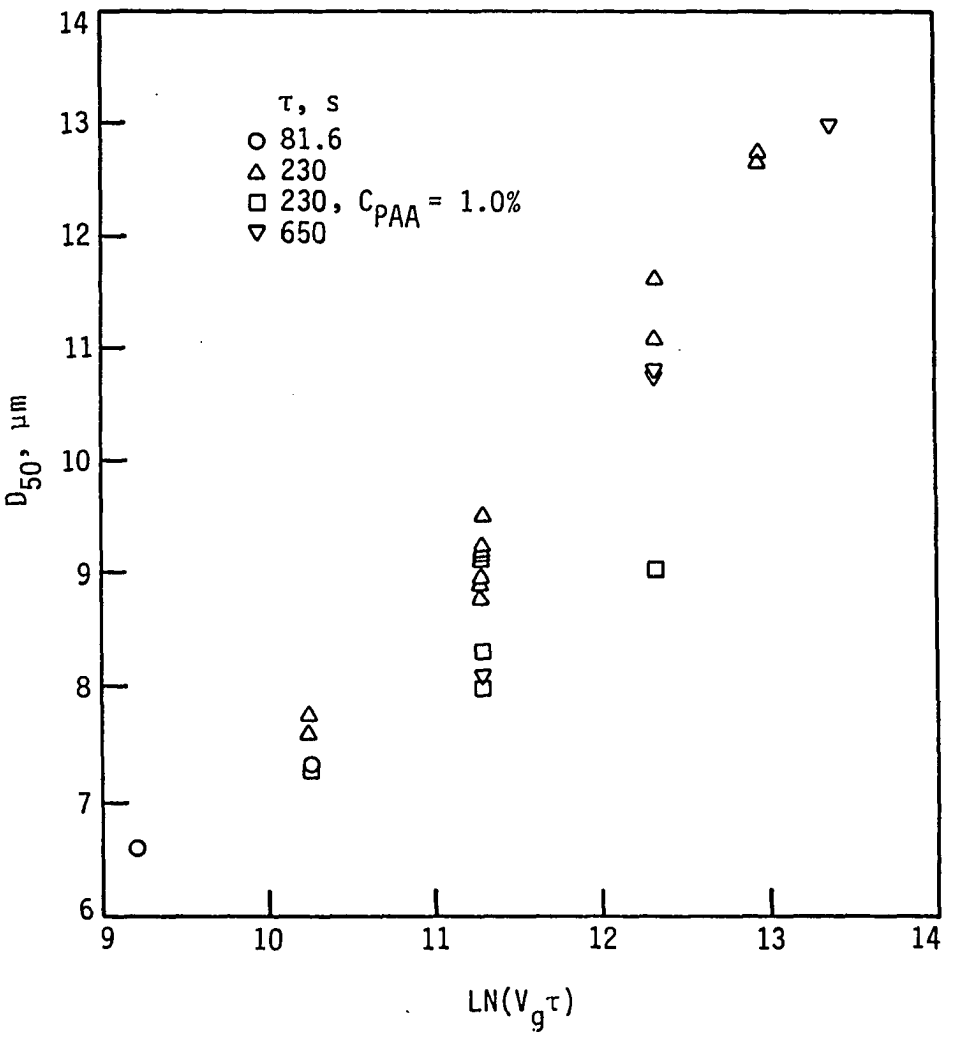

Figure 6. Dependence of mean size, D_{50}, on the Camp number, $V_g\tau$

Figure 7. Scanning electron photomicrographs of typical PAA-precipitated aggregates; bar indicates 1 μm

Zeta potential

In the cases of polymer bridging and patch formation, zeta potential measurements may not present conclusive information regarding particle stability as in isoelectric precipitation (53). But zeta potentials are still useful information when the polymer adsorption is affected by electrostatic forces (54).

Zeta potential measurements of these aggregates present somewhat scattered results (at the high voltages required for electrophoresis, little time (15-30 s) was allowed for measurements before heat-induced convection obscured the observations); all are within the range -10 to 0 mV, the range of electrostatically unstable colloids (1), yet they indicate that a slight excess of PAA or anionic protein has adsorbed onto the aggregate.

Lysozyme recovery and enrichment

The percentage lysozyme recovered in the precipitate is shown in Figure 8, where yields are shown (calculated by difference: feed solution minus supernatant, values adjusted to correct for differences in the feed dosages). Longer residence times lead to higher recoveries (supported by ANOVA), but neither shear rate nor $V_g x\tau$ effects are significant. The lysozyme recovery using a 1.0% PAA solution is significantly lower; the low feed dosage (7.23 mg PAA/g protein in feed) in that case cannot account for such a low recovery.

The lysozyme recovery values are a function of total protein recoveries. The actual fractionating power of the precipitation is quantified by the lysozyme concentration factor (LCF), a ratio of

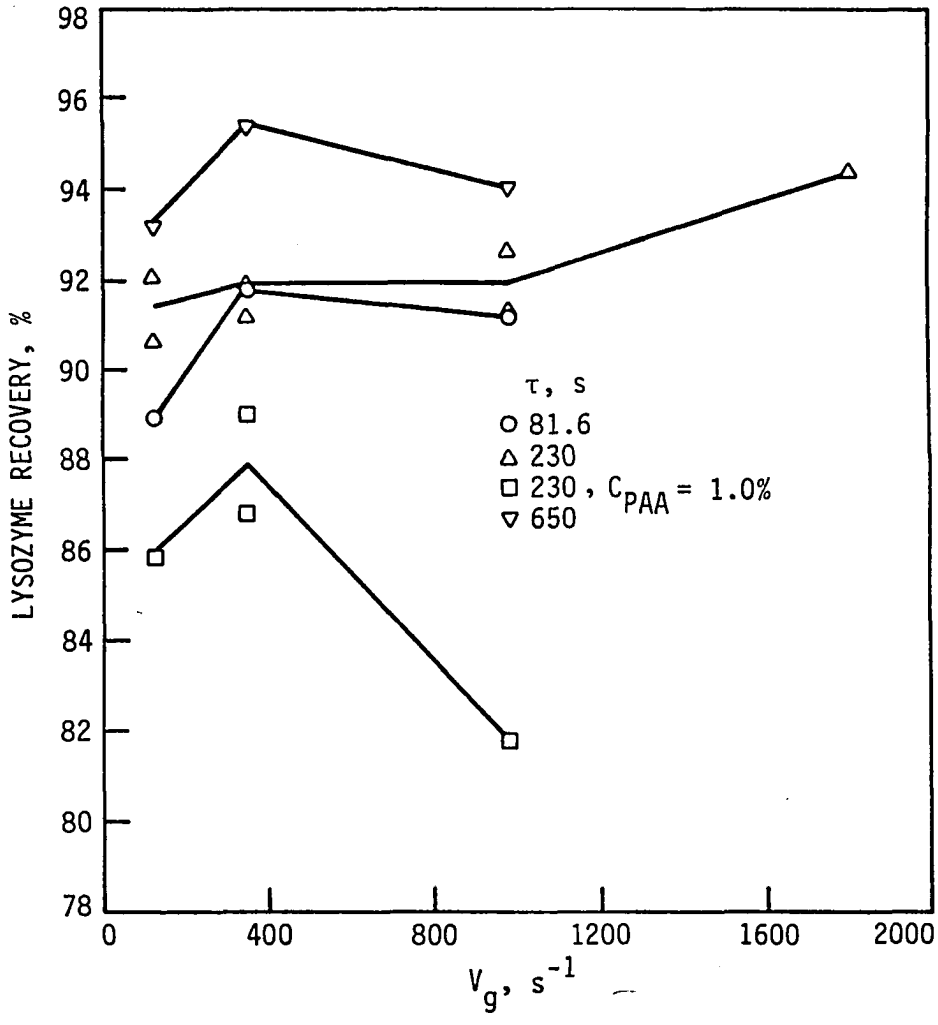

Figure 8. Dependence of lysozyme recovered in the precipitate on V_g

percentage lysozyme in the precipitate (by mass balance difference) to percentage lysozyme in the feed solution. Although the LCF data appear scattered (Figure 9), the ANOVA (for C_{PAA} = 0.1%) indicates that the effects of τ, V_g, and $V_g x \tau$ are all significant, and three of the residence times show an increase in LCF with V_g. It would be expected that the higher shear rates allow for more thorough dispersion of the viscous polymer before adsorption occurs; thus, the more positively charged--yet less concentrated--lysozyme is able to contact more of the PAA and fractionally precipitate, thereby increasing the LCF. However, this would not explain the higher LCF using the 1.0% PAA.

Based on the lysozyme recovery and LCF data described here, it appears that, for this system, the precipitator-specific properties (V_g and τ) do not strongly affect the compositional properties of the precipitate.

Analysis of the precipitate

We attempted to quantify PAA concentrations in the precipitate by size exclusion HPLC and by gravimetric and total protein analyses; each method failed to provide useful information about PAA. Although the protein/PAA separation is possible in a processing sense, the quantitation of PAA in the presence of protein is problematic. An observation regarding the polymer can be made by assuming all of the added PAA was incorporated into the solid phase, whereby the polymer would comprise from 3.6 to 6.6 wt. % of the precipitate.

The gravimetric analysis of the freeze dried precipitate from the continuous runs, although not sufficiently precise to quantitate PAA, did

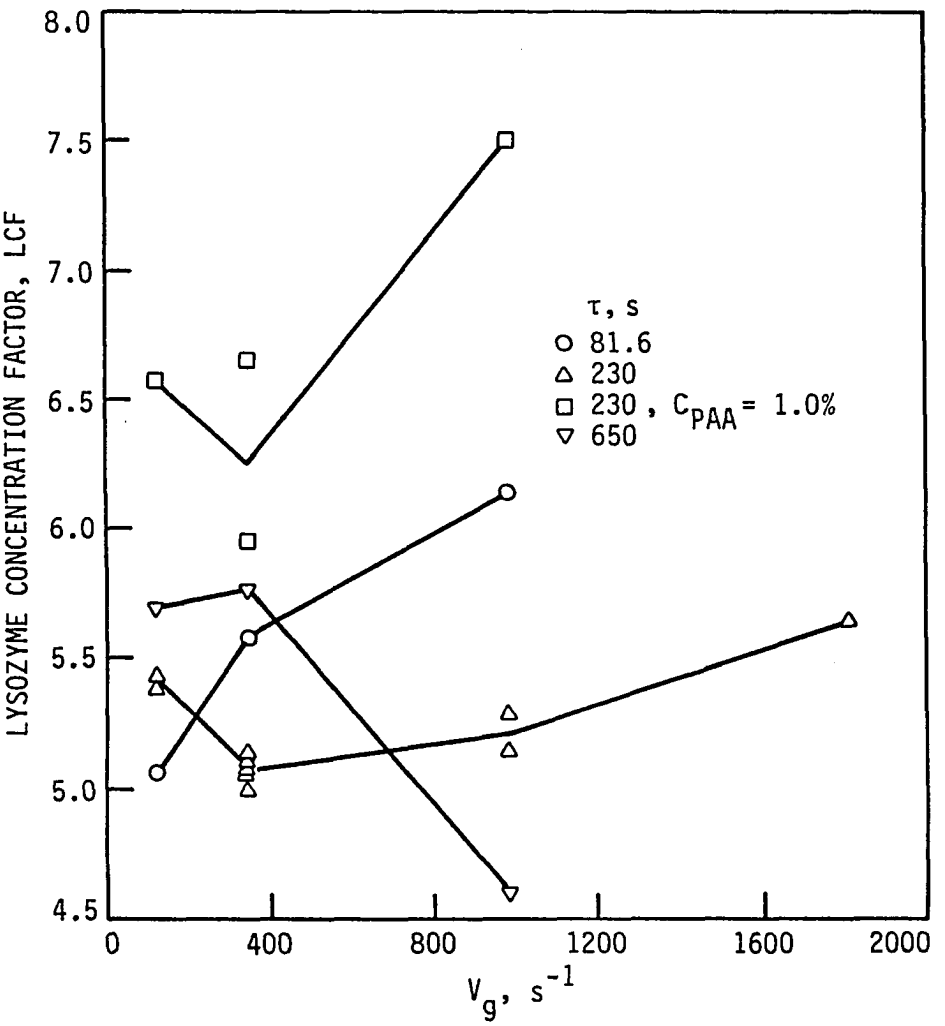

Figure 9. Dependence of lysozyme concentration factor on V_g

show that from 87 to 99% of the lysozyme in the precipitate retained activity after extended frozen storage and freeze-drying. This high stability may be due to the stabilizing effects of collecting the protein in a solid phase (55), to more specific stabilizing properties of polymers (56), and to the inherent stability of lysozyme.

Recovery of lysozyme from the precipitate

Figure 10 demonstrates the solublity behavior of batch-prepared precipitate. It is important to note that these resolubilizations were done at low ionic strength (no added salt), and therefore require high pH conditions to dissociate the complex. (The quantitative analysis of the precipitate phase, described in the preceding section, achieved comparable levels of resolubilization at neutral pH, yet with a high ionic strength.) Further, these recovery methods were performed to show feasibility of such processes, and were not optimized.

Figure 10 also demonstrates the fractional resolubilization behavior which has been exploited to achieve further enrichment of the lysozyme. The results of stepwise pH change are shown in Table 2. At pH 10.50, during stepwise resolubilization, over half of the protein is dissolved yet contains only 4% of the lysozyme. The removal of this fraction leaves a precipitate 70% in soluble lysozyme. Thus, a substantial enrichment of the target protein (from 3% in the original egg white to 70% in the remaining precipitate) has been achieved using one precipitation step and one solubilization step.

The ultrafiltration results in Table 2 demonstrate that the solubilized lysozyme and PAA are not inseparably bound in a soluble

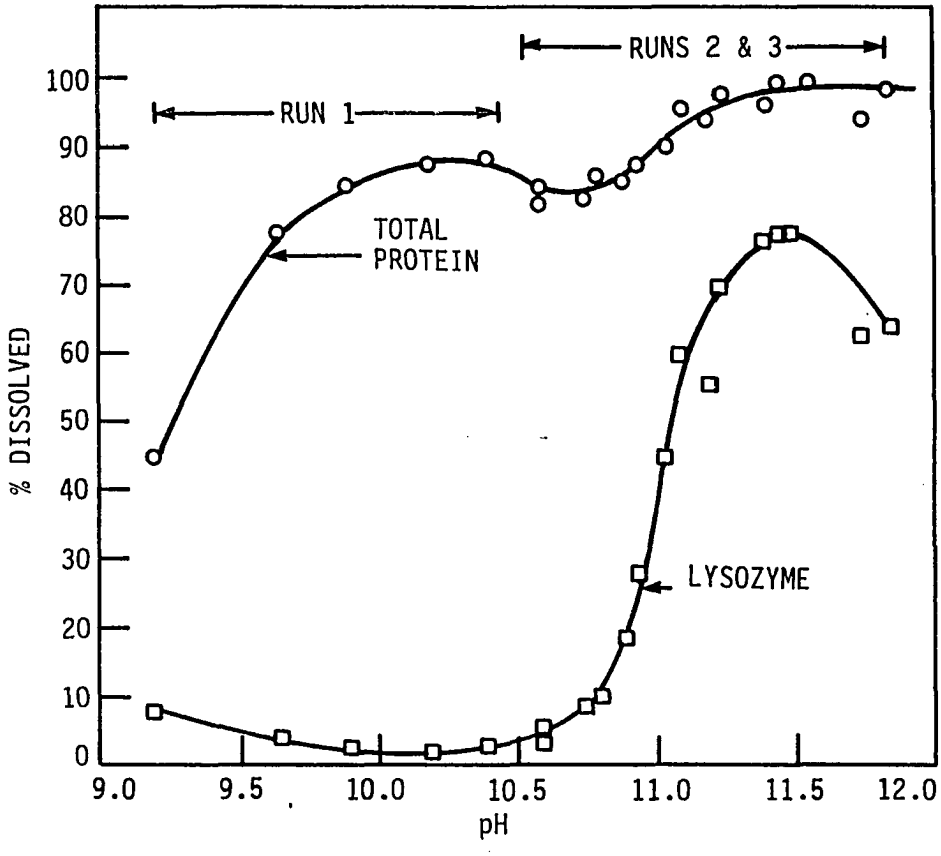

Figure 10. Effect of pH on resolubilization of total protein and lysozyme from the precipitate

Table 2. Representative results from recovery schemes

Stream	$C_{prot.}$ (mg/mL)	prot. diss. (%)	$C_{lys.}$ (mg/mL)	lys. diss. (%)	$\frac{C_{lys}}{C_{prot}}$ (%)	lysozyme yield (%)
fractional resolubilization						
feed to precipitator	3.87		0.0976		2.52	
precipitation supernatant	3.11		0.0078		0.252	92[b] (in ppt)
pH 10.51 supernatant	0.433[a]	52	0.0038	4.2	0.87	
pH 11.49 supernatant	0.0894	11	0.0615	69	68.9	56[b]
ultrafiltration						
feed to precipitator	3.75		0.0968		2.58	
precipitation supernatant	3.32		0.0132		0.398	
XM100A membrane						
feed to cell	2.18		0.312		14.3	
permeate	0.18		0.187		100[d]	54[b], 60[c]
XM300 membrane						
feed to cell	2.12		0.196		9.24	
permeate	0.19		0.164		86	47[b], 84[c]

[a]Using basis of 3.87 mg/mL protein.

[b]Yield calculated on basis of lysozyme in initial feed.

[c]Yield calculated on basis of lysozyme fed to UF cell.

[d]Assays of concentrations below 0.5 mg/mL result in significant error.

complex; lysozyme passes through the 100,000 MW membrane (it is assumed that PAA is retained). The other proteins are excluded using this membrane, probably due to the low ionic strength. (The lysozyme fraction of the filtrate from the 100,000 MW membrane is reported to be greater than unity because the total protein assay is inaccurate at low concentrations.)

CONCLUSIONS

Fractional precipitation of lysozyme from egg white proteins using polyacrylic acid gives substantial yield and enrichment in a continuous process. The aggregates' size and strength are comparable or higher than systems using isoelectric precipitation. In varying the precipitator conditions, it has been found that residence time and mean shear rate significantly affect the resulting particle size distribution, mean size, and lysozyme enrichment. This effect shows nonadditive interactions between V_g and τ for all responses. In a limited number of tests, the effect of inlet polymer concentration has been shown not to be a determinant for physical or compositional properties, in agreement with earlier work (29).

The apparent effect of τ on protein solubility is possibly masked by the particular method used to assay the slurry. If contact time (from 81.6 to 650 seconds) has an effect on lysozyme recovery, then the slowly performed assay (requiring from 1 to 3 hours) would be expected to overwhelm the reactor residence time effect. The persistence of this effect indicates that other phenomena may be responsible for differences in lysozyme recovery with residence time. For example, higher residence times may produce a larger fraction of particles that are recoverable by centrifugation and therefore assayed.

Unique properties and phenomena are evident in this system. The particle size distributions, which do not show the bulge characteristic of fragmentative breakage found in other protein systems (21), appear to be more resistant to breakage. There exists an enhanced growth rate for

particles smaller than 4 μm. Most notably, increasing shear increases the mean size of aggregates, probably a result of the predominance of growth over breakage.

Although, in statistical terms, residence time significantly affects compositional properties--percent lysozyme recovered and the lysozyme concentration factor--the magnitude of these effects is minimal. Given this, and that shear rate does not affect these properties, it can be concluded that compositional properties are not affected by residence time and mean shear rate.

The predominance of the bridging mechanism in these precipitations can be supported by the results. First, the formation of bridges is possible given the low zeta potential of the aggregate (it is assumed the zeta potential of the primary particles is also low); adsorbed polymer will not immediately collapse onto the surface (14) (the zeta potentials indicate that PAA is adsorbed in excess). Second, the continuous operation provides a continuous source of PAA, some of which is available to adsorb on the primary particles and aggregates to act as bridges. Third, the aggregation behavior--larger mean size with residence time and relatively strong aggregates--implicates bridging; the rearrangement of bridges or polymer to form new bridges would require more time than simple particle rearrangements which occur during aggregation by charged patches or simple charge neutralization, and the bridges would be expected to form aggregates stronger than those of electrostatic or hydrophobic particle interaction.

Regardless of which particular mechanism predominates, the outgrowth of these results is that the chemical environment (pH, ionic strength, dosages) can be used to control the composition of the aggregate (57), whereas the mechanical environment (shear rate, residence time) can be adjusted to control the physical properties of the aggregate. Such control is essential for the application of fractional precipitation to large scale protein recovery and purification.

Successful resolubilization of the precipitate and separation of the lysozyme from the polymer have been shown possible, where from 50 to over 95% of the lysozyme activity is recovered in the dissolved precipitate via a variety of schemes, with highly purified protein obtainable in over 50% yields.

ACKNOWLEDGEMENTS

The authors would like to thank Daniel Carlson for his efforts in studying precipitate resolubilization and lysozyme recovery. This work was supported by a grant from the National Science Foundation (ECE 8514865).

REFERENCES

1. D. J. Bell, M. Hoare, and P. Dunnill, Adv. Biochem. Eng. Biotechnol., 26, 1 (1983).

2. A. K. Smith, A. M. Nash, A. C. Eldridge, and W. J. Wolf, J. Agric. Food Chem., 10, 302 (1962).

3. L. Gillberg and B. Tornell, J. Food Sci., 41, 1070 (1976).

4. J. Spinelli and B. Koury, J. Agric. Food Chem., 18, 284 (1970).

5. M. Sternberg and D. Hershberger, Biochim. Biophys. Acta, 342, 195 (1974).

6. J. Cerbulis, J. Agric. Food Chem., 26, 806 (1978).

7. N. S. Gault and R. A. Laurie, Meat Sci., 4, 167 (1980).

8. V. Vandergrift and R. R. Evans, J. Agric. Food Chem., 29, 536 (1981).

9. R. D. Hill and J. G. Zadow, J. Dairy Res., 41, 373 (1974).

10. R. D. Hill and J. G. Zadow, New Zealand J. Dairy Sci. Technol., 13, 61 (1978).

11. C. D. Nelson and C. E. Glatz, Biotechnol. Bioeng., 27, 1434 (1985).

12. G. C. Grabenbauer and C. E. Glatz, Chem. Eng. Commun., 12, 203 (1981).

13. E. Dickinson and G. Stainsby, Colloids in food (Applied Science Publishers, London, 1982).

14. D. R. Kasper, "Theoretical and experimental investigations of the flocculation of charged particles in aqueous solutions by polyelectrolytes of opposite charge," Ph.D. thesis, Calif. Inst. of Tech., Pasadena, CA, 1971.

15. J. Gregory, J. Colloid Interface Sci., 42, 448 (1973).

16. V. K. LaMer and T. W. Healy, Rev. Pure Appl. Chem., 13, 112 (1963).

17. J. C. Kane, V. K. LaMer, and H. B. Linford, J. Am. Chem. Soc., 86, 3450 (1964).

18. W. E. Walles, J. Colloid Interface Sci., 27, 797 (1968).

19. C. E. Glatz, M. Hoare, and J. Landa-Vertiz, AIChE J., 32, 1196 (1986).

20. L. A. Glasgow and R. H. Luecke, Ind. Eng. Chem. Fundam., 19, 148 (1980).

21. D. J. Bell and P. Dunnill, Biotechnol. Bioeng., 24, 1271 (1982).

22. J. O. Hinze, Turbulence, 2nd ed. (McGraw-Hill, New York, 1975).

23. R. A. Stratton, TAPPI J., 66, 141 (1983).

24. L. Jen-Jiang and G. G. Fuller, J. Colloid Interface Sci., 103, 569 (1985).

25. N. D. Sylvester and M. P. Toure, Ind. Eng. Chem. Prod. Res. Dev., 17, 347 (1978).

26. L. A. Glasgow, R. J. Pollock, and W. A. Barkley, Biotechnol. Bioeng., 25, 901 (1983).

27. P. M. Huck, K. L. Murphy, and B. P. LeClair, Proc. 11th Canadian Symp.: Water Pollution Research Canada, 11, 46 (1976).

28. J. W. S. Goossens and P. Luner, TAPPI J., 59, 89 (1976).

29. R. O. Keys and R. Hogg, AIChE Symposium Series No. 190, 75, 63 (1979).

30. M. Hoare, Trans. I. Chem. E., 60, 157 (1982).

31. M. Hoare, Trans. I. Chem. E., 60, 79 (1982).

32. T. R. Camp, Trans. Am. Soc. Civil Eng., 120, 1 (1955).

33. D. J. Salt, R. B. Leslie, P. J. Lillford, and P. Dunnill, European J. Appl. Microbiol. Biotechnol., 14, 144 (1982).

34. A. M. Petenate and C. E. Glatz, Biotechnol. Bioeng., 25, 3059 (1983).

35. R. R. Fisher, C. E. Glatz, and P. A. Murphy, Biotechnol. Bioeng., 28, 1056 (1986).

36. P. Molyneux, Water-soluble synthetic polymers: properties and behavior, Vol. II (CRC Press, Boca Raton, FL, 1984).

37. M. Sternberg, Process Biochem., 11, 11 (1976).

38. M. Sternberg, J. P. Chiang, and N. J. Eberts, J. Dairy Sci., 59, 1042 (1976).

39. F. Rothstein, V. M. Rosenoer, and W. L. Hughes, "Current concepts concerning albumin purification," in V. M. Rosenoer, M. Oratz, and M. A. Rothschild, eds., Albumin structure, function, and uses (Pergamon Press, New York, 1977).

40. B. T. Doumas, Clin. Chem., 21, 1159 (1975).

41. R. M. Parry, Jr., R. C. Chandan, and K. M. Shahani, Proc. Soc. Exp. Biol. Med., 119, 384 (1965).

42. M. C. Cafe and I. D. Robb, J. Colloid Interface Sci., 86, 411 (1982).

43. ASTM standard method A 445-74, Annual book of ASTM standards (American Society for Testing and Materials, Philadelphia, PA, 1974).

44. T. R. Camp and P. C. Stein, J. Boston Soc. Civil Eng., 30, 219 (1943).

45. R. L. Bates, P. L. Fondy, and R. R. Corpstein, Ind. Eng. Chem., 2, 310 (1963).

46. P. M. Huck and K. L. Murphy, J. Environ. Eng. Div., ASCE, 104, 767 (1978).

47. SAS Institute, Inc., SAS users guide: statistics (SAS Institute, Inc., Cary, NC, 1985).

48. A. Randolph and M. Larson, Theory of particulate processes (Academic Press, New York, 1971).

49. R. R. Fisher and C. E. Glatz, "Polyelectrolyte precipitation of proteins. II. Models of the particle size distributions," Iowa State University, Ames, IA (to be published).

50. M. Y. Y. Chan, M. Hoare, and P. Dunnill, Biotechnol. Bioeng., 28, 387 (1986).

51. F. van Voorst Vader and H. Dekker, Proceedings of the VIIth International Congress on Surface Active Substances, paper #147, Moscow, September 12-18, 1976.

52. D. K. W. Smith and J. A. Kitchener, Chem. Eng. Sci., 33, 1631 (1978).

53. G. P. Treweek and J. J. Morgan, J. Water Pollution Control Fed., 51, 1859 (1979).

54. F. Mabire, R. Audebert, and C. Quivoron, J. Colloid Interface Sci., 97, 120 (1984).

55. R. K. Scopes, Protein purification: principles and practice (Springer-Verlag, New York, 1982).

56. J. Hidalgo and P. M. T. Hansen, J. Agric. Food Chem., 17, 1089 (1969).

57. K. M. Clark and C. E. Glatz, "Properties of complexes formed by polyelectrolyte precipitation of protein," presented at AIChE Annual Meeting, Miami Beach, FL, November 2-7, 1986.

SECTION III. POLYELECTROLYTE PRECIPITATION OF PROTEINS
II. MODELS OF THE PARTICLE SIZE DISTRIBUTIONS

ABSTRACT

A population-balance model has been used to characterize continuous polyelectrolyte precipitation of egg white proteins. We have modeled the particle size distributions of aggregates formed using a range of mixing conditions. The models, accounting for aggregate growth (by both shear-driven and Brownian-like collisions), breakage (by hydrodynamic shear or aggregate-aggregate collisions), and birth (by the breakage of larger aggregates), fit the data well. However, the kinetic constants show dependencies on shear rate and residence time that are not theoretically predicted; these dependencies are due in part to aging effects on the aggregate. The model constants show a dominance of growth over breakage, supporting qualitative interpretations of the particle size distributions. A mechanism for growth-rate enhancement, caused by polymer extensions from the particle surfaces, produced slightly improved model performance. A collisional breakage mechanism is supported.

NOMENCLATURE

A, A'	collision-effectiveness factor for growth
A_2	aggregate-breakage constant
b_{12}	binary collision frequency of 1- and 2-particles (# L^{-3} t^{-1})
B	volumetric birth rate of particles (# L^{-4} t^{-1})
C_{pf}	aggregate volume ratio
D	volumetric death rate of particles (# L^{-4} t^{-1})
f	number of equal-volume daughter fragments
g	collision effectiveness constant (Equations 17 and 18)
G	linear growth rate (L/t)
h	length of polymer extension from particle surface (L)
k_h	hydrodynamic death rate constant (Equation 11) ($L^{-\beta}$ t^{-1})
k_c	collisional death rate constant (Equation 13)
k_v	volumetric shape factor (volume = $k_v L^3$)
kT/μ	Boltzmann constant x temperature / viscosity (L^3 t^{-1})
K_0	growth rate constant for orthokinetic growth (Equation 5) (s^{-1})
K_B	growth rate constant for perikinetic growth (Equation 8) (L^2 s^{-1})
L	aggregate diameter (L)
L_1	growth unit diameter (L)
m	enhancement to collision diameter (L)
n	number density of particles (#/L^4)
N_i	particle number concentration (#/L^3)
R_{12}	collision radius (L)
V	particle volume
V_g	root-mean-square velocity gradient (s^{-1})

Greek

α collision efficiency

β breakage power on L

ϕ_1 volume fraction of growth units in solution

η Kolmogorov microscale of turbulence = $(\nu^2\rho/v_g^2)^{1/4}$

μ ionic strength (M)

ν kinematic viscosity ($L^2\ t^{-1}$)

ρ solution density (m/L^3)

σ aggregate yield stress ($m\ L^{-1}\ t^{-2}$)

τ mean residence time of precipitator (t)

Subscripts

1 growth unit or primary particle

a aggregate

c collisional, second-order breakage

e enhanced by polymer extensions

h hydrodynamic, first-order breakage

s shear-driven, orthokinetic

B Brownian

INTRODUCTION

In the bioprocess industry, a large fraction of the overall processing is devoted to the downstream unit operations, where products from often complex streams are recovered and purified. Of the many bioseparations techniques available for protein recovery and enrichment, fractional precipitation offers several advantages:

1. It can be performed in bulk phase and is largely scale independent.
2. The desired product is usually in the solid phase, a stabilizing condition for most proteins (1), and an advantageous state for storage and handling.
3. The process occurs relatively rapidly, minimizing product degradation with time.
4. Many different properties of the target species can be exploited to affect the separation (net charge, hydrophobicity, hydrophilicity, specific interactions on functional protein sites, etc.). (For example, as various binding ligands become available, greatly improved specificity of the fractionation by affinity precipitation will become possible.)

In fractional precipitation, the composition of the precipitate and the final aggregate size and strength are properties that must be controlled. These properties determine the value of the product and the efficacy of solid-liquid separation--by centrifugation/settling or filtration--which occurs downstream from the precipitation. Therefore, in order to design precipitation reactors and processes for optimum

throughput, yield, and enrichment, engineering information on the mechanisms and kinetics of protein precipitation needs to be compiled.

Aggregate-population models accounting for the kinetics of aggregate growth, outflow, and breakage as functions of size have been successfully applied to the isoelectric precipitation of soy proteins in continuous systems (2-4). In this paper, we will employ the population model to study fractional precipitation of proteins using high molecular-weight polyelectrolytes. The model will be fit to steady-state particle size distributions (PSDs) measured during continuous precipitation of proteins (part I of this work (5)), in which lysozyme was fractionally precipitated from egg-white protein using polyacrylic acid (PAA, MW 4 x 10^6). In these experiments (at pH 5.4, where lysozyme has a net positive charge and the PAA is negatively charged), the dissolved lysozyme (diameter approximately 40 Å) and PAA (radius of gyration at experimental conditions is on the order of (6, 7) 1000 Å) are affected predominantly by Brownian forces; the motions of the precipitated solid phase (0.5 - 30 μm) are driven by convective forces.

The purpose of the modeling is to better understand the events during protein precipitation by polyelectrolytes. We are particularly interested in characterizing the unique behavior--apparently due to the high molecular-weight polymer--which we observed.

Models of Precipitation

The mechanisms postulated for precipitation with high molecular-weight polyelectrolytes (5) are analogous to those used in describing precipitation by low molecular-weight precipitants (acid, base, organic

solvent, multivalent metal salt). The modeling of these mechanisms incorporates a mass balance on the precipitated material with the following assumptions and features (4).

First, the removal of the soluble material by the formation of the primary particle is considered to occur instantaneously (relative to the aggregate growth); therefore, the mass balance needs to account for only solid material. Kinetic studies for non-polymer precipitation have shown protein removal from solution to occur in a few seconds (8-10), much less time than the mean residence times used here.

Second, collisions between the growth units (primary particles and smaller aggregates) and growing aggregate collectors (larger aggregates) are driven by turbulent diffusion and are the sole mechanism of growth; collisions between large aggregates do not result in sufficient contacts to survive. Aggregate growth is limited to this incremental addition of small growth units to the aggregate.

Third, the effectiveness (or efficiency, α) of the collisions between small particles and growing aggregates is independent of the growing aggregate size.

Fourth, aggregate breakage yields a small number, f, of equal-volume daughter fragments, which are sufficiently large to require inclusion in the mass balance.

A population balance on aggregates of size L for a CSTR at steady state, mean residence time τ, and with no particles in the feed yields

$$\frac{d(Gn)}{dL} + \frac{n}{\tau} + D - B = 0 \qquad (1)$$

in which n, G, D, and B may be functions of L. Equation (1) describes the particle size distribution of growing aggregates in the precipitator, and requires terms for growth, breakage, and birth (formation).

Aggregate Growth

G is defined as the linear growth rate of the aggregate

$$G \equiv dL/dt \tag{2}$$

In this work, we will use two forms of G. The first, shown here, incorporates the usual shear-driven collision mechanism, with an additional term based on Brownian-driven collisions. The second, to be briefly considered later, is a modification of the first. It incorporates the enhancements to collision frequency caused by polymer extensions from the particle surface. Appendix A shows a detailed derivation of each mechanism, where the polymer-enhanced form condenses to the usual form by neglecting the polymer-enhancement terms.

Previous models (3, 4) have considered growth to be caused by turbulent-shear-driven (orthokinetic) collisions, where the collision frequency for spherical particles smaller than the Kolmogorov scale, of neutral buoyancy, and in isotropic turbulence is (11)

$$b_{12,s} = (A/8)V_g(L_1+L_2)^3N_1N_2 \tag{3}$$

From this, G_s, the shear-driven aggregate growth rate is derived, giving

$$G_s = K_0L \tag{4}$$

where

$$K_0 = \alpha_s \frac{A}{4\pi} V_g \phi_1 \tag{5}$$

in which α_s, the shear-driven collision efficiency, is assumed to be independent of the size of the growing aggregate, and where $\phi_1 = N_1 V_1$.

Based on experimental PSDs, we observed unusually high growth rates for aggregates smaller than approximately 3 μm, indicating the possibility of a superimposed growth mechanism. A term to account for this mechanism was incorporated into the growth term, G. The form of this term is based on a Brownian contribution to particle collision frequency. (The first approximation is that the smaller aggregates, those acting as collectors, undergo Brownian motion in addition to the turbulent motion, thereby showing increased collision frequencies and higher growth rates.) Using the frequency of perikinetic collisions presented by von Smoluchowski (12)

$$b_{12,B} = \frac{2}{3} \frac{kT}{\mu} \left(\frac{1}{L_1} + \frac{1}{L_2} \right) (L_1 + L_2) N_1 N_2 \tag{6}$$

and incorporating the definition for linear growth rate (analogous to the derivation for turbulence-driven collisions (3)), the Brownian (perikinetic) growth rate, G_B, is (assuming spherical particles):

$$G_B = K_B / L \tag{7}$$

where L is the size of the growing aggregate and

$$K_B = \alpha_B \frac{4}{3\pi} \frac{kT}{\mu} \frac{\phi_1}{L_1} \tag{8}$$

Here L_1 is the growth unit size and α_B is the collision efficiency. The ortho- and perikinetic growth contributions are combined to give

$$G = K_0 L + K_B/L \tag{9}$$

Aggregate Breakage

Throughout this work, two parallel models for aggregate breakage (death) will be considered: first order (by hydrodynamic forces) and second order (by collisional forces).

First-order breakage

When considering phenomena possibly responsible for aggregate breakage (death), Petenate and Glatz (3) concluded that forces caused by local shear on the aggregate (entrained in the eddy and smaller than the Kolmogorov microscale) predominate over bulgy rupture and surface erosion (they did not consider collisional breakage). (Hydrodynamic breakage has also been implicated for polymer-aggregated systems (13, 14).) The resulting expression for breakage is

$$D = k_h L^{\beta} n \tag{10}$$

where

$$k_h = A_{2,h} V_g^2/\sigma \tag{11}$$

in which σ is the aggregate strength. The constant β, the breakage power, describes the increased susceptibility of larger aggregates to fragment. Previous modeling of protein precipitations has been characterized by values for β from 1.5 and 2.4 (4) to 3.0 (3).

Second-order breakage

Recent evidence has supported breakage to be second order in particle concentration, caused by aggregate-aggregate collisions as driven by shear. Twineham et al. (15) subjected isoelectric soy protein to high shear ($V_g = 2000\ s^{-1}$) in laminar flow and found breakup to be concentration dependent for concentrations from 0.1 to 2.5% wt/v (the experiments used in this work were performed at 0.4% wt/v). Brown and Glatz (16), in an investigation of protein aggregate breakage in a stirred tank, found the rate of change of particles due to collisional breakage to be

$$D = k_c L^{\beta} n^2 \tag{12}$$

in which

$$k_c = A_{2,c} V_g^{\ 3}. \tag{13}$$

The size dependence of breakage, β, can be derived assuming collisional breakage is a product of collision frequency, energy per collision, and inverse particle strength. Equation 3 shows frequency to be proportional to $V_g L^3 n^2$. The kinetic energy of each collision is a product of aggregate mass (proportional to L^3) and the square of velocity (proportional to $V_g L$); collision energy then depends on $V_g^{\ 2} L^5$. Aggregate strength is assumed to be inversely proportional to size (17-19). The resulting dependence for collisional breakage is

$$D(L) = k_c L^9 n^2 \tag{14}$$

giving $\beta = 9$.

Particle Birth

The breakage of an aggregate is assumed to result in f equal-volume daughter particles, so that

$$B = fD(f^{1/3}L) \tag{15}$$

Bell and Dunnill (17) found capillary shear to break isoelectrically precipitated soy aggregates into two to three daughter particles, with an insignificant volume of fines. The median size of the daughter particles was weakly dependent on the mean shear used (from 9×10^3 to 9×10^4 s^{-1}). Glasgow and Hsu (19) found large flocs of polyacrylamide precipitated kaolin to break into 2 or 3 fragments upon entrainment in a turbulent jet (Re = 1900).

RESULTS AND DISCUSSION

The method and algorithm used to fit the models to the experimental PSDs is outlined in Appendix B. In Appendix C, all of the model fit results are listed.

First-order vs. Second-order Breakage

Given their mathematical forms, it is possible that the first- and second-order-death models cannot be distinguished from one another for certain data. (If so, the models could not be relied upon to indicate the actual order of breakage in the system.) Specifically, if a plot of ln(n) vs. ln(L) produced a straight line with slope z (where z is defined as the difference of the powers of L in either model; $z = \beta_{\text{first-order}} - \beta_{\text{second order}}$), then, for such data, the first- and second-order-breakage terms (Equations 10 and 11) differ only by a constant. In this case, applications of the two models would independently optimize k values and obtain identical fits to the data. We tested the data to preclude such a confounded result.

Using the PSD from a single run (a number of runs were tested in this manner), a ln-ln plot of n vs. L produces a curve (Figure 1) showing a relatively straight segment from 4 to 15 μm, where slope = - 3.3, and a short straight segment above 15 μm, where slope = -6.7. The n and n^2 models depend on $L^{1.5}$ and L^9 respectively (Equations 10 and 14), giving z = -7.5. Since the slope differs from z for either linear segment, the two models are mathematically distinguishable from one another for these data ranges. However, this test does not guarantee that either model will necessarily better represent the data.

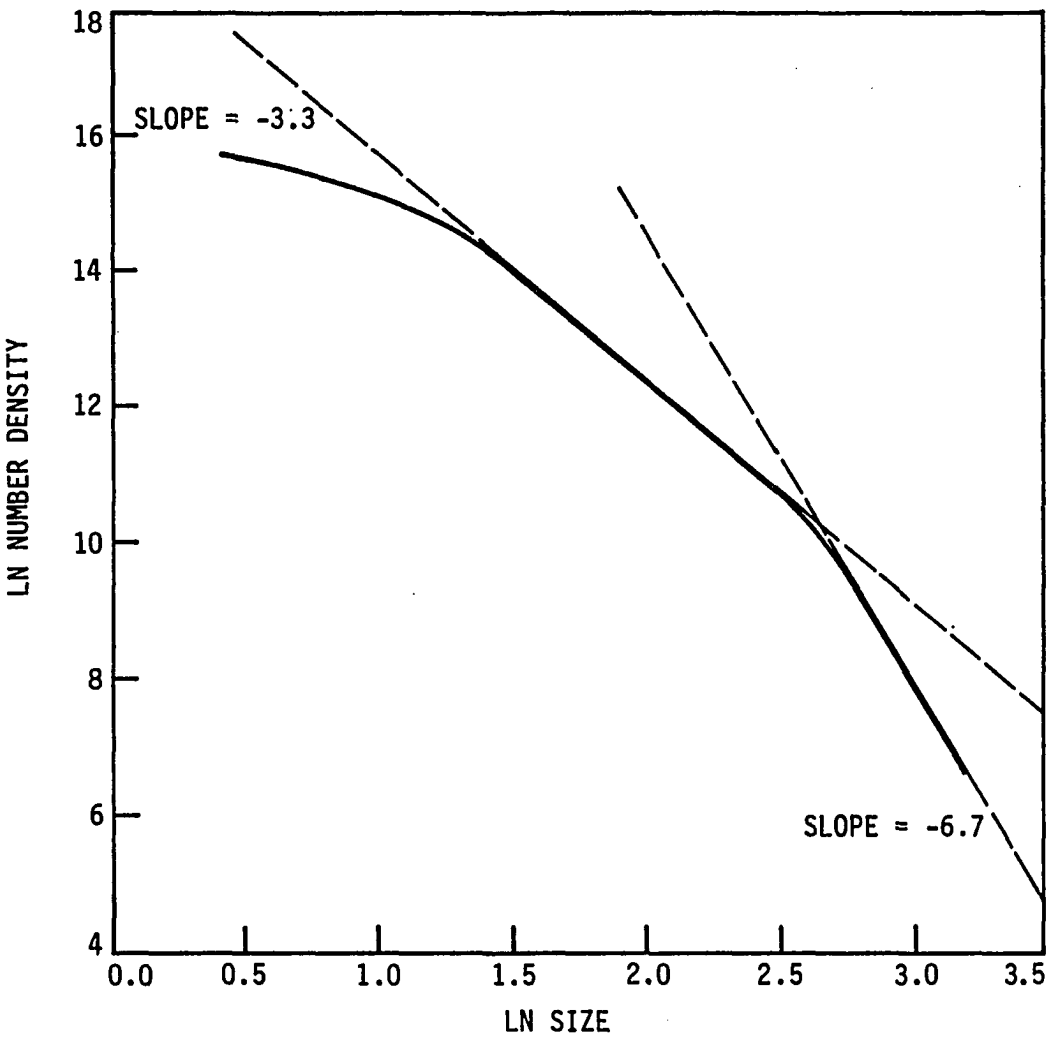

Figure 1. Ln-ln plot of model fit (employing Equations 9 and 10) to particle size distribution for run 8b (τ = 230 s, V_g = 348 s^{-1})

Assessment of Model Fit

Examples of particle size distributions with the model fits for two representative runs are shown in Figure 2. For the model solutions, the choices of β and f had little effect on trends in the behavior of K_0, K_B, and k; therefore, f was fixed at 2 for both models, and β set to 1.5 for the first-order and 9.0 for the second-order breakage model. Other values of β gave no better fit of each model to the data. The sum-of-squares of residuals between the model and data, given for each PSD shown, are based on eleven equispaced positions along the particle size range. Neither model produced significantly better fit to the data based on the sum-of-squares, although the second-order breakage model shows closer fit to the sharper curvature of higher shear conditions.

The features of PSDs representative of all the conditions, shown and discussed previously (5), show progressively larger or increasing particle size with V_g and τ, as well as enhanced growth rates at the small sizes.

Effect of Higher Inlet Polymer Concentration

PSDs were collected for precipitations using 0.10 and 1.0% w/v injected PAA, with equivalent final dosages. Only model characterizations using the 0.10% w/v data are discussed here, although some results using 1.0% wt/v are shown. The model behavior from PSDs of the higher PAA inlet concentration showed no distinguishing characteristics, with trends and values of model constants very similar to those using less concentrated PAA feed.

Figure 2. PSDs showing data and model fits with residual sum of squares (SS), for non-polymer-enhanced growth (Equation 9): (a) first-order death (Equation 10); (b) second-order death (Equation 12). Representative runs shown are 7c (τ = 230 s, V_g = 123 s^{-1}) and $8d_2$ (τ = 230 s, V_g = 1810 s^{-1}). Fits are quantified by residual sum-of-squares values

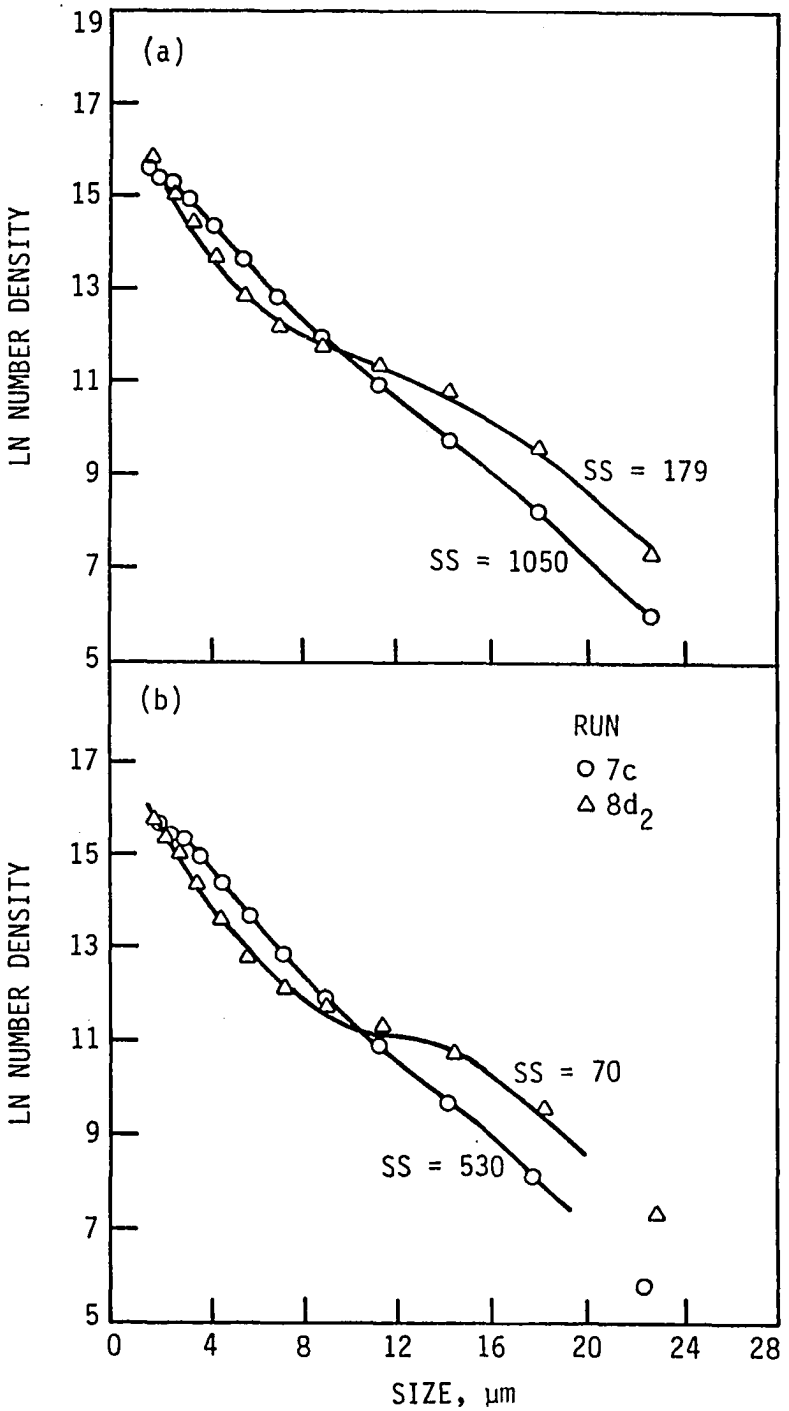
(a)
LN NUMBER DENSITY
19
17
15
13
11
9
7
5
SS = 179
SS = 1050
(b)
RUN
○ 7c
△ 8d2
LN NUMBER DENSITY
17
15
13
11
9
7
5
SS = 70
SS = 530
0
4
8
12
16
20
24
28
SIZE, μm

Values of the Model Constants

The constants for orthokinetic growth (K_0), perikinetic growth (K_B), and breakage (k) are plotted versus mean shear rate, V_g, and mean residence time, τ, in Figures 3, 4, and 5. For all constants, the effects of V_g, τ, and the interaction of V_g and τ ($V_g \times \tau$) are statistically significant (see Table 1). However, equations 5, 8, and 11 do not predict all of these effects.

K_0 increases with V_g as expected (Equation 5), but the effect is very small at high τ, implicating an aging effect to decrease collision efficiency during growth (to be discussed later). K_B shows a decrease with V_g, contrary to the theoretical understanding of the mechanism driving this term (Equation 8). k (Equation 11) decreases with τ and increases slightly with V_g. The notable features of these plots, when compared to reported constants for isoelectric protein precipitation using a similar model (3, 4), are the high values for K_0 and its weak increase with V_g, as well as the relatively small breakage constant, k, and its similar lack of increase with V_g.

In understanding the phenomena and aggregate characteristics responsible for the large values of K_0 in this system, the aggregate microstructure may prove helpful. As reported (5), the aggregates show many elongational structures and a highly porous aggregate built of intermediate structures. (This intermediate structure may be the scale of the growth units, L_1.) The aggregates are clearly more porous on this intermediate level than previously characterized protein precipitates (2, 20). This structural difference is expected to affect growth in two ways. First, as particles approach in solution, they must displace a

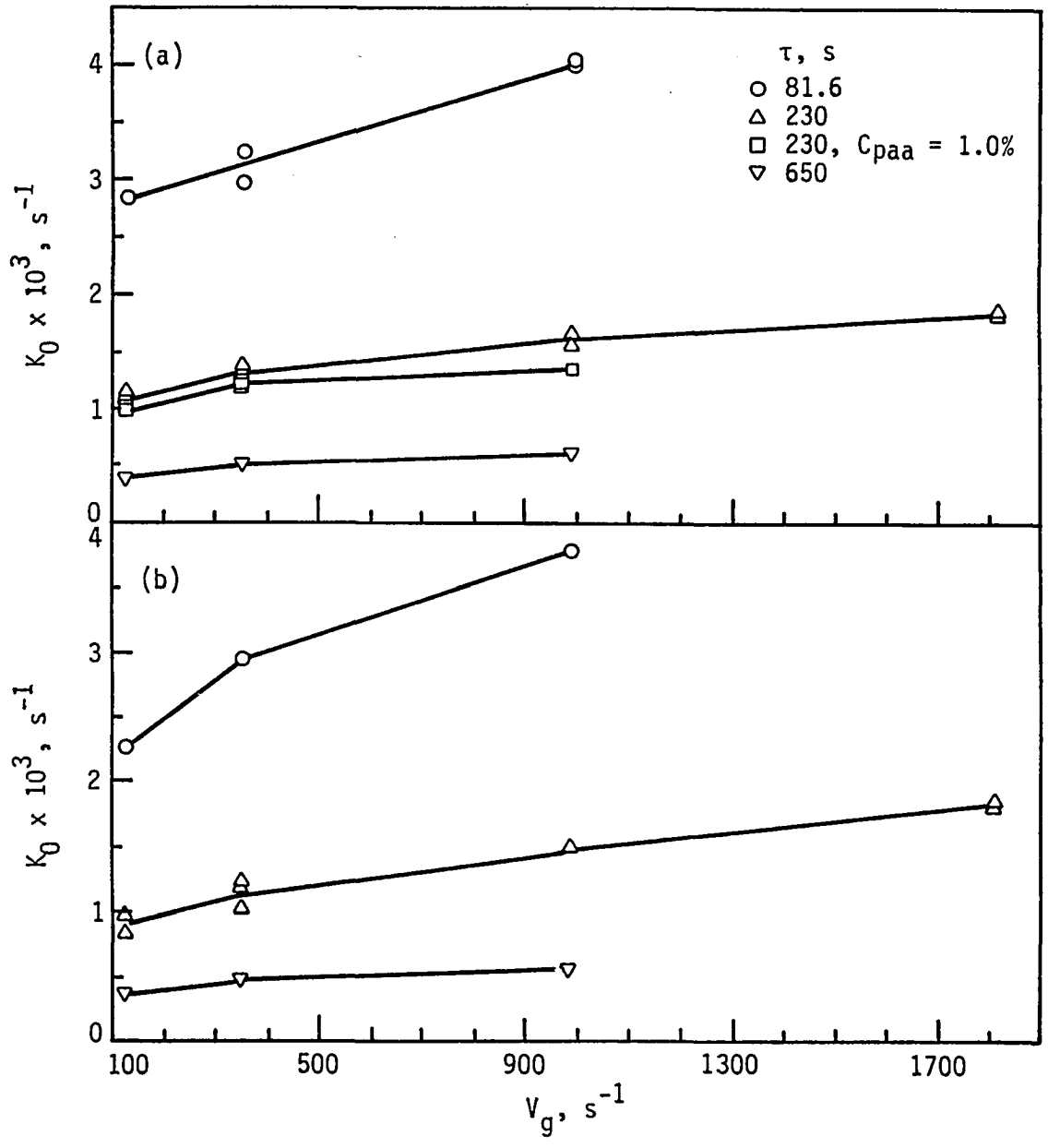

Figure 3. Effects of shear (V_g) and residence time (τ) on K_0 (Equation 5): (a) first-order death, (b) second-order death. Clusters of data points indicate variance

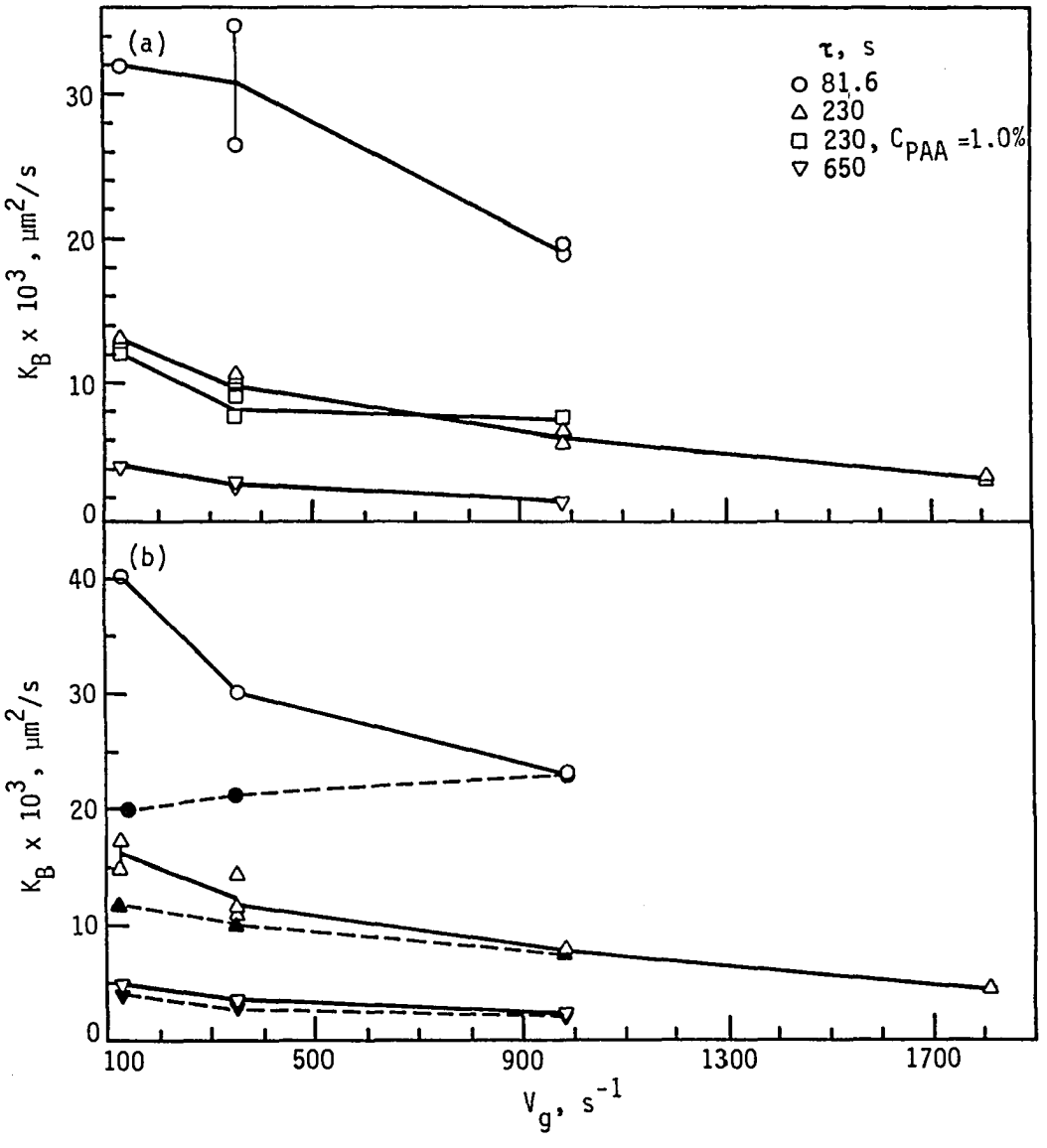

Figure 4. Effects of shear (V_g) and residence time (τ) on K_B (Equation 8): (a) first-order death; (b) second-order death, including data (----) from polymer-enhanced-growth models (Equation 20)

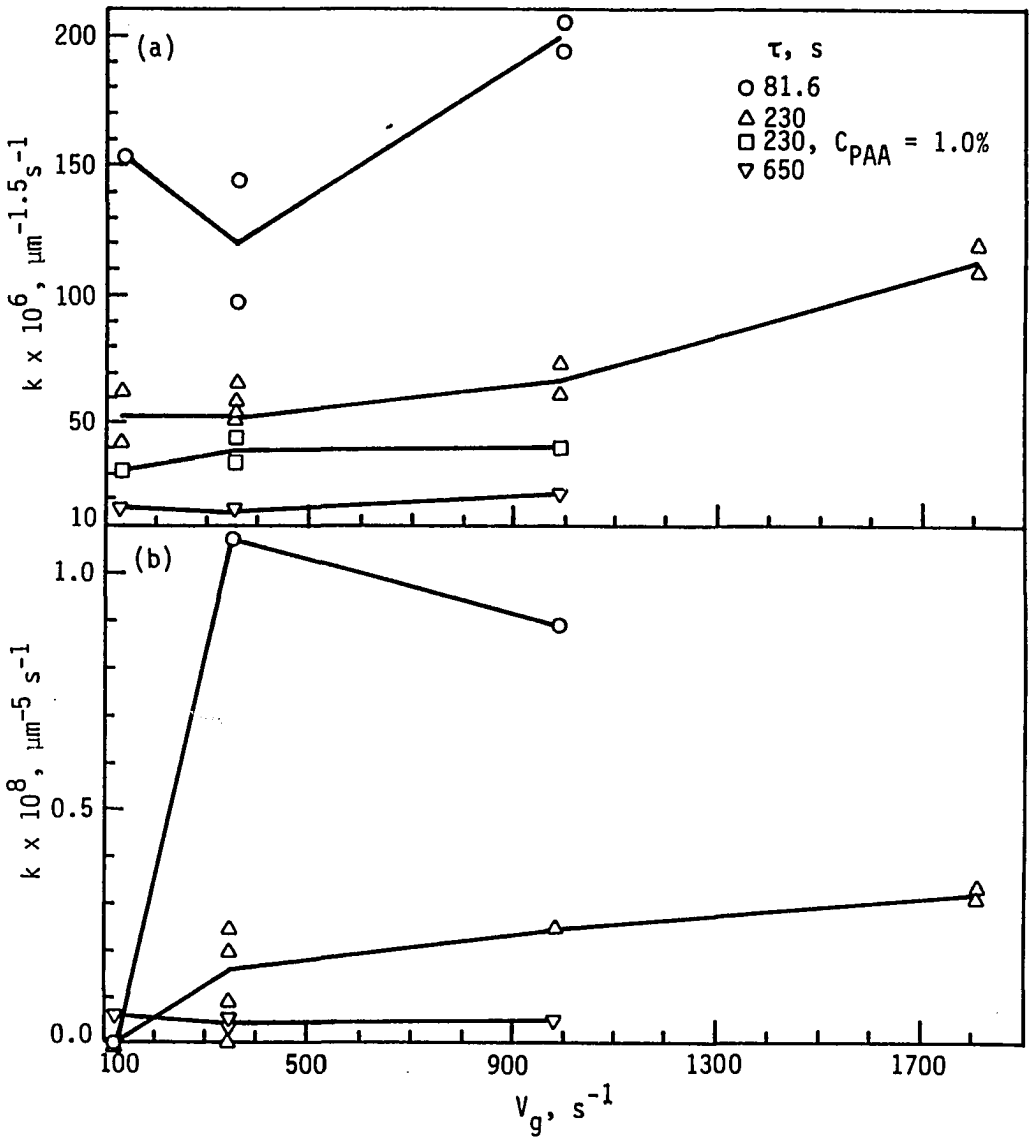

Figure 5. Effects of shear (V_g) and residence time (τ) on k: (a) first-order death (Equations 10 and 11); (b) second-order death (Equations 12 and 13)

Table 1. Analysis of variance[a] of model constants giving probabilities that the variable (V_g, τ, or $V_g x \tau$) does not affect the response (SAS, Type III sum of squares)

Response	V_g			τ			$V_g x \tau$		
	df	F	Pr>F	df	F	Pr>F	df	F	Pr>F
first-order death									
K_0	3	34.61	0.0001	2	272.9	0.0001	4	3.69	0.0352
K_B	3	339.5	0.0001	2	2611.5	0.0001	4	44.02	0.0001
k	3	327.4	0.0001	2	5439.9	0.0001	4	54.03	0.0001
second-order death									
K_0	3	6.86	0.0319	2	39.56	0.0009	4	19.56	0.0030
K_B	3	39.62	0.0007	2	417.0	0.0001	4	9.63	0.0144
k	3	94.05	0.0001	2	1068.7	0.0001	4	23.63	0.0019

[a]ANOVA, SAS General Linear Models using unbalanced data.

layer of solvent; nonporous, smooth, and rigid spheres would require very high attractive energies to overcome this barrier. Wolynes and McCammon (21) have found that hydrodynamic barriers are greatly reduced for porous particles; such effects would give higher collision frequencies. Second, these loosely bound aggregates are also expected to undergo more deformation than a tightly packed aggregate upon collision, leading to an increased adhesive force (22) and a higher collision efficiency.

To quantify the contributions of growth, outflow, breakage, and birth in the population balance (Equation 1), values of each of these terms were calculated for a given L, based on values of n from plots of the model solutions and constants returned from the fit. Table 2 lists selected results. They reveal that breakage played only a minimal role in these precipitations, and, even for large aggregates, particle outflow was as significant as breakage. Using the second-order-breakage model, breakage accounted for less than 2% of the total number density change with time for particles smaller than 8 μm, and less than 50% at 16 μm, even at the higher shear rate. For first-order breakage, the breakage term represented less than 25% of the total at 8 μm and less than 50% at 16 μm. The trends reported here are consistent with the qualitative characterization of the PSDs which show little breakage of larger particles.

Theoretical values of growth constants

Values of the kinetic constants K_0 and K_B can be theoretically approximated based on Equations 5 and 8. To calculate K_0 (Equation 5), we first assume $C_{pf} = 1$. The volume fraction of growth units, ϕ_1, is obtained from the model solution as the volume of counted aggregates

Table 2. Contributions of growth, outflow, breakage, and birth to the population-balance equation; calculated using kinetic constants returned by the models (Equations 9 and 10 or 12)

Run	Breakage mechanism	L μm	Population balance term (μm^{-3} ml^{-1} s^{-1})			
			D(k,L,β,n)	B(D)	$\frac{n}{\tau}$	$\frac{-d(Gn)}{dL}$[a]
8a[b]	$D=k_h L^{1.5} n$	16	55.8	52.6	65.2	68.4
		8	307	432	1057	932
		4	980	1380	9521	9120
8a	$D=k_c L^9 n^2$	16	13.8	44.4	955	924
		8	2.19	12.9	8620	8610
		4	0.047	0.51	28600	28600
8c[c]	$D=k_h L^{1.5} n$	16	205	129	117	193
		8	485	914	783	354
		4	938	1454	4283	3770
8c	$D=k_c L^9 n^2$	16	101	66.1	106	141
		8	7.24	28.6	640	619
		4	1.15	5.55	5780	5770

[a] Calculated by difference, so that Equation 1 is satisfied.

[b] $V_g = 348\ s^{-1}$, $\tau = 230$ s.

[c] $V_g = 984\ s^{-1}$, $\tau = 230$ s.

smaller than 2.06 μm (an arbitrarily chosen upper size limit for the growth units). It has been reported (23) that A = 1.67, for particles within the viscous subrange such that L < η, neglecting electrostatic repulsion, and assuming $\alpha_s = 1$, where

$$\eta = \left[\frac{\nu^2 \rho}{V_g^2}\right]^{1/4} \tag{16}$$

Using these constants, values for K_0 are in order-of-magnitude agreement with those returned from the model (see Table 3). It is reasonable that, for these apparently strong aggregates, larger particles may serve as growth units. For example, if L_1 is increased to 3.1 μm, ϕ_1 increases a factor of 3 to 4 and brings the theoretical and model values of K_0 into closer agreement.

Table 3 shows (for each τ) that increases in V_g reduce the ratio of (model K_0)/(theory K_0). This observation is consistent with the physical understanding of the aggregate formation. We know that increasing V_g will decrease the Kolmogorov microscale. Thus the size where convective overcome diffusive forces will also decrease with V_g. As a result, it is expected that L_1--thus ϕ_1 and K_0--will also decrease with V_g. This effect may explain the trends of model and theory shown in Table 3. Alternatively, if the V_g effects on K_0 are attributed to collision efficiency, one would expect (24) increased shear to lead to a reduction in α_s, which is also shown.

K_B, when calculated from Equation 8 using L_1 = 1.66 μm (the mean size of the growth unit) and ϕ_1 as before, returns values four orders of magnitude smaller than those of the model solution. Clearly, Brownian

Table 3. Values of growth-rate constants returned by the model and calculated from theory (Equation 5)

Run	V_g s^{-1}	τ s	$K_{0,model}$[a] x 10^6 s^{-1}	$K_{0,theory}/\alpha_s$[b] x 10^6 s^{-1}	$\left(\frac{K_{0,model}}{K_{0,theory}}\right)$
4b	123	650	409	271	1.51
7c	123	230	1114	227	4.91
5a	123	81.6	2847	258	11.0
$4c_1$	348	650	527	707	0.75
7a	348	230	1298	601	2.16
$3b_1$	348	81.6	2980	643	4.63
4a	984	650	636	2080	0.31
7b	984	230	1571	1830	0.86
3a	984	81.6	4041	1960	2.06

[a]Solution using model form of Equation 9 and second-order death (Equation 12).

[b]Based on Equation 5.

growth alone does not account for the high growth rates at the small sizes.

Characteristics of the Model Constants

By considering the constants K_0, K_B, and k in relation to system parameters (as suggested by their derivations), we can gain insight into the validity of the mechanisms used.

Hydrodynamic growth

The growth constant, K_0, has been plotted versus $V_g\phi_1$ for both first- and second-order-breakage models (Figure 6). Because the curves are not linear for all τ and do not extrapolate to the origin, as per Equation 5, the growth mechanism is not fully supported.

One assumption implicit with the description of K_0 is that α_s is invariant with time, as well as aggregate size, during precipitation. Figure 7 shows the effect of aggregate aging on α_s, as reflected in $A = K_0/(\phi_1 V_g)$ (Equation 5). It demonstrates that α_s is not constant, and that $V_g\tau$, the Camp number, accurately reflects the interaction of V_g and τ to decrease α_s. Further, Figure 7 shows a power law relationship between A and $V_g\tau$, such that for first-order breakage

$$A_h = g_h(V_g\tau)^{-0.84} \tag{17}$$

and for second-order breakage

$$A_c = g_c(V_g\tau)^{-0.80} \tag{18}$$

where g_h and g_c are independent of $V_g\tau$. The effects of the Camp number can be explained in terms of aging, where repeated aggregate-aggregate

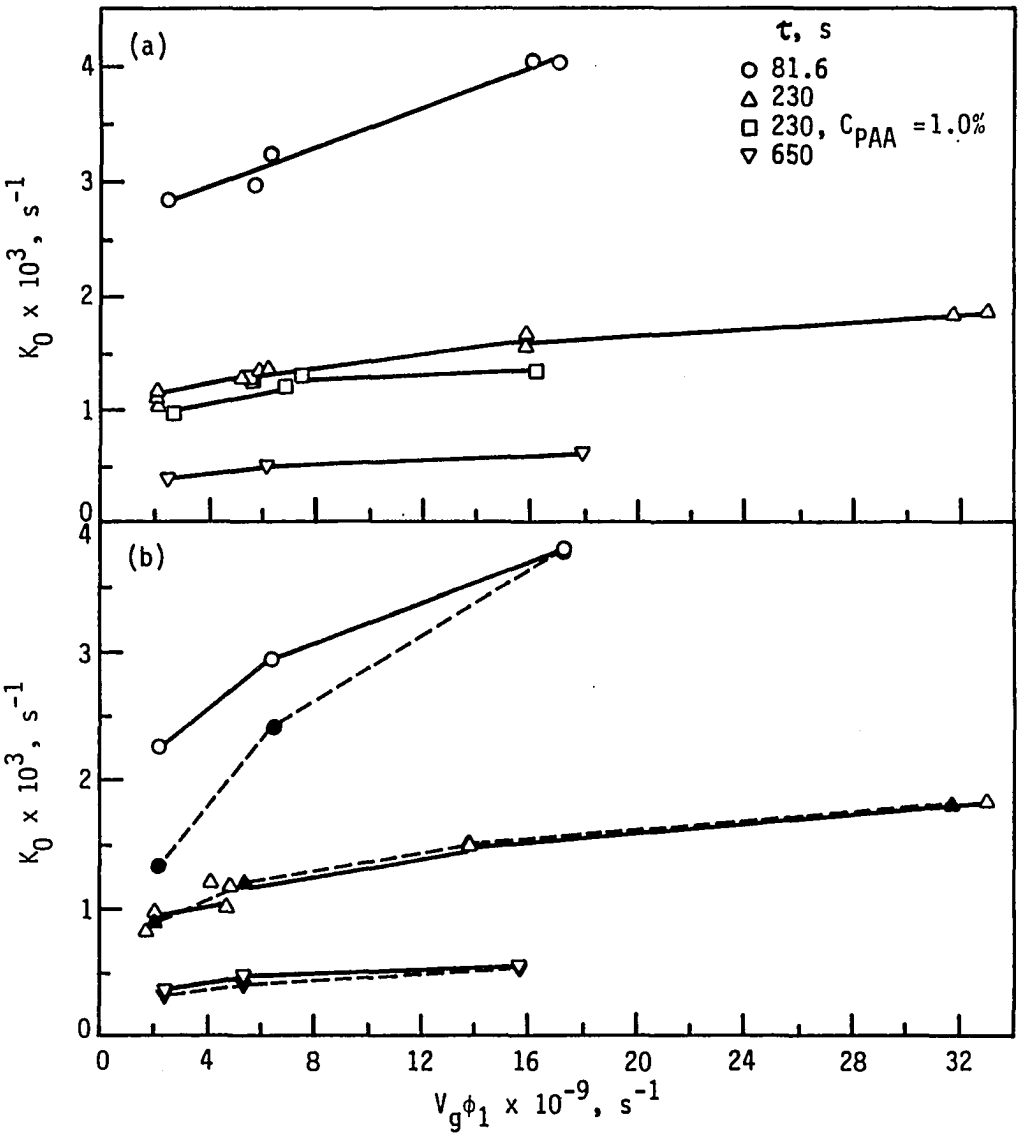

Figure 6. Dependence of K_0 on $V_g\phi_1$ (Equation 5): (a) first-order death; (b) second-order death, including data (----) from polymer-enhanced-growth model (Equation 20)

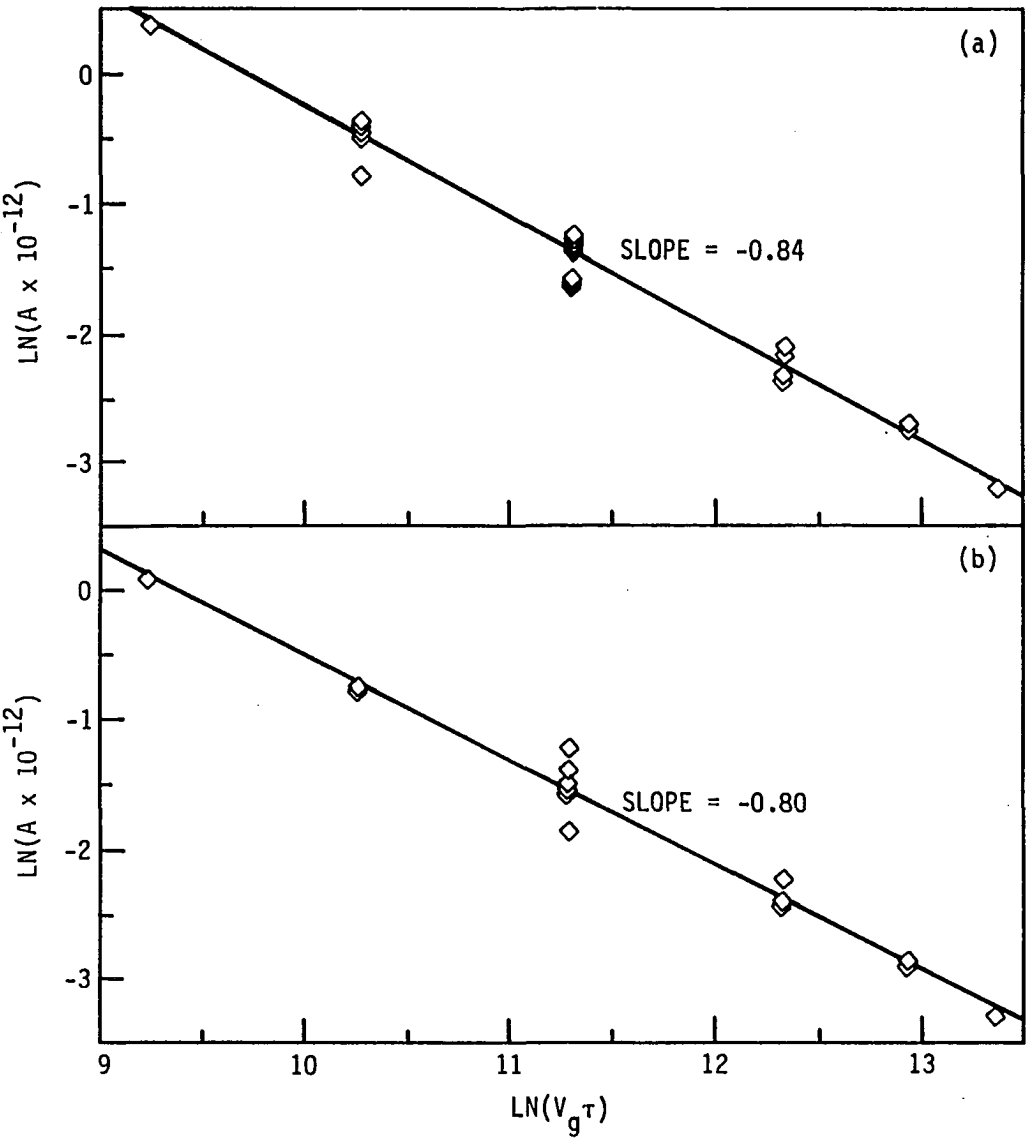

Figure 7. Dependence of collision-effectiveness factor (A) on $V_g\tau$: (a) first-order death; (b) second-order death

collisions--increasing with longer residence times and higher shear rates--are expected to reduce the porosity of the surviving aggregates (17) and lower the collision efficiencies by "polishing" the aggregate surface (25); each of these changes would reduce A. Further, scission of the polymer, possible in a turbulent environment (26), and increasing with V_g and τ (27), would reduce A when bridging or patch formation were the predominant mechanisms for aggregation.

Brownian-type growth

For the range of conditions used, ϕ_1 varies little, from 13 x 10^6 to 18.4 x 10^6; therefore, the effect of ϕ_1 on K_B as indicated by Equation 8 is difficult to assess. Calculations using Equation 8 predict that for this range of ϕ_1, K_B will vary less than 0.001%; Figure 8, showing no observable change of K_B with ϕ_1, supports this prediction.

Breakage

From Equations 11 and 13, the dependence of k on V_g is shown theoretically for either model. The plots in Figure 9 show V_g effects to be small and scattered. Possibly, for the conditions used, aggregate breakage is not sufficiently pronounced to adequately test the death term in the model.

Growth Enhancement by Polymer Extensions

As discussed, the form of the second term in the growth-rate equation is based on a Brownian enhancement at small sizes. The ratio of theoretically derived Brownian growth rate to shear-driven growth rate is given by the ratio of collision rates (Equations 6 and 3).

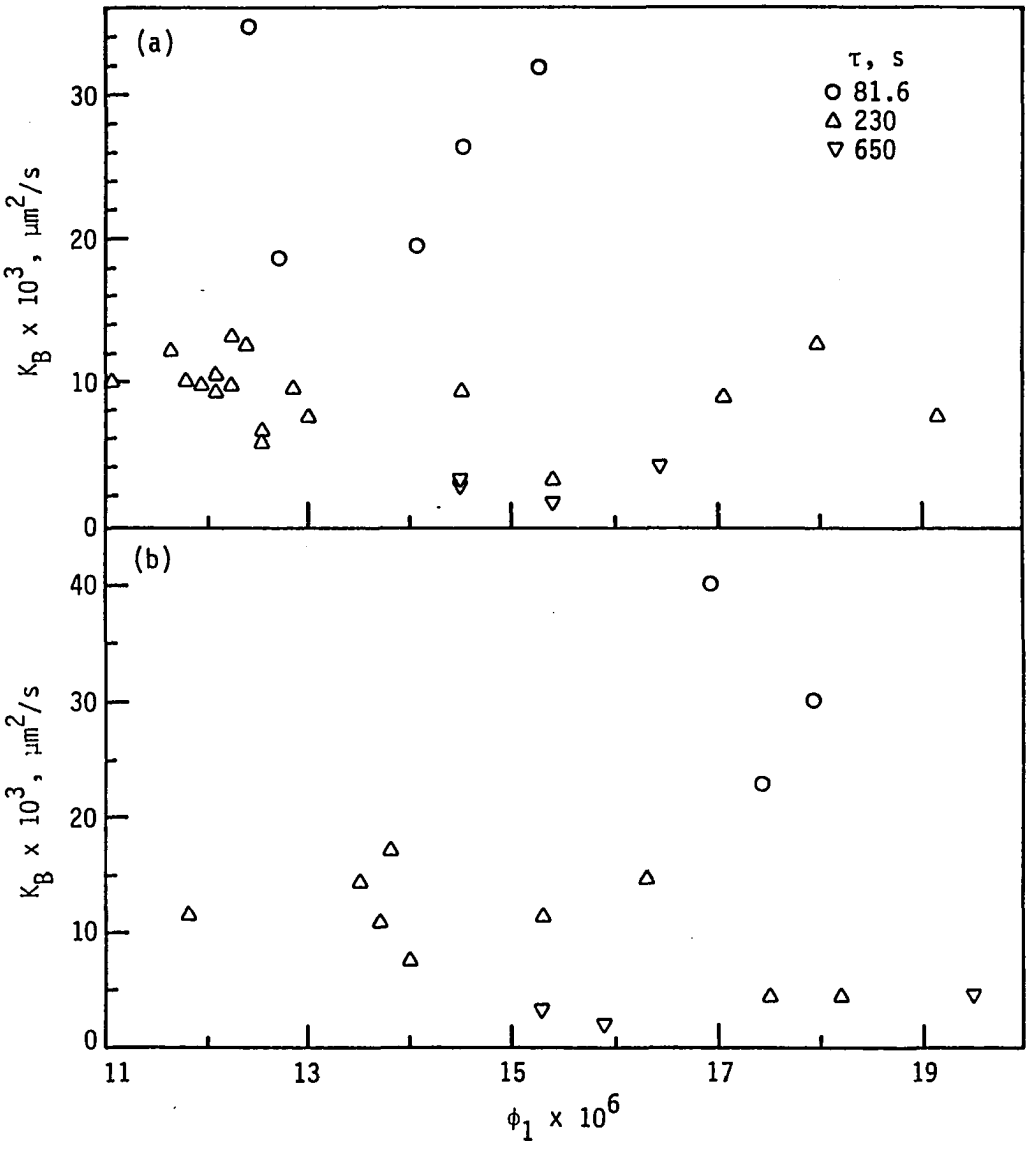

Figure 8. Dependence of K_B on ϕ_1 (Equation 8): (a) first-order death; (b) second-order death

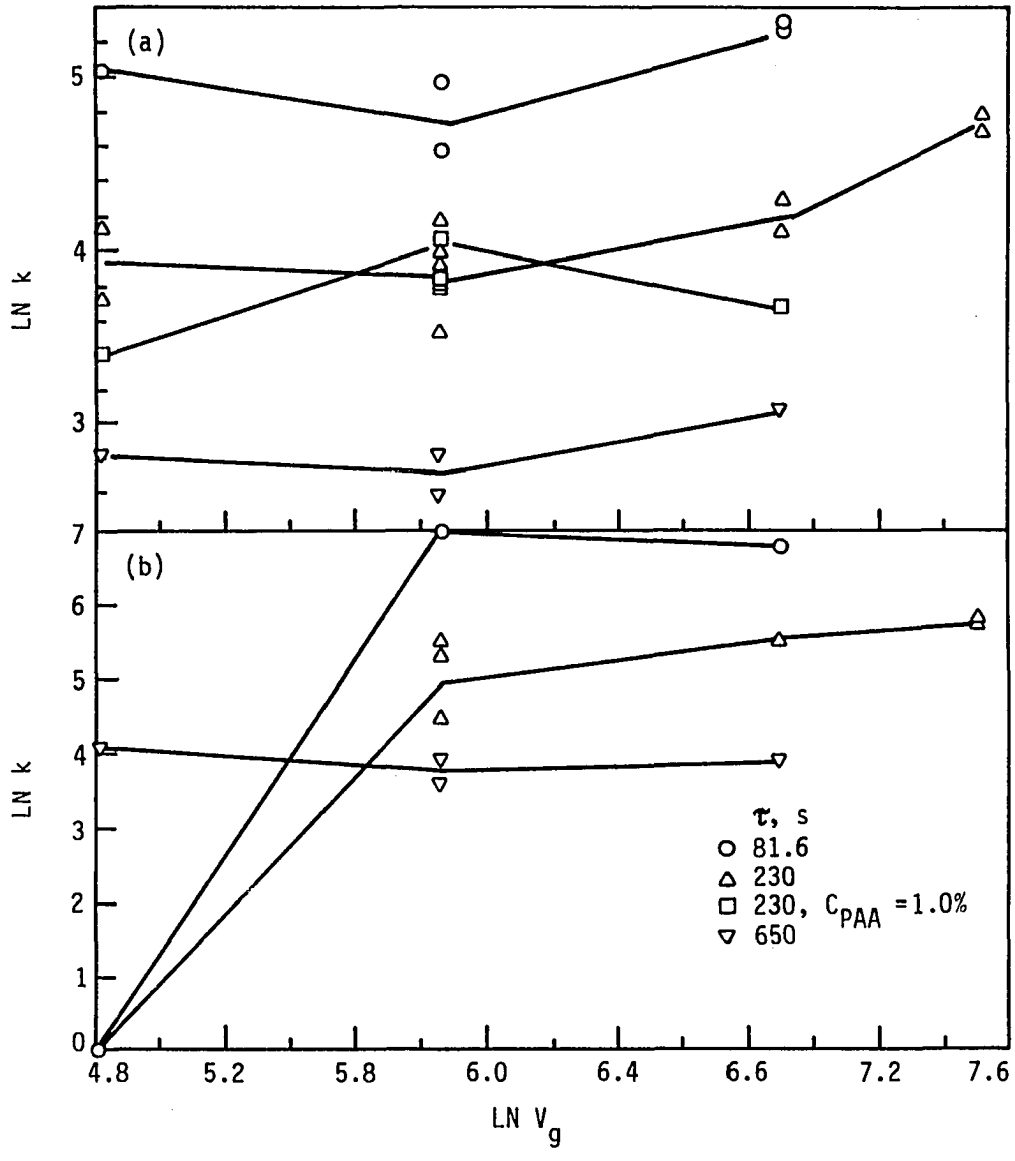

Figure 9. Dependence of k on V_g: (a) first-order death (Equation 11); (b) second-order death (Equation 13)

Assuming collision efficiencies are equivalent for each mechanism, the result shows a dependence on particle sizes and V_g

$$\frac{G_B}{G_s} = \frac{\frac{2}{3}\frac{kT}{\mu}\left(\frac{1}{L_1} + \frac{1}{L}\right)(L_1 + L)}{\frac{1.67}{8} V_g (L_1 + L)^3} = \frac{12.03}{V_g (L_1 L)(L_1 + L)} \tag{19}$$

for μ = 1.1 cP, L_1 in μm, and V_g in s^{-1}. In Table 4, values for this ratio and the analogous ratio calculated from the model constants--$(K_B/L)/(K_0 L)$--for representative conditions are compared, assuming primary particles of 0.5 μm. Clearly, the Brownian enhancement cannot account for the magnitude of the increased growth rates for small aggregates. The enhancement due to polymer extensions, proposed as a mechanism to bring better agreement to the theory, will be now shown to account for only a small part of this discrepancy.

Walles (28) has considered the effect of polymer extensions from colloidal particle surfaces during Brownian collisions and has derived an expression for enhancement of the collision rate as a function of h/L, where h is the length of the polymer extension from the particle surface. In this treatment, the particle with the extended polymer segments acts with an unchanged mass and mobility but with a larger collision radius.

The effects of the polymer extensions on the mechanistic forms of the growth-rate constants of the population model are derived in Appendix A, for the case where the polymer extensions are capable of forming an aggregate-aggregate bridge. The resulting growth rate is

$$G_e = K_0(L + m) + K_{B,e}/L \tag{20}$$

Table 4. Theoretical and model-derived ratios of Brownian- to shear-driven growth rate

Run	V_g s^{-1}	τ s	L μm	$\left(\frac{G_B}{G_s}\right)^a_{model}$	$\left(\frac{G_B}{G_s}\right)^b_{theory}$
8a	348	230	1.42	4.74	0.025
			5.69	0.296	0.0020
			9.97	0.097	0.00066
5a	123	81.6	1.42	8.78	0.072
			4.89	0.743	0.0074
			11.84	0.127	0.0013

[a] $\left(\frac{K_B/L}{K_0 L}\right)$, for second-order death (Equation 12), non-polymer-enhanced growth (Equation 9).

[b] From Equation (19), using L_1 = 0.5 μm (small growth unit).

where

$$m = 3L_1 + 2h \tag{21}$$

and

$$K_{B,e} = (1 + 2h/L_1)K_B \tag{22}$$

The PAA used in the present experiments will result in h values from 0.1 μm (6, 7), for a coiled polymer with 50% counterion binding, to h = 5 μm, for a 30% extended chain. Given a particle mass concentration of 0.08%, Walles shows that the theoretical Brownian collision rates will be enhanced up to 50-fold.

Model results using polymer enhancement

The population model incorporating the enhancement of polymer extension was run for both first- and second-order breakage, for various input values of m. In both models, with m = 4 μm, the Brownian/shear-growth ratio (G_B/G_s) decreased only 5% for low shear and 50% for high shear conditions. Thus, for reasonable values of h, the polymer enhancement did not account for the large K_B values at small sizes.

The polymer enhancement growth mechanism did not affect model fit to the data for the first-order-death model; the best fits--based on the sum-of-squares of residuals (SS)--for all precipitation conditions were for m = 0. In the first-order-death model, we have shown that breakage and birth are more important at the small sizes than for the second-order-death model (see Table 2). Apparently, because growth's relative role

is diminished at small sizes for first-order death, the effects of the enhancement on the fit are insignificant.

Using the second-order-death model, the polymer enhancement did improve fits for low-shear conditions, where m values (giving minimum SS) increase for decreasing $V_g\tau$ (see Table 5). The magnitudes of h are reasonable, where a 0.5 μm extension would give m = 3.5 μm, assuming a 0.5 μm growth unit. These results are consistent with the polymer-enhancement phenomena. As mean shear and aging increase, the polymer extensions are subjected to increasing magnitudes of tangential shear and more time available for the extension to flatten onto the particle surface; these effects additively reduce the extension length, h.

The physical interpretation of m = 0 requires some explanation. The derivation of K_0 (shown in Appendix A) requires assumptions regarding relative sizes. In the model for no polymer enhancement (where h is neglected), the assumption that $L_1 << L$ is typically used in the K_0 derivation. But since, in this case, h and L_1 are similar in size, L_1 cannot be summarily neglected. The assumption is made less strongly as $L_1^2 << L^2$, and L_1 remains in the term for m (Equation 21). However, as Table 5 shows, m for best fit is zero only at higher V_g conditions, where L_1 and h are expected to be smallest, and where $L_1 << L$ does hold. Thus, at high shear, m = 0 is equivalent to h = 0.

The growth constants returned by the polymer-enhanced growth, second-order-breakage model show improved agreement with the theory used to derive them. First, the data for K_0 vs. $V_g\phi_1$ (Figure 6(b)), show a slightly better extrapolation to the origin, as Equation 5 predicts.

Table 5. Data from fits of polymer-enhanced growth model (Equation 20) using second-order death (Equation 12)

Run	V_g s^{-1}	τ s	m_{opt} [a] μm	% Decrease in SS [b]
4b	123	650	2	58
7c	123	230	2	77
5a	123	81.6	8	78
$4c_2$	348	650	0.5	1
8a	348	230	1	54
$3b_2$	348	81.6	2	67
4a	984	650	0	0
8c	984	230	0	0
$3a_1$	984	81.6	0	0
$8d_2$	1810	230	0	0

[a] Value of m (Equation 21) giving minimum residual-sum-of-squares.

[b] $(SS_{m=m_{opt}} - SS_{m=0})/SS_{m=0}$.

Second, the data in Figure 4(b) show that $K_{B,e}$ is less dependent on V_g, more in agreement with Equation 8.

Although the growth rate enhancement due to polymer extensions gives a better fitting model (for second-order breakage) with improved behavior from the growth constants, the large Brownian contribution to growth is not sufficiently accounted for. For the Brownian enhancement factor $(1 + \frac{2h}{L_1})$ to account for the 100-fold discrepancy between the model results and theory shown in Table 4, an h of 100 μm is required. (Walles (28) shows an h of 6 μm to increase the Brownian collision rate by a factor of 100, but in the present model, shear growth is also enhanced with h, causing $G_{B,e}/G_{s,e}$ to remain relatively constant.)

Consideration of the hydrodynamic environment may explain the unusually high $K_{B,e}$ values returned by the model. In a shear field, the tangential component of viscous shear-force on the surface of a suspended particle will increase with the square of the particle size (11). Given this, it is possible that the shear forces compress the polymer extensions more quickly on larger particles. As a result, the growth rates for smaller aggregates would be selectively enhanced, and the model fit would return a higher $G_{B,e}/G_{s,e}$ than predicted by the theory in Equation 19.

CONCLUSIONS

A population-balance model, used previously with PSDs created by small molecular-weight precipitants, has been applied to polyelectrolyte precipitation of proteins. The model has been altered to include an additional mechanism for growth at small aggregate sizes and to allow collisional (second-order) aggregate breakage. Also, we tested an enhancement to growth caused by polymer extensions from the protein particle surface.

The shear-growth constants showed an unexpected dependence on residence time, probably due to aging effects on collision efficiency. The values of the Brownian-growth constant are too high to be explained by the Brownian mechanism, even when the polymer enhancement is incorporated. Some other mechanism for preferential growth at small sizes, possibly of the form shown by the Brownian term, is supported by the model.

This system displayed unusually high rates of growth, even for large aggregates; the breakage phenomenon, usually dominant in protein precipitation, played a lesser role.

Based on residual sum-of-squares values, the model fits do not discriminate between either breakage mechanism, although second-order death produced dependencies in the polymer-enhanced growth consistent with a physical understanding of the phenomenon.

The effects of mean shear rate and residence time on the kinetic constants for growth (shear and Brownian) and death are all significant, yet not all predicted by theory. Given these dependencies, modifications

to or new forms of the mechanisms are in order for application of the model to polyelectrolyte precipitation.

The picture presented by the models is not inconsistent with that supported by the data (5), where bridging was implicated as the dominant mechanism for primary particle aggregation. A possible description for growth includes Brownian and shear collisions superimposed for small particles ($L < 3$ μm), where surface shear is sufficiently low to allow polymer tails to extend up to a few micrometers (at the impeller, where the polymer is introduced, the Kolmogorov microscale is on the order of 10 μm). Higher shear rates suppress the polymer extensions and reduce the relative effect of Brownian collisions. At larger sizes, the Brownian effect is negligible and the polymer enhancement effect is small.

ACKNOWLEDGEMENTS

This work was supported by a grant from the National Science Foundation (ECE 8514865).

REFERENCES

1. R. K. Scopes, Protein purification: principles and practice (Springer-Verlag, New York, 1982).

2. G. C. Grabenbauer and C. E. Glatz, Chem. Eng. Commun., 12, 203 (1981).

3. A. M. Petenate and C. E. Glatz, Biotechnol. Bioeng., 25, 3059 (1983).

4. C. E. Glatz, M. Hoare, and J. Landa-Vertiz, AIChE J., 32, 1196 (1986).

5. R. R. Fisher and C. E. Glatz, "Polyelectrolyte precipitation of proteins. I. The effects of reactor conditions," Iowa State University, Ames, IA (to be published).

6. F. Rodriguez, Principles of polymer systems, 2nd ed. (McGraw-Hill, New York, 1982).

7. S. A. Rice and F. E. Harris, J. Phys. Chem., 58, 725 (1954).

8. T. G. Parker and D. G. Dalgleish, Biopolymers, 16, 2533 (1977).

9. P. D. Virker, M. Y. Y. Chan, M. Hoare, and P. Dunnill, Biotechnol. Bioeng., 24, 871 (1982).

10. M. Y. Y. Chan, M. Hoare, and P. Dunnill, Biotechnol. Bioeng., 28, 387 (1986).

11. V. Levich, Physiochemical hydrodynamics (Prentice-Hall, Englewood Cliffs, NJ, 1962).

12. K. J. Ives, "Rate theories," in K. J. Ives, ed., The scientific basis of flocculation (Sijthoff and Noordhoff, Alphen aan den Rijn, The Netherlands, 1978).

13. L. A. Glasgow and R. H. Luecke, Ind. Eng. Chem. Fundam., 19, 148 (1980).

14. P. M. Huck and K. L. Murphy, J. Environ. Eng. Div., ASCE, 104, 767 (1978).

15. M. Twineham, M. Hoare, and D. J. Bell, Chem. Eng. Sci., 39, 509 (1984).

16. D. L. Brown and C. E. Glatz, Chem. Eng. Sci. (to appear).

17. D. J. Bell and P. Dunnill, Biotechnol. Bioeng., 24, 1271 (1982).

18. B. A. Firth and R. J. Hunter, J. Colloid Interface Sci., 57, 266 (1976).

19. L. A. Glasgow and J. P. Hsu, AIChE J., 28, 779 (1982).

20. C. D. Nelson and C. E. Glatz, Biotechnol. Bioeng., 27, 1434 (1985).

21. P. G. Wolynes and J. A. McCammon, Macromolecules, 10, 86 (1977).

22. B. Dahnke, J. Colloid Interface Sci., 40, 1 (1972).

23. S. Yuu, AIChE J., 30, 802 (1984).

24. P. M. Adler, J. Colloid Interface Sci., 83, 106 (1981).

25. M. Hoare, Trans. Inst. Chem. Eng., 60, 157 (1982).

26. A. H. Abdel-Alins and A. E. Hamlec, J. Appl. Polym. Sci., 17, 3769 (1973).

27. N. D. Sylvester and M. P. Toure, Ind. Eng. Chem. Prod. Res. Dev., 17, 347 (1978).

28. W. E. Walles, J. Colloid Interface Sci., 27, 797 (1968).

SUMMARY AND RECOMMENDATIONS

Summary

Isoelectric precipitation in a batchwise stirred vessel has been characterized. The mixing during acid addition--or, alternatively, the homogeneity of the change in pH--significantly affected the primary particle and aggregate size but not the final compositional character. Mixing effects on primary particle size and surface properties are understood in terms of protein "supersaturation" and the speed of protein incorporation into the primary particle. The primary particle properties in turn have effects on the strength and surface properties of the aggregate, as shown by size distributions and hindered settling behavior of the precipitate. The measured aggregate sizes were consistent with trends predicted by a floc model, where primary particle binding potential and size are important. Hindered settling, which occurs via further aggregation in a low-shear environment, is understood to occur more rapidly for particles with higher residual binding potential.

The use of polyacrylic acid to fractionally precipitate lysozyme from egg white proteins in a continuous system is characterized by high growth rates and large aggregates. The mixing properties of the reactor--mean shear rate and mean residence time--are shown to affect the aggregate size distribution of the product, but not its composition. Also, for this reactor configuration, a ten-fold difference in the inlet concentration of the polymer does not affect the precipitate properties. The size distributions show an augmented growth rate for particles smaller than 3 μm (implicating an additional mechanism at those sizes) and increases

of aggregate size with shear and residence time (indicating the dominance of growth over breakage). The Camp number is demonstrated to accurately incorporate the interaction of shear and residence time as affecting mean particle size. Resolubilization studies show that high yields of enriched lysozyme can be recovered from the precipitate, by way of a number of dissolution methods.

A population-balance model, applied to the continuous polyelectrolyte precipitation data, provides a means to test various mechanisms of growth, breakage, and birth. The model accounts for growth driven by turbulent shear, aggreage breakage due to hydrodynamic shear or aggregate-aggregate collisions, and sudden formation (birth) of aggregates due to breakage of larger aggregates. Model fits suggest that collisional breakage is the predominant breakage mode in this system. For adequate fit to the data, the model required an additional term to provide for growth at small sizes. This modification, theoretically based on Brownian-driven collisions, allowed good fit to the data, but returned growth rates in excess of predicted Brownian effects. A second modification to growth tested in the model allowed polymer extensions from the particles to enhance collision frequencies and growth rates. This mechanism slightly improved the model's fit to the data and agreement to theory, although it did not account for high growth rates seen in smaller aggregates. The precipitation shear rate and residence time affected all constants for growth and breakage, but not in total agreement with theoretically predicted dependencies. Collision effectiveness for growth was shown to decrease with aggregate aging, an effect not accounted for in the model.

Recommendations for Further Work

My recommendations for continued work in this area are generally concerned with an understanding of the fundamental phenomena occurring at various stages of the precipitation. A few areas of further investigation on polyelectrolyte precipitation are also suggested.

Experimental

1. Precipitations run at higher residence times, to increase the aggregate sizes and the relative importance of breakage, will allow a more complete test of the death term in the model.

2. Changes in the molecular weight of the polymer have been used to test the existence of bridging or patch formation (17); such changes are suggested here.

3. The distribution of the polyelectrolyte in the system is valuable information, especially when testing for dosage effects on the precipitation; however, the assay of charged polymers in the presence of proteins (charged biopolymers) is difficult. Ion exchange chromatography and labelled polymer scintillation (49) are possible methods to accurately assay the polymers.

4. The assays for polymer should also include a method to determine the extent of scission, especially to test the link between collision efficiency decreases and polymer breakdown.

5. Studies of the effects of protein concentration, pH, ionic strength, and polymer dosage on the precipitate properties can give information concerning important mechanisms. Such work for continuous

systems is needed. Most solubility work of this type is performed in batch studies, where micro-environments and mechanisms may be significantly different.

6. Precipitations run in a known shear field (couette or laminar tube flow) would reduce the effects of different shear zones in the precipitator, which are difficult to characterize and model.

7. Measurements of aggregate strength, possible by a number of methods, could be related to aggregate size; the effects of polymer size, aging, and other conditions on strength could then be studied.

8. The natures of the primary particle and growth unit are very important to the development of a physical model of aggregation. The use of probes which give information about these species during the precipitation is recommended. For example, in batch studies, the use of in situ light scattering techniques (41) may allow transient measurements of primary particle formation and size, or may provide measurements of spacial variation in flow precipitators.

9. Improvements in precipitant dispersion and aggregate aging are expected using motionless mixers as precipitators. Continuous flow precipitations--possibly with a recycle stream--using a variety of motionless-mixer geometries are suggested.

Theory and modeling

1. The data and analysis suggest that collision effectiveness for growth is a function of $V_g\tau$. Such a dependence could be incorporated into the development of the K_0 term, where K_0 would be expected to decrease with increasing $V_g\tau$.

2. The model does not account for the up to 200-fold variation in local shear rates (14) in a stirred tank. Variations in the shear environment during circulation, resulting in separate regions of growth and breakage (50), have been characterized by models of fluid hydrodynamics (51). Incorporating such zonal or temporal changes into the population balance may greatly extend the model's applicability to different reactor types.

3. If the polyelectrolyte system gives growth units as large as 3 μm, as has been postulated to explain high K_0 values, then the model assumption of incremental addition may be violated; if so, more discrete summations may be required in the particle accounting scheme.

ADDITIONAL LITERATURE CITED

1. E. Bjurstrom, Chem. Engrg., 92, 126 (1985).

2. M.-R. Kula, H. Hustedt, K. H. Kroner, H. Schutte, Biotech '83, January, 359 (1983).

3. A. Wiseman, ed., Principles of biotechnology (Chapman and Hall, New York, 1983).

4. J. E. Bailey and D. F. Ollis, Biochemical engineering fundamentals, 2nd ed. (McGraw-Hill, New York, 1986).

5. M. D. Scawen and J. Melling, "Practical aspects of large-scale protein purification," in A. Wiseman, ed., Handbook of enzyme biotechnology, 2nd ed. (John Wiley, New York, 1985).

6. D. J. Bell, M. Hoare, and P. Dunnill, Adv. Biochem. Eng., 26, 1 (1983).

7. M. Scheider, C. Guillot, and B. Lamy, Ann. N. Y. Acad. Sci., 369, 257 (1981).

8. R. D. Hill and J. G. Zadow, New Zealand J. Dairy Sci. Technol., 13, 61 (1978).

9. M. Hoare, D. J. Bell, and P. Dunnill, "Process design for the recovery of food proteins by precipitation and centrifugation," in B. M. McKenna, ed., Engineering and food, Vol. 2. Processing applications (Elsevier Applied Science Publishers, New York, 1984).

10. F. Rothstein, V. M. Rosenoer, and W. L. Hughes, "Current concepts concerning albumin purification," in W. M. Rosenoer, M. Oratz, and M. A. Rothschild, eds., Albumin structure, function, and uses (Pergamon Press, New York, 1977).

11. B. L. Ramaley, D. F. Lawler, W. C. Wright, and C. R. O'Melia, J. Envir. Engr. Div. ASCE, 107, 547 (1981).

12. J. W. S. Goossens and P. Luner, TAPPI J., 59, 89 (1976).

13. E. Dickenson and G. Stainsby, Colloids in food (Applied Science Publishers, London, 1982).

14. D. T. Tomi and D. F. Bagster, Trans. I. Chem. E., 56, 1 (1978).

15. R. K. Scopes, Protein purification: principles and practice (Springer-Verlag, New York, 1982).

16. J. T. G. Overbeek, "Electrochemistry of the double layer," in H. R. Kruyt, ed., Colloid science, Vol. I (Elsevier Publishing Company, New York, 1952).

17. D. R. Kasper, "Theoretical and experimental investigations of the flocculation of charged particles in aqueous solutions by polyelectrolytes of opposite charge," Ph.D. thesis, Calif. Inst. of Tech., Pasadena, CA, 1971.

18. J. Lyklema, in K. J. Ives, ed., The scientific basis of flocculation (Sijthoff and Noordhoff, Alphen aan den Rijn, The Netherlands, 1978).

19. G. C. Grabenbauer and C. E. Glatz, Chem. Eng. Commun., 12, 203 (1981).

20. C. D. Nelson and C. E. Glatz, Biotechnol. Bioeng., 27, 1434 (1985).

21. K. J. Ives, "Rate theories," in K. J. Ives, ed., The scientific basis of flocculation (Sijthoff and Noordhoff, Alphen aan den Rijn, The Netherlands, 1978).

22. C. E. Glatz, M. Hoare, and J. Landa-Vertiz, AIChE J., 32, 1196 (1986).

23. D. J. Bell and P. Dunnill, Biotechnol. Bioeng., 24, 1271 (1982).

24. J. O. Hinze, Turbulence, 2nd ed. (McGraw-Hill, New York, 1975).

25. L. A. Glasgow and R. H. Luecke, Ind. Eng. Chem. Fundam., 19, 148 (1980).

26. M. Twineham, M. Hoare, and D. J. Bell, Chem. Eng. Sci., 39, 509 (1984).

27. D. L. Brown and C. E. Glatz, Chem. Eng. Sci. (to appear).

28. Y. Argaman and W. J. Kaufman, J. Sanitary Eng. Div., Proc. ASCE, 96, 223 (1970).

29. D. T. Tomi and D. F. Bagster, Trans. I. Chem. E., 56, 9 (1978).

30. F. B. Birkner and J. J. Morgan, J. AWWA, 60, 175 (1968).

31. A. Randolph and M. Larson, Theory of particulate processes (Academic Press, New York, 1971).

32. A. M. Petenate and C. E. Glatz, Biotechnol. Bioeng., 25, 3059 (1983).

33. N. S. Tavare and J. Garside, "Mixing, reaction and precipitation in an MSMPR crystallizer: effects of reaction kinetics on the limits of micromixing," in S. J. Jancic and E. J. de Jong, eds., Industrial crystallization '84 (Elsevier Science Publishers B.V., Amsterdam, 1984).

34. L. A. Glasgow and J. P. Hsu, AIChE J., 28, 779 (1982).

35. F.J. Glavis, "Poly(acrylic acid) and its homologs," in R. L. Davidson and M. Sittig, eds., Water-soluble resins (Reinhold, New York, 1968).

36. M. Sternberg, Proc. Biochem., 11, 11 (1976).

37. M. Sternberg, J. P. Chiang, and N. J. Eberts, J. Dairy Sci., 59, 1042 (1976).

38. K. Hamaguchi and K. Hayashi, "Lysozyme," in M. Funatsu, K. Hiromi, K. Imahori, T. Murachi, and K. Narita, eds., Proteins, structure and function, Vol. 1 (John Wiley, New York, 1972).

39. R. C. Warner, "Egg proteins," in H. Neurath and K. Baily, eds. The proteins; chemistry, biological activity, and methods (Academic Press, New York, 1954).

40. I. D. Robb, "Stereo-biochemistry and function of polymers," in K. C. Marshall, ed., Microbial adhesion and aggregation (Springer-Verlag, New York, 1984).

41. J. Gregory, "Effects of polymers on colloid stability," in K. J. Ives, ed., The scientific basis of flocculation (Sijthoff and Noordhoff, Alphen aan den Rijn, The Netherlands, 1978).

42. R. A. Stratton, TAPPI J., 66, 141 (1983).

43. J. Gregory, J. Colloid Interface Sci., 42, 448 (1973).

44. V. K. LaMer and T. W. Healy, Rev. Pure Appl. Chem., 13, 112 (1963).

45. T. R. Camp and P. C. Stein, J. Boston Soc. Civil Eng., 30, 219 (1943).

46. R. L. Bates, P. L. Fondy, and R. R. Corpstein, Ind. Eng. Chem., 2, 310 (1963).

47. R. O. Keys and R. Hogg, AIChE Symposium Series No. 190, 75, 63 (1979).

48. R. R. Fisher, "Studies of the effects of reactor conditions during precipitation on the physical and compositional properties of proteins using acid or polyelectrolytes. A preliminary research report," Iowa State University, Ames, Iowa, 1985 (unpublished).

49. A. P. Black, F. B. Birkner, and J. J. Morgan, J. Colloid Interface Sci., 21, 626 (1966).

50. M. Tanaka, Can. J. Chem. Engrg., 63, 723 (1985).

51. M. A. Zeitlin and L. L. Tavlarides, Can. J. Chem. Engrg., 50, 207 (1972).

ACKNOWLEDGEMENTS

My sincere appreciation goes to Chuck Glatz, for guiding me through this task and for helping me develop a scientific style and ethic. I am thankful for his counsel and friendship.

I also wish to thank those on my program-of-study committee--Dick Seagrave, Peter Reilly, Karl Gwiasda, and Pat Murphy--for their assistance and advice throughout my studies.

Finally, I thank Nancy, my very patient partner and wife.

APPENDIX A

Derivation of the Growth Constants Incorporating the Effects of Polymer Extensions from the Particles

The derivation is parallel to that of Petenate (1), in which the total flux of particles (radius r_1) approaching a growing aggregate, (radius r_2) is, at steady state, invariant with r, the distance from the center of the aggregate. It is assumed that the polymer-coated particles have the same mass and mobility as an uncoated particle, but that the total collision radius is increased by h, the distance that the polymer extends away from the surface (2).

Modification of the shear-growth term

The diffusion equation (3) describes the distribution of N_1

$$\frac{d}{dr}\left(D_T r^2 \frac{dN_1}{dr}\right) = 0 \qquad \text{(A1)}$$

with boundary conditions (4)

1. $N_1 = 0$ at $r = R_{12} + h$ ($= r_1 + r_2 + h$); 1-particles become 2-particles upon collision, and the polymer extension increases the effective collision radius for each particle in the collision (i.e., both particles in the collision have the polymer extensions, and the extensions may link to form a bridge).

2. $N_1 = N_{1,0}$ as $r \to \infty$; far from the collector, the 1-particles are at some original concentration.

D_T is the turbulent diffusion coefficient, a function of shear and length scale (3)

$$D_T = A' V_g r^2 \tag{A2}$$

The solution of Equation A1 yields a gradient of 1-particles at the collision surface of the collector

$$\frac{dN_1}{dr} = \frac{3\ N_{1,0}}{r^4}\ (R_{ij} + h)^3 \tag{A3}$$

From the gradient, the flux of particles across the $R_{12} + h$ surface gives the collision frequency for a single collector

$$\frac{dN_1}{dt} = 12\pi N_{1,0}\ (R_{12} + h)\ D_T \tag{A4}$$

The total number of collisions in the system is then given using Fick's first law for diffusion to a sphere

$$\frac{dN_{12}}{dt} \equiv b_{12,s} = 12\ N_1 N_2\ A' V_g\ (R_{12} + h)(R_{12})^2 \tag{A5}$$

The values prediced by such collision theory may be significantly wrong, as noted by Petenate (1), but the functional form of the collision rate is considered correct.

Following the method used in the development of the model, the volume rate of change of the aggregate, assuming spherical particles, becomes

$$\frac{dV_2}{dt} = \frac{\pi}{2} L_2^2 \frac{dL_2}{dt} = \frac{\alpha_s b_{12} V_1}{N_2} = \alpha_s 12\pi A' V_g (R_{12} + h)(R_{12})^2\ N_1 V_1 \tag{A6}$$

The linear growth rate is then given by

$$G_s \equiv \frac{dL_2}{dt} = K_0(L_2 + m) \tag{A7}$$

where

$$K_0 = \frac{A}{4\pi} V_g \phi_1 \tag{A8}$$

where $A = 12\pi A'$,

$$\phi_1 = N_1 V_1 \tag{A9}$$

and

$$m = 3L_1 + 2h \tag{A10}$$

As before, the 2-particle is the collecting aggregate ($L_2 = L$), and the 1-particle may be larger than the primary particle. In simplifying the form of K_0, it was assumed that $L_1^2 << L_2^2$.

Modification of the Brownian growth term

Beginning as for shear growth enhancement, the shell balance on 1-particles is used (Equation A1) using the same boundary conditions, where now the diffusion is Brownian and is given by (5)

$$D_1 = \frac{kT}{6\pi\mu}\left(\frac{1}{r_1}\right) \tag{A11}$$

The particle gradient becomes

$$\frac{dN_1}{dr} = \frac{N_0 (R_{12} + h)}{r^2} \tag{A12}$$

and the collision frequency for a single 1-particle is

$$\frac{dN_1}{dt} = 4 \pi N_{1,0} (R_{12} + h) D_1 \tag{A13}$$

The total collision frequency is

$$\frac{dN_{12}}{dt} = b_{12,B} = \frac{2}{3} \frac{kT}{\mu} N_1 N_2 \left(\frac{1}{r_1} + \frac{1}{r_2} \right) (r_1 + r_2 + h) \tag{A14}$$

Making the same substitution for volume change with time as in Equations A6 and A7 gives

$$G_B = K_{B,e}/L_2 \tag{A15}$$

where, assuming $L_1 << L_2$,

$$K_{B,e} = \left(1 + \frac{2h}{L_2} \right) K_B \tag{A16}$$

and K_B is given as before (Equations 7 and 8). The assumption just used is weakest at small aggregate sizes, where the enhancement factor in Equation A16 approaches $(2 + 4h/L_2)$. However, since the predictions of h will be approximate, the exact power of the enhancement is subject to large variations. We observe that the Brownian-growth term is significant only at small sizes, and can therefore make $K_{B,e}$ independent of L_2 by substituting the growth-unit size into Equation A16,

$$K_{B,e} = \left(1 + \frac{2h}{L_1} \right) K_B \tag{A17}$$

REFERENCES

1. A. M. Petenate, "Kinetics of protein aggregate growth and breakage during isoelectric precipitation," Ph.D. thesis, Iowa State University, Ames, IA, 1982.

2. W. E. Walles, J. Colloid Interface Sci., 27, 797 (1968).

3. V. Levich, Physiochemical hydrodynamics (Prentice-Hall, Engelwood Cliffs, NJ, 1962).

4. K. J. Ives, "Coagulation and flocculation: Part II - Orthokinetic flocculation," in L. Svarovsky, ed., Solid liquid separation, 2nd ed. (Butterworths, London, 1981).

5. A. Einstein, Investigations on the theory of the Brownian movement (E. P. Dutton, New York, 1926).

APPENDIX B

Algorithm for the Solution of the Model

The population balance equations (from Equation 1) to be solved take this form:

$$\frac{dn}{dL} = \frac{n}{L}\left[\frac{k}{K_0} L^{\beta}\left[f^{1+\beta/3}\,\frac{n(f^{1/3}L)}{n(L)} - 1\right] - \left[1 + \frac{1}{K_0\tau}\right] + \frac{K_B}{K_0}\frac{1}{L^2}\right] \times \left[\frac{1}{1 + \frac{K_B}{K_0}\frac{1}{L^2}}\right] \tag{B1}$$

for first-order breakage and

$$\frac{dn}{dL} = \frac{n}{L}\left[\frac{k}{K_0} nL^{\beta}\left[f^{1+\beta/3}\,\frac{n^2(f^{1/3}L)}{n^2(L)} - 1\right] - \left[1 + \frac{1}{K_0\tau}\right] + \frac{K_B}{K_0}\frac{1}{L^2}\right] \times \left[\frac{1}{1 + \frac{K_B}{K_0}\frac{1}{L^2}}\right] \tag{B2}$$

for second-order breakage. These equations were fit to a sixth-order Chebyshev polynomial representation of the size distribution data using a nonlinear least-squares routine. Data were fit from 1.42 to 22.8 or 28.7 μm, where upper-size data were truncated due to low counts.

The solution of the differential equation, by a fourth-order Runga-Kutta method, required an initial guess of n at the largest aggregate size, and a backward solution of the equations (required because breakage of larger (mother) aggregates is needed to determine

birth at a given size). The boundary condition was the total aggregate volume, measured experimentally.

β and f values were first estimated from literature and exploratory runs of the model. The least-squares routine for the fit (ROUTINE ZXSSQ, IMSL Library, Iowa State University Computation Center) then returned a best fit of K_0, K_B, and k simultaneously. Fits of more than three parameters required inordinant computation time. The routine returned residuals at eleven equispaced points for the sum of squares, and convergence required a reduction in this value. The good-fit criterion that was always satisfied (others are possible) required that upon successive iterations, all three parameter estimates agree to three significant digits.

Typically, solutions required from twenty to forty runs of the integration subroutine, with five to ten adjustments of the model parameters.

Using the second-order breakage model, solutions were not obtainable for eight of the 24 conditions tried (usually an exponent overflow or underflow in the CPU caused the error). Apparently, the equations, having the n^3 term, were highly sensitive to parameter values, and certain combinations of data and constants acted to produce this behavior.

Fortran Program for First-Order Breakage Model

```
1.      C  LS3P1
2.
3.      C  FORTRAN PROGRAM LISTING
4.      C  USED 1986 BY ROD FISHER
5.
6.      C   LS3P(3 PARAMETERS) (AUG86) IS TO FIT THE LS MODEL--INCLUDING
7.      C      THE BROWNIAN GROWTH AT SMALL SIZES-- TO THE WHOLE RANGE
8.      C      OF DATA, SIMULTANEOUSLY.
9.      C
10.     C
11.     C   THIS MODEL USES TURBULENT-SHEAR DRIVEN GROWTH WITH BROWNIAN GROWTH
12.     C       AND BREAKAGE INTO A FEW FRAGMENTS.  BREAKAGE IS BY HYDRODYNAMIC
13.     C       SHEAR (FIRST ORDER IN n).
14.     C
15.     C *THIS PROGRAM HAS BEEN ALTERED TO MAKE IT AGREE WITH D.L.B.'S
16.     C    ALTERATIONS ON PFIT (OR PSD); DLOW AND DHIGH ARE READ IN--THESE
17.     C    ARE LOWEST EDGE OF SMALLEST CHANNEL AND HIGHEST EDGE OF LARGEST
18.     C    CHANNEL.
19.     C
20.           IMPLICIT REAL*8 (A-H,O-Z)
21.           DIMENSION A(8),X(3),Y(200),D(200),SCALE(4),TITLE(10)
22.           DIMENSION PARM(4),F(11),XJAC(11,3),XJTJ(6),WORK(43)
23.           COMMON /BLOCK1/A,EXVOL,BETA,VTOL,D,BDRYY,DAU,SCALE,IDP,IMAX
24.          1 /BLOCK2/DMIN,DMAX,DELD,Y,DLOW,DHIGH,GAM,TAU
25.           EXTERNAL FUNGM
26.           DATA NIN,NOUT/11,6/
27.           READ (NIN,55555) TITLE
28.     55555 FORMAT(10A8)
29.           READ (NIN,*) N,M,IDP,IMAX,DMIN,DMAX,DGROW
30.     C N,# PARAMETERS; M,# OF RESIDUES CALCULATED; IDP,CHEBYSHEV DEGREE + 1;
31.     C IMAX, #RK STEPS + 1; DMIN,DMAX, SMALLEST AND LARGEST PARTICLE SIZES.
32.           READ (NIN,*) VTOL,DLOW,DHIGH
33.     C VTOL IS FRACTIONAL ERROR ALLOWED IN VOL BALANCE BOUNDARY CONDITION.
34.           READ (NIN,*) (A(I),I=1,IDP)
35.           READ (NIN,*) (X(I),I=1,N),BETA,BDRYY
36.           READ (NIN,*) DAU,SCALE,TAU,GAM
37.     C X, PARAMETERS; A, CHEBYSHEV COEFFICIENTS.
38.           WRITE (NOUT,*) '   THE KO*L+GKB/L**GAM MODEL, 3 PARAMS. '
39.           WRITE (NOUT,55554)TITLE
40.     55554 FORMAT(1X,10A8)
41.           WRITE (NOUT,99999) N,M,IDP,IMAX,DMIN,DMAX,VTOL,DLOW,DHIGH
42.           WRITE (NOUT,99998) (A(I) ,I=1,IDP)
43.           WRITE (NOUT,99997) BDRYY,(X(I), I=1,N)
44.           WRITE(NOUT,99996) BETA,GAM,TAU
45.     C   BETA IS POWER ON n OF BREAKAGE FUNCTION
46.     C   GAM IS POWER OF SIZE IN BROWNIAN GROWTH TERM
47.     C   TAU IS MEAN RESIDENCE TIME
48.           WRITE(NOUT,88887) DAU,SCALE
49.     C   DAU IS "f", THE NUMBER OF DAUGHTER FRAGMENTS UPON BREAKAGE
50.     C   SCALE IS HOW THE PARAMETERS X(I) ARE SCALED TO MAKE ZXSSQ WORK BEST
51.     99999 FORMAT (1H ,'NUMBER OF PARAMETERS =',I2/' NUMBER OF RESIDUALS =',
52.          1 I2/' DEGREE OF POLYNOMIAL FIT TO EXPTL DATA +1 =',I2/' NUMBER OF'
53.          2 ,'GRID POINTS =',I3/' MIN AND MAX SIZE',2F7.2/' TOLERANCE ON VOL'
54.          3 ,F7.4/' DLOW AND DHIGH FOR CHEBY VOLUME:',2F7.2)
55.     99998 FORMAT (' CHEBYSHEV COEFFICIENTS'/1H ,(E13.4))
56.     99997 FORMAT (' Y(IMAX)=BDRYY ESTIMATE',F7.0/' INITIAL PARAMETER ESTIMA'
57.          1 ,'TES:',(E13.3))
58.     99996 FORMAT(' BETA = ',F8.2,' GAMMA, TAU= ',2F8.3)
59.     88887 FORMAT(' DAU=',F4.1/' PARAMETER SCALE FACTORS=',4(F6.0))
60.           DELD = (DMAX-DMIN)/(IMAX-1)
```

```
      EXVOL = 0.
      DO 30 I=1,IMAX
      D(I) = DMIN + (I-1)*DELD
      IFAIL = 1
      CALL CHEBY(IDP,A,DLOW,DHIGH,D(I),8,EXLNY,IFAIL)
      IF (IFAIL .NE. 0) GO TO 32
      IF (I .EQ. 1 .OR. I .EQ. IMAX) GO TO 22
      EXDVOL = DEXP(EXLNY)*D(I)**3.*DELD
      GO TO 24
   22 EXDVOL = 0.5*DEXP(EXLNY)*D(I)**3.*DELD
   24 EXVOL = EXVOL + EXDVOL*0.5236D0
      IF(D(I) .LT. DGROW) GO TO 30
      VCUT = EXVOL
      DCUT = D(I)
      DGROW = DMAX + 1.
   30 CONTINUE
      WRITE (NOUT,88888) EXVOL,VCUT,DCUT
88888 FORMAT(/' CALCULATED EXPTL VOL IS ',E11.3,' OF WHICH',E11.3,' IS
     1SMALLER THAN',F6.2,' MICRON'/)
      GO TO 100
   32 WRITE(NOUT,88889) IFAIL
      GO TO 300
88889 FORMAT(' ERROR IN EXPERIMENTAL VOLUME CALCULATION--CHEBY  IFAIL=',
     1 I2)
C  THE FOLLOWING SECTION CALLS IMSL ROUTINE ZXSSQ TO FIND THE
C  BEST VALUES OF THE TWO PARAMETERS.
  100 NSIG = 3
      EPS = 0.
      DELTA = 0.
      MAXFN = 200
      IOPT = 1
      IXJAC = 11
      CALL ZXSSQ(FUNGM,M,N,NSIG,EPS,DELTA,MAXFN,IOPT,PARM,X,SSQ,F,
     1 XJAC,IXJAC,XJTJ,WORK,INFER,IER)
  150 WRITE (NOUT,99995) INFER,SSQ,(X(I), I=1,N)
C CALCULATION OF GROWTH AND BREAKUP CONSTANTS, CORRECTING FOR SCALING
      GK = 1.D0/(TAU*(X(2)/SCALE(2)-1.D0))
      BK = GK*X(1)/SCALE(1)
      GKB = GK*X(3)/SCALE(3)
      WRITE(NOUT,99993) BK,GK,GKB
99993 FORMAT(' CALCULATED BREAKUP,GROWTH,AND BROWNIAN CONSTANTS'/3E13.4)
C       NEXT LINE ALTERED (5 NOW 10) TO ALLOW IMAX=101
      WRITE (NOUT,99994) (D(I),Y(I),DLOG(Y(I)),F(1+(I-1)/10),
     1  100.*GKB/(GK*D(I)**(GAM+1.)),I=1,IMAX,10)
99995 FORMAT(1H ,'LEAST SQUARES RESULTS WITH INFER =',I2/' SUM OF SQUAR'
     1 ,'ES =',E11.3/' FINAL PARAMETER VALUES',3E13.4)
99994 FORMAT(1X,'DIAMETER',8X,' NUMBER DENSITY',5X,'LN NUMBER DENSITY',
     1  5X,'RESIDUAL',5X,'%BROWNIAN',
     1    //(1X,F7.2,9X,E12.4,9X,F7.2,13X,F8.3,5X,F6.2))
      WRITE(NOUT,44449)
44449 FORMAT(1X,//' OTHER FITTING DIAGNOSTICS---WORK(1-5),XJAC-',
     1 'THE JACOBIAN')
      WRITE(NOUT,*) (WORK(I), I=1,5),XJAC
      WRITE(NOUT,66666) IER
66666 FORMAT(1X,//' IER, THE ERROR PARAMETER = ',I2)
  300 STOP
      END
C     .....---------.....----------
      SUBROUTINE FUNGM(X,M,N,F)
      IMPLICIT REAL*8 (A-H,O-Z)
```

```
      DIMENSION XC(3),X(3),F(11),Y(200),D(200),A(8),SCALE(4)
      COMMON /BLOCK1/A,EXVOL,BETA,VTOL,D,BDRYY,DAU,SCALE,IDP,IMAX
     1  /BLOCK2/DMIN,DMAX,DELD,Y,DLOW,DHIGH,GAM,TAU
      DATA NOUT/6/
      DO 1020 I=1,N
      XC(I)=X(I)/SCALE(I)
 1020 CONTINUE
C THE ABOVE ASSIGNMENTS PERMIT SCALING OF THE PARAMETERS.
      EF = BETA/3.DO + 1.DO
      DYFAC = DAU**EF
C INITIALIZE RUNGA-KUTTA PARAMETERS
      NSHOT = 0
      Y(IMAX) = BDRYY
 1050 VOL = 0.
C SHOOT THROUGH A RK SOLUTION
      IMAX1 = IMAX - 1
      DO 1100 I = 1,IMAX1
        J = IMAX - I + 1
      X1 = D(J)
        X2 = Y(J)
        X3 = YMOTH(X1,DAU)
        RK1 = X2/X1*(XC(1)*(DYFAC*X3/X2-1.)*X1**BETA-XC(2)
     1   +(XC(3)*GAM/X1**(GAM+1.))) / (1.+XC(3)/X1**(GAM+1.))
        X1 = D(J) - DELD/2.
        X2 = Y(J) - RK1/2.*DELD
        X3 = YMOTH(X1,DAU)
        RK2 = X2/X1*(XC(1)*(DYFAC*X3/X2-1.)*X1**BETA-XC(2)
     1   +(XC(3)*GAM/X1**(GAM+1.))) / (1.+XC(3)/X1**(GAM+1.))
        X2 = Y(J) - RK2/2.*DELD
        RK3 = X2/X1*(XC(1)*(DYFAC*X3/X2-1.)*X1**BETA-XC(2)
     1   +(XC(3)*GAM/X1**(GAM+1.))) / (1.+XC(3)/X1**(GAM+1.))
        X1 = D(J) - DELD
        X2 = Y(J) - RK3*DELD
        X3 = YMOTH(X1,DAU)
        RK4 = X2/X1*(XC(1)*(DYFAC*X3/X2-1.)*X1**BETA-XC(2)
     1   +(XC(3)*GAM/X1**(GAM+1.))) / (1.+XC(3)/X1**(GAM+1.))
      Y(J-1) = Y(J) - DELD*(RK1+2.*(RK2+RK3)+RK4)/6.
66667 FORMAT(1X,I2,5X,F7.2,5X,E12.4)
      IF (Y(J-1) .LE. 0.) GO TO 1700
      DVOL = (Y(J)*D(J)**3. + Y(J-1)*D(J-1)**3.)*DELD/2.
      VOL = VOL + DVOL*0.5236DO
 1100 CONTINUE
C  HAVING COME UP WITH A TRIAL SOLUTION, A TEST IS MADE TO SEE IF THE
C  BOUNDARY CONDITION ON VOLUME IS MET.  IF NOT A NEW ESTIMATE IS MADE OF
C  THE NUMBER DENSITY AT DMAX.
      ERRVOL = EXVOL - VOL
      FERV = ERRVOL/EXVOL
      IF (DABS(FERV) .LT. VTOL) GO TO 1500
      NSHOT = NSHOT + 1
C FOR THE SECOND SHOT THE INITIAL GUESS IS CHANGED BY A % OF THAT USED IN
C THE FIRST SHOT. THEREAFTER THE CHANGE IS A LINEAR EXTRAPOLATION BASED ON
C THE RATE OF CHANGE OF ERRVOL WITH STARTING POINT.
      IF (NSHOT .NE. 1) GO TO 1200
      SERR = ERRVOL
      SYIMAX = Y(IMAX)
      Y(IMAX) = BDRYY + 0.3*DSIGN(BDRYY,ERRVOL)
      GO TO 1050
 1200 TEMPY = Y(IMAX)
      Y(IMAX) = Y(IMAX) - ERRVOL*((Y(IMAX) - SYIMAX)/(ERRVOL-SERR))
      IF (Y(IMAX) .LT. 0.) GO TO 1240
```

```
181.           GO TO 1250
182.      1240 Y(IMAX) = 0.
183.           IF (TEMPY .EQ. 0.) GO TO 1500
184.      1250 SERR = ERRVOL
185.           SYIMAX = TEMPY
186.           GO TO 1050
187.      C CALCULATION OF RESIDUALS FOR THE CONVERGED SOLUTION.  THESE ARE RETURNED TO
188.      C THE CALLING LEAST SQUARES PROGRAM FOR NEXT PARAMETER ADJUSTMENT.
189.      1500 DO 1600 J = 1,M
190.           I = (IMAX-1)/(M-1)*(J-1) + 1
191.           IFAIL = 1
192.           CALL CHEBY(IDP,A,DLOW,DHIGH,D(I),8,EXLY,IFAIL)
193.           IF (IFAIL .NE. 0) GO TO 1550
194.           F(J) = (DLOG(Y(I)) - EXLY)/SCALE(4)
195.           GO TO 1600
196.      1550 WRITE(NOUT,99992) IFAIL,J
197.      C THE RESIDUALS ARE FOR THE LN N VS D AND TAKEN AT EQUISPACED RATHER THAN
198.      C EXPERIMENTAL POINTS.  MAY NEED TO CHANGE THIS.
199.      1600 CONTINUE
200.           RETURN
201.      1700 WRITE(NOUT,*) 'NEGATIVE Y AT XC(1)=',XC(1),' XC(2)=',XC(2),' D=',
202.          1 X1,' XC(3)=', XC(3)
203.           DO 1750 J=1,M
204.           F(J) = 5.D0
205.      1750 CONTINUE
206.           RETURN
207.      99992 FORMAT(' RESIDUE ERROR',I2,'IN CHEBY OF FUNGM AT RESIDUE NO',
208.           1 I3)
209.           END
210.      C
211.      C THE FOLLOWING FUNCTION IS CALLED BY FUNGM TO CALCULATE THE NUMBER AT THE
212.      C MOTHER SIZE, CONVERTING SIZE TO A GRID POINT IN THE PROCESS.  SIZES GREATER
213.      C THAN DMAX ARE ASSUMED TO HAVE ZERO POPULATION.
214.      C
215.           FUNCTION YMOTH(D,DAU)
216.      C DAU IS THE NUMBER OF FRAGMENTS RESULTING FROM BREAKUP; D IS THE FRAGMENT
217.      C SIZE; Y IS THE LN N DISTRIBUTION.
218.           IMPLICIT REAL*8 (A-H,O-Z)
219.           DIMENSION Y(200)
220.           COMMON/BLOCK2/DMIN,DMAX,DELD,Y,DLOW,DHIGH,GAM,TAU
221.           DATA NOUT/6/
222.           DMOTH = DAU**(1./3.)*D
223.           IF (DMOTH .LT. DMAX) GO TO 2000
224.           YMOTH = 0.
225.           RETURN
226.      2000 RIMOTH = (DMOTH - DMIN)/DELD + 1.
227.           IMOTH = IDINT(RIMOTH)
228.      66668 FORMAT(6X,I2,5X,E12.3,5X,E12.3)
229.           YMLOG = DLOG(Y(IMOTH))+(RIMOTH-IMOTH)*(DLOG(Y(IMOTH+1)) -
230.          1 DLOG(Y(IMOTH)))
231.           YMOTH = DEXP(YMLOG)
232.      C  THE ABOVE TWO STATEMENTS INTERPOLATE LINEARLY ON LOG Y.
233.           RETURN
234.           END
235.           SUBROUTINE CHEBY(IDP,A,XMIN,XMAX,X,LA,P,IFAIL)
236.           IMPLICIT REAL*8 (A-H,O-Z)
237.           DIMENSION A(LA),T(10)
238.           XN=(2.D0*X-(XMAX+XMIN))/(XMAX-XMIN)
239.           IF((XN .LT. -1.) .OR. (XN .GT. 1.)) GO TO 3200
240.           IF (IDP .GT. LA) GO TO 3300
```

```
241.           T(1) = 1.0D0
242.           T(2) = XN
243.           P=T(1)*A(1) +T(2)*A(2)
244.           IDP1 = IDP - 1
245.           DO 3100 I=2,IDP1
246.             T(I+1) = 2.D0*XN*T(I) - T(I-1)
247.             P = P + A(I+1)*T(I+1)
248.      3100 CONTINUE
249.           IFAIL = 0
250.           RETURN
251.      3200 IFAIL = 1
252.           RETURN
253.      3300 IFAIL = 2
254.           RETURN
255.           END
256.      $ENTRY
257.      //
```

```
C     THESE LINES ARE THE RUNGA-KUTTA KERNAL USED IN THE SECOND ORDER
C        BREAKAGE MODEL
C
C SHOOT THROUGH A RK SOLUTION
      IMAX1 = IMAX - 1
C       WRITE(NOUT,*) 'Y(IMAX)--B.C. GUESS-- =',Y(IMAX)
      DO 1100 I = 1,IMAX1
        J = IMAX - I + 1
      X1 = D(J)
        X2 = Y(J)
C       TEMPORARY WRITE.....--------.........-------
C        WRITE(NOUT,66667) J,D(J),Y(J)
        X3 = YMOTH(X1,DAU)
        RK1 = X2/X1*(XC(1)*X2*(DYFAC*(X3/X2)**2.-1.)*X1**BETA-XC(2)
     1   +(XC(3)*GAM/X1**(GAM+1.))) / (1.+XC(3)/X1**(GAM+1.))
        X1 = D(J) - DELD/2.
        X2 = Y(J) - RK1/2.*DELD
        X3 = YMOTH(X1,DAU)
        RK2 = X2/X1*(XC(1)*X2*(DYFAC*(X3/X2)**2.-1.)*X1**BETA-XC(2)
     1   +(XC(3)*GAM/X1**(GAM+1.))) / (1.+XC(3)/X1**(GAM+1.))
        X2 = Y(J) - RK2/2.*DELD
        RK3 = X2/X1*(XC(1)*X2*(DYFAC*(X3/X2)**2.-1.)*X1**BETA-XC(2)
     1   +(XC(3)*GAM/X1**(GAM+1.))) / (1.+XC(3)/X1**(GAM+1.))
        X1 = D(J) - DELD
        X2 = Y(J) - RK3*DELD
        X3 = YMOTH(X1,DAU)
        RK4 = X2/X1*(XC(1)*X2*(DYFAC*(X3/X2)**2.-1.)*X1**BETA-XC(2)
     1   +(XC(3)*GAM/X1**(GAM+1.))) / (1.+XC(3)/X1**(GAM+1.))
```

APPENDIX C

Table C1. Data returned by population-balance models

Run	V_g s^{-1}	τ s	$V_g\tau$	V_T[a]$\times 10^6$	For growth (Equation 9) and first-order death (Equation 10)				
					$\phi_1\times 10^{6}$[b]	SS$\times 10^6$	k$\times 10^6$ $\mu m^{-1.5} s^{-1}$	$K_0\times 10^6$ s^{-1}	$K_B\times 10^3$ $\mu m^2 s^{-1}$
4b	123	650	79950	1020	16.6	157	16.86	409	4.346
$5b_1$	123	230	28290	823	13.4	341	62.7	1148	12.27
$5b_2$	123	230	28290	819	13.8	234	41.32	1060	13.14
7c	123	230	28290	835	13.9	179	62.4	1114	12.64
5a	123	81.6	10036.8	662	15.8	184	153.8	2847	32.11
$4c_1$	348	650	226200	966	15.3	448	13.3	525.8	3.036
$4c_2$	348	650	226200	934	15.3	501	16.73	526.4	2.932
$5c_1$	348	230	80040	812	13.5	158	53.85	1296	10.19
$5c_2$	348	230	80040	823	13.7	202	34.15	1281	10.62
7a	348	230	80040	777	13	417	58.17	1298	10.09
$7d_1$	348	230	80040	809	13.6	171	46.56	1324	9.839
$7d_2$	348	230	80040	847	14.2	308	43.96	1356	9.511
$7d_3$	348	230	80040	799	13.8	217	50.49	1320	9.739
8a	348	230	80040	939	15.3	686	58.07	1369	9.421
8b	348	230	80040	767	13.7	48.5	50.06	1328	9.323
$3b_1$	348	81.6	28396.8	715	13.9	218	97.65	2983	34.94
$3b_2$	348	81.6	28396.8	621	15.3	149	144.6	3255	26.61
4a	984	650	639600	972	15.9	1360	22.02	636.3	1.78
7b	984	230	226320	768	14	744	60.96	1571	6.605
8c	984	230	226320	809	14	1190	73.11	1675	5.771
$3a_1$	984	81.6	80294.4	693	15	436	194.2	4041	19.63
$3a_2$	984	81.6	80294.4	614	14.1	712	205.3	4062	18.8
$8d_1$	1810	230	416300	988	15.9	1640	119	1867	3.189
$8d_2$	1810	230	416300	892	15.3	1050	108.5	1854	3.272
6b	123	230	28290	861	17.6	343	30.67	996	12.7
6a	348	230	80040	800	18.4	2120	65.34	1319	7.704
6d	348	230	80040	760	17	87.9	45.09	1231	9.06
6c	984	230	226320	622	14.3	67.3	39.98	1361	7.523

[a] Total volume of solids per unit volume of slurry (fit to 22.8 μm).

[b] Volume of growth units (L_1 < 2.06 μm) per unit volume slurry.

[c] Calculated for L_1 < 2.16 μm (upper limit of fit was 19.8 μm).

[d] Value of m (Equation 21) giving minimum SS.

For growth (Equation 9) and second-order death (Equation 12)					For polymer-enhanced growth (Eqn. 20) and second order death (Equation 12)				
$\phi_1 x10^{6}$[b]	$SSx10^{6}$	$kx10^{8}$ $\mu m^{-5}s^{-1}$	K_0x10^{6} s^{-1}	K_Bx10^{3} $\mu m^{2}s^{-1}$	m^{d}_{opt}	$SSx10^{6}$	$kx10^{8}$ $\mu m^{-5}s^{-1}$	K_0x10^{6} s^{-1}	K_Bx10^{3} $\mu m^{2}s^{-1}$
19.5	148	61.6	373.3	4.89	2	62.2	45.2	311.7	3.80
13.8	4130	0	821	17.35					
16.3[c]	70	0	966	14.8	2	15.9	289	805	11.9
16.9[c]	1400	0	2274	40.47	8	311	0	1320	19.7
15.3	252	37.01	487	3.47					
15.3	503	51.9	479	3.47	0.5	497	49.3	458	3.09
13.5	6010	0	1023	14.54					
11.8	133	86.3	1217	11.69					
15.3	1260	196	1206	11.59	1	1260	196	1206	11.59
13.7	191	244	1190	10.96					
17.9[c]	131	1078	2955	30.3	2	43.8	779	2454	22.0
15.9	636	51.2	580	2.32	0	63.6	51.2	580	2.32
14	731	249	1502	7.61	0	731	249	1502	7.61
17.4[c]	57.2	894	3810	23.1	0	57.2	894	3810	23.1
18.2[c]	503	312	1858	4.611					
17.5[c]	530	336	1831	4.603	0	530	336	1831	4.603